UNIVERSIDADE DE SÃO PAULO
FFCLRP - DEPARTAMENTO DE FÍSICA
PÓS-GRADUAÇÃO EM FÍSICA APLICADA À MEDICINA E BIOLOGIA

LEONARDO VINÍCIUS DA SILVA FRANÇA

Development and characterization of new borate-based compounds for X-rays, gamma rays and neutron luminescence dosimetry

(Desenvolvimento e caracterização de novos compostos à base de boro para dosimetria luminescente usando raios-X, gama e nêutrons)

Ribeirão Preto - SP
2022

LEONARDO VINÍCIUS DA SILVA FRANÇA

Development and characterization of new borate-based compounds for X-rays, gamma rays and neutron luminescence dosimetry

Thesis presented to Faculty of Philosophy, Sciences and Literature of the University of São Paulo, as part of the requirements for the degree of Doctor of Sciences.

Concentration area:

Physics Applied to Medicine and Biology

Advisor:

Oswaldo Baffa Filho

Original version

Available at FFCLRP - USP

Ribeirão Preto - SP

2022

FICHA CATALOGRÁFICA

França, Leonardo Vinícius da Silva

Desenvolvimento e caracterização de novos compostos à base de boro para dosimetria luminescente usando raios-X, gama e nêutrons / Leonardo Vinícius da Silva França; Orientador: Oswaldo Baffa Filho. Ribeirão Preto - SP, 2022.

75 f.:il.

Tese (Doutorado - Programa de Pós-Graduação em Física Aplicada à Medicina e Biologia) - Faculdade de Filosofia, Ciências e Letras de Ribeirão Preto of the Universidade de São Paulo, 2022.

1. Optically Stimulated Luminescence. 2. Borates. 3. Lanthanides. 4. Silver. 5. Radiation Dosimetry.

Name: FRANÇA, Leonardo Vinícius da Silva

Title: Development and characterization of new borate-based compounds for X-rays, gamma rays and neutron luminescence dosimetry

Thesis presented to Faculty of Philosophy, Sciences and Literature of the University of São Paulo, as part of the requirements for the degree of Doctor of Sciences.

Approved in:___/___/___.

Examination Board

Prof. Dr. : _____ Institution:_____

Judgement:_____ Signature: _____

Prof. Dr. : _____ Institution:_____

Judgement:_____ Signature: _____

Prof. Dr. : _____ Institution:_____

Judgement:_____ Signature: _____

Prof. Dr. : _____ Institution:_____

Judgement:_____ Signature: _____

Prof. Dr. : _____ Institution:_____

Judgement:_____ Signature: _____

Acknowledgements

Não apenas o meu esforço levou-me a realizar este trabalho. Contribuições de diversas pessoas, de diferentes lugares e contextos foram relevantes para isso. Gostaria de deixar isso aqui registrado.

Agradeço ao meu orientador, Prof. Baffa, pela parceria, paciência, apoio, engajamento e prontidão, mesmo estando super-ocupado e até mesmo fora do horário de trabalho, nesses quatro anos.

Agradeço também ao Dr. Eduardo Yukihara pelo apoio, paciência e contribuição relevante na minha formação profissional durante meu período de intercâmbio no PSI e até agora.

Agradeço também a Fernanda Hediger pelas medidas de fotoluminescência realizadas e a Prof. Rogéria Gonçalves por permitir isso.

I also thank Elisabeth Gübler for collecting the STEM images from my samples.

Agradeço também ao Lourenço Rocha pela ajuda técnica sempre que necessária e pelas conversas que tivemos.

Ao Eldereis de Paula, deixo também meus agradecimentos pelas várias irradiações realizadas no cidrinha.

Agradeço também a Cassiana Viccari pelas irradiações no CIDRA.

I also thank Federico Geser for the irradiations performed.

Aos companheiros de café e de conversa durante esse tempo, Guilherme Turato, Renan Matsuda, Gabriela Tardelli (a Vegita), Fernando (o Bagaço) e o Matheus Silveira: muito obrigado! A Nilza Marino por todo apoio e paciência em sanar as minhas dúvidas quanto a prazos e submissão de documentos desde o início até agora (e mais adiante).

Ao meu amigo, Leonardo Machado, deixo também meus agradecimentos pela parceria, conversas e apoio.

Agradeço também, em especial, a Mayara Lima, por ter me mostrado que a vida é

mais bela.

A minha família pelo infindável apoio, mesmo eu estando longe.

Finalmente, agradeço também a Deus e seu filho Jesus, por me proporcionar tudo isso.

Resumo

FRANÇA, L. V. S. **Desenvolvimento e caracterização de novos compostos à base de boro para dosimetria luminescente usando raios-X, gama e nêutrons**. 2022. 75 f. Tese (Doutorado - Programa de Pós-Graduação em Física Aplicada à Medicina e Biologia) - Faculdade de Filosofia, Ciências e Letras de Ribeirão Preto, Universidade de São Paulo, Ribeirão Preto - SP, 2022.

Dosimetria de radiações ionizantes é necessária em diversos contextos, tais como imageamento por raios-X, medicina nuclear, centros de pesquisa expostos à radiação, síncrotrons e o espaço sideral. Com base nisso, uma técnica baseada na luminescência opticamente estimulada (OSL), que é a luz emitida por um material previamente irradiado quando estimulado oticamente, tem se estabelecido. Após mais de 20 anos de pesquisa, apenas dois dosímetros OSL baseados nos compostos de Al_2O_3:C e BeO estão comercialmente disponíveis.

O principal objetivo deste estudo é propor novos fósforos que emitam OSL baseados em um borato de cálcio, i.e., CaB_6O_{10} (Z_{eff}=11.5) dopado com lantanídeos (Gd^{3+}, Tb^{3+} or Ce^{3+}) e prata (Ag^+). O composto dopado com Tb e Ag, por exemplo, apresentou sensibilidade OSL comparável ao do Al_2O_3:C (usando os filtros Hoya U340), linearidade em uma ampla faixa de doses (30 mGy até 20 Gy), desvanecimento de ∼30% depois de 24 h, seguido de estabilidade do sinal, sensibilidade a nêutrons, e mostrou ser reprodutível e repetível. O composto dopado com Gd e Ag mostrou características dosímetricas similares. A OSL dos diferentes compostos apresentaram tempos de vida desde microsegundos até nanosegundos, dependendo do tipo de dopante usado. Isso satisfaz os requisitos da dosimetria 2D por varredura com laser e da OSL pulsada, usando o mesmo composto.

Palavras-chave: 1. Luminescência Opticamente Estimulada. 2. Boratos. 3. Lantanídeos. 4. Prata. 5. Dosimetria das Radiações.

Abstract

FRANÇA, L. V. S. **Development and characterization of new borate-based compounds for X-rays, gamma rays and neutron luminescence dosimetry**. 2022. 75 f. Thesis (Ph.D. - Postgraduate Program in Physics Applied to Medicine and Biology) - Faculty of Philosophy, Sciences and Literature, University of São Paulo, Ribeirão Preto - SP, 2022.

Radiation dosimetry is required in several contexts, such as X-ray imaging, nuclear medicine, radiotherapy, radiation-exposed research facilities, synchrotrons and space, to name a few. In view of this, a technique based on the optically stimulated luminescence (OSL) phenomenon, which is the light emission of a previous irradiated material when optically stimulated, has emerged. After more than 20 years of research, there are only two commercially available OSL dosimeters, which are based on Al_2O_3:C and BeO compounds.

The main objective of this work is to propose new OSL phosphors based on a calcium borate compound, i.e., CaB_6O_{10} (Z_{eff}=11.5) doped with lanthanides (Gd^{3+}, Tb^{3+} or Ce^{3+}) and silver (Ag^{+}). Tb,Ag-doped compound, for instance, exhibited OSL sensitivity comparable to that of Al_2O_3:C (using U340 Hoya filters), wide linear dose-range with no signs of saturation (30 mGy up to 20 Gy), fading of ∼30% after 24 h following stability, neutron sensitivity, and showed to be reproducible and repeatable. Gd,Ag-doped compound exhibited similar dosimetric features. OSL from different compounds exhibited luminescence lifetimes ranging from microsecond to nanosecond time-scale, depending on the dopant used. This addresses both 2D laser scanning dosimetry and pulsed OSL dosimetry requirements using the same host compound.

Key-words: 1. Optically Stimulated Luminescence. 2. Borates. 3. Lanthanides. 4. Silver. 5. Radiation Dosimetry.

x

Contents

List of Papers

[1] L. V. S. França and O. Baffa, "Boosted UV emission on the optically and thermally stimulated luminescence of CaB_6O_{10}:Gd,Ag phosphors excited by X-rays," *Applied Materials Today*, vol. 21, p. 100829, 2020.

[2] L. V. S. França, E. Müller, E. G. Yukihara, and O. Baffa, "Swiss-cheese like Structure in a Borate-Based Compound Forms a High Sensitive X-ray, Gamma-ray and Neutron Luminescence Detector," Forthcoming.

[3] L. V. S. França, F. H. Borges, R. R. Gonçalves, O. Baffa, and E. G. Yukihara, "Influence of lanthanide (Gd, Tb or Ce) and silver doping on the luminescence lifetimes of calcium borate investigated by pulsed optically stimulated luminescence," *Journal of Luminescence*, vol. 248, p. 118809, 2022.

Influential Contributions

[1] O. Pakari, L. Bossin, J. B. Christensen, and E. G. Yukihara, "On the analysis of photon arrival time distributions obtained using the pulsed optically stimulated luminescence technique," *Journal of Luminescence*, vol. 245, p. 118796, 2022.

[2] E. G. Yukihara, A. J. J. Bos, P. Bilski, and S. W. S. McKeever, "The quest for new thermoluminescence and optically stimulated luminescence materials: Needs, strategies and pitfalls," *Radiation Measurements*, vol. 158, p. 106846, 2022.

I. General Introduction

1 Radiation Dosimetry

X-ray imaging, computed tomography, nuclear medicine, radiotherapy, nuclear reactors, synchrotrons, nuclear accidents, space, food irradiation. These are a few examples of where radiation dosimetry takes place. Here the radiation is monitored to ensure the safety of the radiation-exposed individuals and to fulfill the requirements of the radiation-dependent procedures. Several types of detectors have been utilized to monitor or quantify radiation: gas filled detectors (e.g. ionization chambers and Geiger counters), Fricke dosimeters, solid state detectors, scintillators, luminescence dosimeters (radiophotoluminescent (RPL), thermoluminescent (TL) and optically stimulated luminescent (OSL) dosimeters), to name a few. A short description of how these detectors operate is presented below.

An ionization chamber is an enclosed device containing a gas where an electric field can be applied within (through an external voltage). By interacting with the gas, the ionizing radiation generates ion pairs, which are then drifted by the applied electric field. Then, the electric current, the output signal, is correlated with the exposure rate of radiation; Geiger counters which are mostly used for surface contamination and ambient exposure rates work in a similar way, but electric pulses are the output signal instead and the energy of the radiation can not be discriminated; Fricke dosimeters are ferrous solutions which change the iron oxidation state (from Fe^{2+} to Fe^{3+}) after exposure to radiation. That causes a change in their optical absorbance, hence their color, which is directly related to the absorbed dose; solid state detectors (or semiconductor diode detectors) release electron-hole pairs after interacting with the incident radiation. Then, an applied electric field promotes the motion of those charge carriers, leading to an electric signal; Scintillators emit prompt visible light under exposure to ionizing radiation. The visible light is then

collected by a photodiode or a photomultiplier coupled to the scintillator; RPL dosimeters emit visible light under UV stimulation after exposure to radiation. Their luminescence output then can be correlated with the absorbed dose and their signal are not erased during readout; TL dosimeters also store the radiation similar to radiophotoluminescent dosimeters, but the dosimetric signal, i.e., luminescence usually in the UV-visible region, is read during a controlled increase of temperature; OSL dosimeters are similar in nature to the TL dosimeters. If previously irradiated, they emit an anti-stokes emission after optical stimulation, i.e., emission wavelength shorter than stimulation wavelength, usually in the UV region. RPL, TL and OSL dosimeters are called passive dosimeters, i.e., the operation of the detectors do not need power supply and readout is performed apart from irradiation. Also, their response is cummulative over exposure to radiation.

The principle of operation and specificities of all these radiation detection techniques are described elsewhere [1–5]. Now a more in depth description of the optically stimulated luminescence, in which this work is based on, is presented.

2 Optically Stimulated Luminescence

Semiconductors and insulators are the typical materials where OSL phenomenon takes place. Some modifications in their structure, e.g. the presence of intrinsic defects or incorporation of (extrinsic) defects originate the called trapping centers, which are responsible for the introduction of new energy levels within the forbidden energy gap of the material. When the trapping centers lie near and below the bottom of the conduction band they act as electron trapping centers, and if they lie near and above the top of the valence band they work as hole trapping centers. Holes are positive charge carriers which appear in the absence of electrons.

In addition to the trapping centers, defects in a material can also introduce recombination centers. These centers are usually more energetic stable than the trapping centers and they can capture an electron and eventually a hole or vice-versa. If this process is radiative, the recombination center is also a luminescence center. For an in depth description of the formation of defects in solids, as well as, the creation of trapping and luminescence centers in different compounds, one can refer to the following references [6, 7].

Considering a material with both trapping and recombination (luminescence) cen-

ters. If sufficient energy is provided to the material, e.g. by irradiating it with X-rays, electrons can escape from the valence band to the conduction band, and then holes become free in the valence band. These charges can eventually be captured by the trapping and recombination centers via their intrinsic electric fields. If these centers are thermally stable enough, the charges can remain trapped for long periods until be detrapped by a stimulation source. If trapping centers release their charges during an optical stimulation and these charges are retrapped by the active (charge-trapped) recombination centers, leading to emission of light, then the OSL have occurred (Figure 1). When the luminescence takes place during thermal stimulation, then we have the thermoluminescence. Therefore, trapping and recombination centers play special roles in both OSL and TL processes.

Regarding the luminescence readout, OSL is usually collected during continuous stimulation of the material, and the luminescence intensity is recorded as a function of the stimulation time. Then a typical exponential decay curve is obtained, which is how the concentration of trapped charges (n) changes with the stimulation time:

$$n(t) = n_0 \exp(-pt), \tag{1}$$

for a model that neglects retrapping of charges. Here n_0 represents the initial concentration of trapped charges and p represents the transition probability per unit time for the trapped

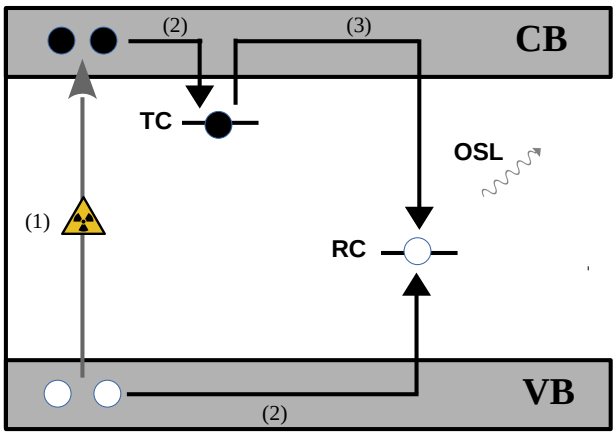

Figure 1: Schematic of how OSL takes place in semiconductors and insulators (the simplest model). 1) represents the excitation of charges by ionizing radiation; 2) represents the capture of charges by trapping centers (TC) and by recombination centers (RC) and 3) represents the radiative recombination process after optical stimulation (OSL). The black and the white circles represent the electrons and the holes, respectively.

electron (hole) to escape to the conduction band (valence band) under stimulation. On the other hand, the TL is collected during a controlled increase of temperature, i.e., at a specific heating rate, and the TL intensity is collected as a function of the temperature. A typical TL curve is composed of peaks centered at specific temperatures which are related to the energy needed to release the electrons (or the holes) from their trapping centers. That energy may be determined by using the several heating rates method, for instance. If both TL and OSL have a common trapping center, then the TL can be used to probe the OSL trapping center. Theoretical and experimental aspects of OSL and TL phenomena are thoroughly described by Yukihara, McKeever and Bøtter-Jensen books [4, 5, 8]. For a comparison of TL and OSL dosimetries and technical specificities, one can refer to the works mentioned herein [9, 10].

There are two physical parameters of high relevance with respect to the nature of OSL: the emission wavelength and the luminescence lifetime. The former is dependent on the luminescence center and its intrinsic energy levels, which may be affected by the surroundings (lattice, in a crystal) [11]. The latter is mostly dependent on the nature of the transition responsible for the luminescent center emission [12]. Determining the OSL emission wavelength is important for the optimization of the OSL response readout and to fulfill emission wavelength designed applications. The luminescence lifetime can be a limiting factor on dosimetric applications as reported in the "OSL dosimetry requirements" section.

3 OSL instrumentation

Three are the main components for an OSL reader: stimulation sources, luminescence detector and optical filters. Stimulation sources are usually LEDs or lasers of high power to allow for an efficient and fast readout of the dosimetric response. The luminescence detection is usually performed using PMTs coupled to optical filters. Optical filters are needed to allow for the detection of luminescence with wavelength shorter than the stimulation wavelength. In addition to the optical filters in front of the PMT, other filters are usually placed in front of the stimulation source to avoid detection of undesirable light components i.e., short wavelength scattered light. Therefore, for a specific OSL emission, one has to make an appropriate choice of stimulation sources, detection filters and stimulation

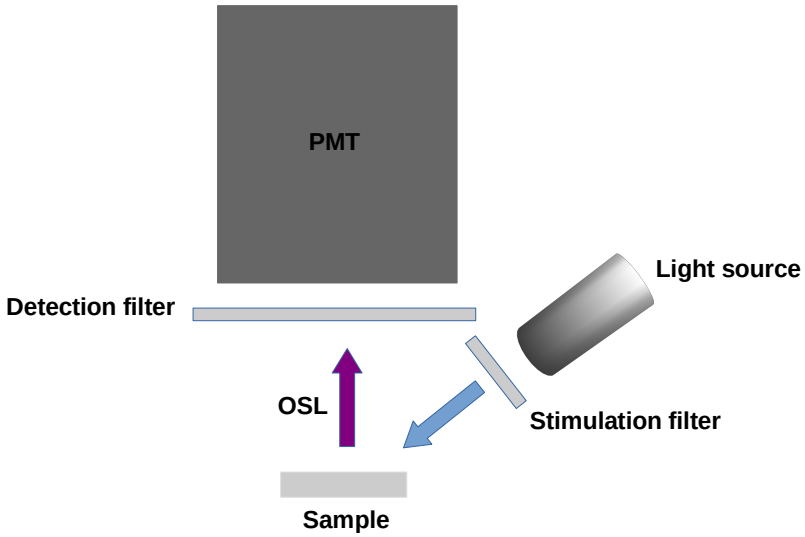

Figure 2: Diagram showing the main components for detection of OSL.

filters. Figure 2 shows a simple schematic for OSL detection. It is worth mentioning that the OSL can be composed of luminescence with wavelength longer than stimulation wavelength, but blocking longer wavelength light is a convenient way to prevent overlap with photoluminescence from the phosphors. For more details about the instrumental aspects for OSL readout, the reader can refer to the classical books on OSL [5, 8].

Different readout modes can be used to collect the OSL: continuous-wave, pulsed and linear modulated modes [5]. In the continuous-wave mode, the stimulation light power is kept constant, while the OSL is continuously collected. It is the simplest mode regarding both stimulation and light collection, but efficient regarding the measurement of the dosimetric response. In the pulsed mode, a train of light pulses stimulates the sample, while the luminescence is collected in between the pulses [13, 14]. That allows for a higher signal-to-noise ratio of the luminescence response compared to the continuous-wave mode, since it allows for the discrimination of the decay components and hence the elimination of undesirable components. However, the acquisition setup needs additional components for the high-frequency light pulses collection and synchronization of stimulation and light detection. In addition, data acquisition and analyses are not as simple as in the continuous-wave mode. At last, the linear modulated mode: here the stimulation light power is linearly increased during stimulation and the OSL is continuously collected [15]. Instead of exponential curves, the OSL here exhibits peak-shape curves, which are asso-

ciated to specific trapping centers. It has been suggested that the advantage of this mode compared to the continuous-wave mode is the possibility of discriminating different trapping center components contributing to the OSL curves [16–18]. However the need of modulation of the stimulating light and its complications must be considered.

4 OSL dosimetry requirements

There are requirements that need to be fulfilled by passive dosimeters in general. Also, there are other ones which are dependent on the type of application in which the OSL dosimeter will be used. The main general requirements are: high sensitivity, dose linearity response in a wide dose range, low or negligible fading, tissue-equivalent effective atomic number, reproducibility and repeatability [19, 20].

Perhaps the first parameter to be evaluated in a potential radiation dosimeter is its sensitivity, i.e., the amount of measurable radiative recombinations due to optical stimulation after irradiation. This is crucial since personal dosimetry require monitoring of doses as low as 1 μSv [20]. There are many reports showing new OSL phosphors with low sensitivities or only tested at high dose irradiation conditions [21–24]. Although it is desirable that an OSL dosimeter presents sensitivity adequate for personal and medical dosimetries, other applications such as dose planning in radiotherapy and emergency dosimetry require radiation detectors working at high-dose irradiation conditions [20, 25].

In radiation dosimetry, one needs to correlate the dosimeter response with the absorbed dose. The simplest correlation between two quantities proportional to each other is a linear dependence, and therefore, a linear-responsive dosimeter facilitates the routines of dose calculation in radiation facilities. Several new OSL phosphors have presented non-linear dose-response dependence for a wide range analysed and therefore are not useful for practical applications [26–28]. Furthermore, it is desirable that the linear response be applicable to a wide range, covering low doses, e.g. for personal dose monitoring and also high doses, e.g. for dose planning in radiotherapy.

In addition, passive dosimeters such as TLDs and OSL dosimeters need to store the trapped charges for long periods, since the dosimetric response is usually measured minutes, hours and even days after radiation exposure in practical applications. Therefore, dosimeters whose response fades with time are not desirable. However, if a dosimeter

presents a consistent percentage fading, followed by stability, that may be a minor issue in applications such as emergency dosimetry.

In personal and medical dosimetries, there is a need of estimating doses absorbed by radiation-exposed staff and patients. To perform an accurate estimation, one has to consider that the absorbed dose is dependent on the properties of the absorbing medium, specially on its effective atomic number. Here the medium of interest is the human tissue and therefore the phosphors that compose the radiation dosimeters should have effective atomic number similar to that of human tissue ($Z_{eff} = 7.6$). Otherwise, one may get an over-estimation (under-estimation) of the absorbed dose for X-ray irradiation at low energies, if the dosimeter has an effective atomic number higher (lower) than that of tissue [19]. Al_2O_3:C, for instance, has a $Z_{eff} = 11.3$, which causes a 4x over-response to low-energy X-rays (mean energy: 20-30 keV) [29].

Regarding the manufacturing processes of the dosimeter, two requirements need to be fulfilled: reproducibility and repeatability. The reproducibility is related to the ability of manufacturing the dosimeters with consistency, i.e., different dosimeters synthesized at the same conditions must present similar dosimetric features (e.g. dose-response, fading) to not compromise inter-comparisons among the dosimeters. On the other hand, the repeatability is related to the ability of obtaining similar dosimetric responses using the same dosimeter when evaluated at different times (under the same conditions). Both reproducibility and repeatability are crucial requirements since they can estimate how reliable the dosimeter synthesis processes and the dose readout protocols are.

If one consider the OSL lifetimes, two different OSL dosimetry modalities may be explored: 2D laser scanning dosimetry and pulsed OSL dosimetry. In the case of 2D laser scanning dosimetry, the OSL signal is fastly and sequentially read at different spots of the dosimeter, so that one can reconstruct a 2D dose distribution. To accomplish that, the OSL phosphor needs to have a fast luminescence center, typically of nanoseconds, to avoid the called pixel bleeding [30]. On the other hand, the pulsed OSL dosimetry requires slow luminescence centers. Since this method relies on the separation of the stimulation stage and the luminescence readout stage, OSL lifetimes should be longer than the stimulating light pulse widths, longer than the dead time, i.e., period in which the PMT is off and longer than the luminescence acquisition time [31]. Typical lifetimes suggested for pulsed OSL dosimetry are in the millisecond timescale, which allows for an easy discrimination

from undesirable components.

From these requirements, it is not hard to see that fulfilling the requirements for all different modalities of radiation dosimetry and different readout modes is unrealistic, since an OSL phosphor is evaluated at specific conditions. One has to be aware of both potentialities and limitations of an OSL phosphor, to not exclude non-envisioned applications and to not overestimate their features.

5 Search and development of new OSL phosphors

As already said, OSL takes place due to an effective combination of trapping and recombination centers. Finding or developing this effective combination for practical applications has shown to be a hard task, since more than 20 years of research has passed and there is only two commercially available OSL detectors, which are based on Al_2O_3:C and BeO phosphors [19].

Al_2O_3:C dosimeter is by far the most used OSL detector in personal dosimetry. That is due to its excellent features, such as high sensitivity (minimum detectable dose in the order of nGy), wide dose range (up to 50 Gy) and no fading []. When excited with blue or green stimulation sources, it presents a main broad emission centered at 420 nm reaching UV detection range, which allows for the light collection at the most sensitive region of the majority of the PMTs. Its emission associated with a 35 ms lifetime is also adequate for the pulsed OSL dosimetry [32]. Several applications have been demonstrated by using Al_2O_3:C based detectors, such as space dosimetry [33], 2D dosimetry in magnetic resonance guided radiotherapy [34], real time in vivo dosimetry [35].

However, Al_2O_3:C presents some limitations. It has a low sensitivity to neutrons, i.e., neutron irradiation does not induce an efficient OSL response. Attempts to overcome this have been made by mixing Al_2O_3:C with ^{6}LiF and $^6Li_2CO_3$ neutron converters, presenting sensitivity of 60% compared to that of ^{6}LiF:Mg,Ti (TLD-600) [36]. However, the neutron conversion process here is not effective, since the secondary particles have short ranges and are produced outside the Al_2O_3:C grains [37]. In addition, Al_2O_3:C is not tissue equivalent (Z_{eff}=11.3). That compromises applications in medical dosimetry, since corrections would be needed to a better estimation of the absorbed doses. Also, the slow luminescence lifetime of Al_2O_3:C (~35 ms) is not adequate for 2D laser scanning

dosimetry applications.

BeO phosphors also present outstanding dosimetric features such as, sensitivity comparable to that of Al_2O_3:C, negligible fading within 6 months, it is almost tissue equivalent (Z_{eff}=7.2), which facilitates its use in medical dosimetry and it is relatively cheap since it is a ubiquitous material used by electronic industry [38–40]. However BeO is toxic in powder form and similar to Al_2O_3:C and has low sensitivity to neutrons [40].

In order to fill this gap of alternative OSL phosphors, many research groups have proposed new compounds with interesting luminescent and dosimetric features, but most of them are either part of preliminary studies or present one or more undesirable features. In this context, significant efforts have been made by exploring borate-based compounds.

5.1 Borate-based compounds

Several types of borate-based compounds have been proposed for OSL dosimetry applications. These include crystalline compounds, e.g. lithium borates, magnesium borates, calcium borates, as well as, glass compounds and nanosize borate compounds. Features and limitations of some of these OSL phosphors are presented below.

Lithium borate with the formula $Li_2B_4O_7$ is almost tissue-equivalent (Z_{eff}=7.4) and have been explored with different dopants and codopants [41–44]. Cu-doped $Li_2B_4O_7$ was shown to have a linear dose-response up to 12 Gy but there is no record of its OSL fading [43]. Kananen et al. showed that Ag-doped $Li_2B_4O_7$ exhibits OSL but basic dosimetric features such as dose-response and fading were not reported [42]. $Li_2B_4O_7$ codoped with Cu and Ag presented a minimum detectable dose of 10 mGy [44], which is too high for personal dosimetry. When codoped with Ag and Gd, $Li_2B_4O_7$ exhibited a fading of 27% after 24h following irradiation, considering the initial OSL intensity [41].

Magnesium tetraborate (MgB_4O_7) has attracted too much attention for OSL dosimetry applications as well [37,45–47]. It has a relatively low effective atomic number (Z_{eff}=8.4) and the use of Ce and Li as dopants has produced a potential OSL phosphor for 2D laser scanning dosimetry applications [37]. Although it presents some interesting features such as high sensitivity (50% compared to that of Al_2O_3:C), linear dose response up to almost 1 kGy and neutron sensitivity, the main issue of this compound is its fading: 10-15% after the first 6 days following irradiation, considering the total OSL area [37]. Studies with other combination of dopants such as Ce-Gd and Ce-Na did not present significant advances:

Ce,Gd- codoped MgB_4O_7 showed dose linearity in a short dose range (0.1-10 Gy), as well as anomalous irradiation storage properties, i.e., increase of 4.5% after 1 day from irradiation, following fading of almost 11% after 7 days from irradiation [45]; The Ce,Na-codoped compound showed a relatively high minimum detectable dose (0.73 mGy) and strong fading of almost 50% after 4 weeks [46]. Using other combination of dopants, i.e., Dy and Li, was not advantageous: MgB_4O_7 presented complete fading after 40 days [47].

Several borate glass compounds have been proposed as alternative OSL phosphors for dosimetry applications. The majority of these works, if not all, however, is part of preliminary investigations of new OSL phosphors. For instance, a new synthesis route for production of MgB_4O_7: Ce,Li has been achieved by heat treatment of a magnesium borate glass [48]. However this work is part of a preliminary study of the new compound, lacking basic dosimetric investigations such as dose-response [48]. In addition, the compound presented OSL fading of 13-40%, depending on the heat treatment temperatures [48]. Preliminary studies using lead borate and lead-aluminum borate glasses have shown either a sublinear or supralinear dose range behaviors for most part of the range analyzed (0.5-100 Gy) [28]. Studies with borate glasses with lithium and potassium carbonates did not show fading investigations and the dose-response of the proposed compounds (0.1-7 Gy) did not exhibit a clear linear dependence [49]. Li_3PO_4-B_2O_3 glass was shown to produce OSL after X-ray irradiation, but no other feature related to OSL dosimetry applicability was reported [50].

Nanostructured compounds have also been explored in view of luminescence (OSL) dosimetry applications. For instance, nanophosphors of $Li_2B_4O_7$:Al exhibited a linear dose-response in the 1-200 Gy range but showed a fading of 20% after 30 days following irradiation, with no signs of stability [21]. Nanoparticles of $Li_2B_4O_7$ have also been investigated with other dopants: Cu- and Ag- singly doped and Cu,Ag- codoped compounds. Although the compounds exhibited high sensitivity under beta irradiation, i.e., minimum detectable dose of 15 μGy and linear dose response in the range of 20 mGy to 50 Gy, they exhibited significant fading after 4 days following irradiation (>30% for the Ag-doped compound and >50% for the Cu,Ag-codoped compound) [51]. Another report showed that nanoparticles of CaB_4O_7:Tb exhibits OSL after X-ray irradiation. The compound exhibited fading of ~40% after 10 days following stability and the report lacks dose-response studies [52]. At last, a novel nanocomposite material based on LiF:Cu was shown to be a

potential candidate for 3D dosimetry applications [53]. The nanoparticles showed linear dose response in a wide range (three orders of magnitude up to ∼20 Gy), but the report lacks fading studies of the compound [53].

5.2 Lanthanide doping

As mentioned before, the OSL requires the presence of trapping and recombination centers. Since these centers are introduced by defects in a crystal, one possible route of manufacturing efficient OSL phosphors is by a trial-and-error approach. This approach takes into account previous materials proposed and their potentialities, but it lacks a rational design on the choice of host and dopants used. It is worth mentioning that this approach has been the most used one for proposing new OSL phosphors.

An alternative approach that has gained some attention in the last years is based on the energy levels introduced by lanthanide-doping with respect to the valence and conduction bands of a compound. This approach is based on a model proposed by Dorenbos, which predicts the energy levels of divalent and trivalent lanthanides for a compound, by considering a few spectroscopic parameters [54–58]. As a result, one can determine if a divalent/trivalent lanthanide acts as a hole trapping center or an electron trapping center in a specific host. This approach has led to the design of several compounds to a variety of applications, such as information storage, stress sensing, anticounterfeiting, X-ray imaging, as well as, TL and OSL dosimetries [59–63]. Other model-guided approaches for the development of new OSL phosphors are reported in a recent work authored by Yukihara et al. [19].

In addition to the level location of energy levels within the band-gap of a compound, the use of lanthanides is also advantageous due to their intrinsic luminescence properties. It is well known that most of trivalent lanthanides present characteristic emissions, which are associated with their $4f^n$ configurations [11]. As a result, applications that require specific wavelength emissions can be envisioned and emission tunability can be achieved by appropriate choice of combination of lanthanides. Reports on the emission tunability by using combination of lanthanides can be found elsewhere [64–66]. The characteristic emissions of most of trivalent lanthanides lie in the visible and IR regions. Only Ce^{3+}, Gd^{3+} and Pr^{3+} present energy levels that allows for UV emission. Regarding UV emission, a transition metal that is worth to be mentioned: silver.

5.3 Silver doping

Silver doping has shown to be effective regarding the introduction of UV luminescence centers in different compounds [67–69]. That is due to the $4d^9 5s \rightarrow 4d^{10}$ transitions of isolated Ag^+, as reported in a study with crystalline and glassy SrB_4O_7:Ag compounds [67]. In this work, the compounds exhibited main emissions centered at 290 nm and 330 nm for the crystalline and glassy compounds, respectively, when excited at 235 nm [67]. Based on this, new OSL phosphors with broad UV emission have been proposed, e.g. Ag-doped lithium borates [42, 70]. It is worth mentioning that Kananen et al. reported that $Li_2B_4O_7$:Ag presented an OSL emission centered at 270 nm [42], which is in a good agreeement with the emission of isolated Ag^+ in crystalline SrB_4O_7:Ag, as reported by Meijerink et al. [67].

6 Motivation and thesis outline

The optically stimulated luminescence has demonstrated to be an effective and reliable technique in passive dosimetry. This encompasses a variety of radiation-exposed environments that need to be routinely monitored, e.g. radiodiagnostics/radiotherapy facilities, synchrotrons and other radiation-exposed research facilities, space, as well as, eventually exposed environments, e.g. in nuclear incidents and accidents. Not restricted to the passive approach, OSL has also the potential to be used to assess real-time and in-vivo doses in patients during radiotherapy, as demonstrated by using Al_2O_3:C detectors [35, 71, 72]. That is possible due to the high-sensitivity of the detectors, which can be manufactured as small as required for the application. Although the potentiality of the OSL in radiotherapy is clearly demonstrated, Al_2O_3:C is not a tissue-equivalent material.

As already mentioned, there are only two commercially available OSL dosimeters currently, namely, Al_2O_3:C- and BeO- based detectors. It is the difficulty in developing efficient OSL phosphors which fulfill the dosimetry requirements that accounts for the scarcity of alternative OSL dosimeters. Furthermore, neither Al_2O_3:C- nor BeO- based detectors is sensitive to neutrons. This is perhaps the main drawback of OSL dosimetry in the current stage.

In view of this, new OSL compounds based on a calcium borate, i.e., CaB_6O_{10} (CBO, hereinafter) doped with lanthanides (Gd^{3+}, Tb^{3+} or Ce^{3+}) and silver (Ag^+) were

developed. This host has a relatively low effective atomic number (Z_{eff}=11.5), which is similar to that of Al_2O_3:C (Z_{eff}=11.3). Furthermore the similarity of the radius of the seven-coordinated Ca^{2+} ions in CBO compared to that of trivalent lanthanides suggests a possible introduction in the matrix by substitution. Borates usually present intrinsic defects in their structure, e.g. oxygen vacancies and the called boron-oxygen-hole-centers (BOHC), which is a defect created by an oxygen that bridges one BO_3 and one BO_4 groups or two BO_4 groups []. As a result, these defects may create the required trapping centers for the OSL processes. The use of Gd^{3+} and Ag^{+} as dopants here is justified by their intrinsic UV emission, which matches the most sensitive region of the majority of PMTs. On the other hand, the use of Tb^{3+} and Ce^{3+} as dopants is desirable since these lanthanides usually act as hole trapping centers in different compounds. This can facilitate the understanding of the trapping and recombination processes and therefore can be useful to optimize the luminescent properties of the phosphor.

In addition to the potentialities of the dopants to be used, the relatively high amount of boron contents in the host structure suggests the use in neutron dosimetry, since the ^{10}B isotope has a high cross section for neutrons [73], and therefore its use can enhance the neutron sensitivity of the phosphor. Some research groups have proposed new detectors, e.g. a combination of a neutron sensitive material with Al_2O_3:C detectors to overcome their limitation of not being sensitive to neutrons. For instance, some reports suggested the use of Al_2O_3:C mixed with boron and lithium-based materials to be used in a mixed field (neutron and gamma-rays) [36,74]. In the first work, the authors proposed a material (Al_2O_3:C + $LiCO_3$, Luxel-N) with a response equivalent to 60% of that of the standard thermoluminescent dosimeter TLD-600 [36]. More recently, a novel material (MgB_4O_7:Ce,Li) with neutron sensitivity approximately 2.5 times higher than that of Luxel-N was suggested [37]. However, more detailed studies, i.e., energy dependence, dose-response and other studies need to be carried out for validation of these materials.

Thesis outline

In this work, CBO doped with lanthanides (Gd, Tb or Ce) and silver were developed and characterized in view of OSL dosimetry applications. The thesis is composed of three main chapters, and each chapter corresponds to a paper already published or to be published (**Paper I**, **Paper II** and **Paper III**). **Paper I** reports the synthesis and optimization,

as well as, luminescent and dosimetric characterizations of CBO:Gd,Ag compounds using X-rays. **Paper II** reports structural, luminescent and dosimetric characterizations of CBO:Tb,Ag compounds using X-rays, gamma-rays and neutrons. In parallel, **Paper III** reports the main features of the luminescent centers responsible for the OSL of CBO:Ln,Ag (Ln=Gd,Ce,Tb) compounds, i.e., their wavelength emissions and luminescence lifetimes.

References

[1] G. F. Knoll, *Radiation Detection and Measurement*. Wiley, 2010.

[2] M. G. Stabin, *Radiation Protection and Dosimetry*. Springer, 2007.

[3] J. H. Schulman, R. J. Ginther, C. C. Klick, R. S. Alger, and R. A. Levy, "Dosimetry of X-Rays and Gamma-Rays by Radiophotoluminescence," *Journal of Applied Physics*, vol. 22, no. 12, pp. 1479–1487, 1951.

[4] S. W. S. McKeever, *Thermoluminescence of Solids*. Cambridge University Press, 1985.

[5] E. G. Yukihara and S. W. S. McKeever, *Optically Stimulated Luminescence - Fundamentals and Applications*. Wiley, 2011.

[6] J. H. Schulman and W. D. Compton, *Color centers in solids*. Pergamon Press, 1962.

[7] R. J. D. Tilley, *Defects in Solids*. Wiley, 2008.

[8] L. Bøtter-Jensen, S. W. S. McKeever, and A. G. Wintle, *Optically Stimulated Luminescence Dosimetry*. Elsevier, 2003.

[9] L. Bøtter-Jensen, "Luminescence techniques: instrumentation and methods," *Radiation Measurements*, vol. 27, no. 5, pp. 749–768, 1997.

[10] S. W. S. McKeever and M. Moscovitch, "Topics under Debate - On the advantages and disadvantages of optically stimulated luminescence dosimetry and thermoluminescence dosimetry," *Radiation Protection Dosimetry*, vol. 104, pp. 263–270, 05 2003.

[11] G. Blasse and B. C. Grabmaier, *Luminescent Materials*. Springer, 1994.

[12] M. L. Chithambo and R. B. Galloway, "On the slow component of luminescence stimulated from quartz by pulsed blue light-emitting diodes," *Nuclear Instruments and Methods in Physics Research Section B: Beam Interactions with Materials and Atoms*, vol. 183, no. 3, pp. 358–368, 2001.

[13] M. L. Chithambo, *An Introduction to Time-Resolved Optically Stimulated Luminescence*. Morgan and Claypool Publishers, 2018.

[14] M. S. Akselrod and S. W. S. McKeever, "A Radiation Dosimetry Method Using Pulsed Optically Stimulated Luminescence," *Radiation Protection Dosimetry*, vol. 81, pp. 167–175, 02 1999.

[15] E. Bulur, "An alternative technique for optically stimulated luminescence (OSL) experiment," *Radiation Measurements*, vol. 26, no. 5, pp. 701–709, 1996.

[16] A. J. J. Bos and J. Wallinga, "Optically stimulated luminescence signals under various stimulation modes assuming first-order kinetics," *Phys. Rev. B*, vol. 79, p. 195118, May 2009.

[17] J. Singarayer and R. Bailey, "Component-resolved bleaching spectra of quartz optically stimulated luminescence: preliminary results and implications for dating," *Radiation Measurements*, vol. 38, no. 1, pp. 111–118, 2004.

[18] C. K. Kuhns, N. A. Larsen, and S. W. S. McKeever, "Characteristics of LM-OSL from several different types of quartz," *Radiation Measurements*, vol. 32, no. 5, pp. 413–418, 2000.

[19] E. G. Yukihara, A. J. J. Bos, P. Bilski, and S. W. S. McKeever, "The quest for new thermoluminescence and optically stimulated luminescence materials: Needs, strategies and pitfalls," *Radiation Measurements*, vol. 158, p. 106846, 2022.

[20] T. Rivera, "Thermoluminescence in medical dosimetry," *Applied Radiation and Isotopes*, vol. 71, pp. 30–34, 2012.

[21] Sahil, R. Kumar, M. K. Yadav, and P. Kumar, "OSL and TA-OSL properties of $Li_2B_4O_7$:Al for radiation dosimetry," *Journal of Alloys and Compounds*, vol. 908, p. 164628, 2022.

[22] V. Guckan, V. Altunal, G. S. Polymeris, A. Ozdemir, Y. Zhydachevskyy, and Z. Yegingil, "TL and OSL characteristics of the fluoroperovskite $KMgF_3$:Eu,Yb, Li for dosimetry applications," *Journal of Luminescence*, vol. 251, p. 119213, 2022.

[23] M. S. Nikam, Y. K. More, B. Butey, M. Jog, S. P. Wankhede, S. B. Kondawar, and S. V. Moharil, "Study of optically stimulated luminescence dosimetric properties of submicron $BaSO_4$:eu phosphor," *Journal of Physics: Conference Series*, vol. 1913, p. 012040, may 2021.

[24] M. Isik, M. Yüksel, M. Topaksu, and N. M. Gasanly, "TL and OSL studies on gallium sulfide (GaS) single crystals," *Journal of Luminescence*, vol. 225, p. 117362, 2020.

[25] I. K. Bailiff, S. Sholom, and S. W. S. McKeever, "Retrospective and emergency dosimetry in response to radiological incidents and nuclear mass-casualty events: A review," *Radiation Measurements*, vol. 94, pp. 83–139, 2016.

[26] L. Pan, S. Sholom, S. W. S. McKeever, and L. Jacobsohn, "Magnesium aluminate spinel for optically stimulated luminescence dosimetry," *Journal of Alloys and Compounds*, vol. 880, p. 160503, 2021.

[27] S. U. Gaikwad, R. R. Patil, M. S. Kulkarni, C. M. Dudhe, and S. V. Moharil, "Development of NaCl-based optically stimulated luminescent phosphors for the possible applications in dosimetry," *Radiation Protection Dosimetry*, vol. 192, pp. 27–35, 12 2020.

[28] G. R. Barrera, L. F. Souza, A. L. F. Novais, L. V. E. Caldas, C. M. Abreu, R. Machado, E. M. Sussuchi, and D. N. Souza, "Thermoluminescence and optically stimulated luminescence of PbO-H_3BO_3 and $PbOH_3BO_3$-Al_2O_3 glasses," *Radiation Physics and Chemistry*, vol. 155, pp. 150–157, 2019.

[29] P. B. R. Gasparian, F. Vanhavere, and E. G. Yukihara, "Evaluating the influence of experimental conditions on the photon energy response of Al_2O_3:C optically stimu-

lated luminescence detectors," *Radiation Measurements*, vol. 47, no. 4, pp. 243–249, 2012.

[30] E. G. Yukihara and M. F. Ahmed, "Pixel Bleeding Correction in Laser Scanning Luminescence Imaging Demonstrated Using Optically Stimulated Luminescence," *IEEE Transactions on Medical Imaging*, vol. 34, no. 12, pp. 2506–2517, 2015.

[31] M. S. Akselrod and S. W. S. McKeever, "A Radiation Dosimetry Method Using Pulsed Optically Stimulated Luminescence," *Radiation Protection Dosimetry*, vol. 81, pp. 167–175, 02 1999.

[32] S. W. S. McKeever, M. S. Akselrod, and B. G. Markey, "Pulsed Optically Stimulated Luminescence Dosimetry Using Alpha-Al_2O_3:C," *Radiation Protection Dosimetry*, vol. 65, pp. 267–272, 06 1996.

[33] E. G. Yukihara, G. O. Sawakuchi, S. Guduru, S. W. S. McKeever, R. Gaza, E. R. Benton, N. Yasuda, Y. Uchihori, and H. Kitamura, "Application of the optically stimulated luminescence (OSL) technique in space dosimetry," *Radiation Measurements*, vol. 41, no. 9, pp. 1126–1135, 2006.

[34] N. Shrestha, E. G. Yukihara, D. Cusumano, and L. Placidi, "Al_2O_3:C and Al_2O_3:C,Mg optically stimulated luminescence 2D dosimetry applied to magnetic resonance guided radiotherapy," *Radiation Measurements*, vol. 138, p. 106439, 2020.

[35] M. C. Aznar, C. E. Andersen, L. Bøtter-Jensen, S. Å. J. Bäck, S. Mattsson, F. Kjær-Kristoffersen, and J. Medin, "Real-time optical-fibre luminescence dosimetry for radiotherapy: physical characteristics and applications in photon beams," *Physics in Medicine and Biology*, vol. 49, pp. 1655–1669, apr 2004.

[36] E. G. Yukihara, J. C. Mittani, F. Vanhavere, and M. S. Akselrod, "Development of new optically stimulated luminescence (OSL) neutron dosimeters," *Radiation Measurements*, vol. 43, no. 2, pp. 309–314, 2008.

[37] E. G. Yukihara, B. A. Doull, T. Gustafson, L. C. Oliveira, K. Kurt, and E. D. Milliken, "Optically stimulated luminescence of MgB_4O_7:Ce,Li for gamma and neutron dosimetry," *Journal of Luminescence*, vol. 183, pp. 525–532, 2017.

[38] E. Bulur and H. Y. Göksu, "OSL from BeO ceramics: new observations from an old material," *Radiation Measurements*, vol. 29, no. 6, pp. 639–650, 1998.

[39] E. G. Yukihara, A. B. Andrade, and S. Eller, "Beo optically stimulated luminescence dosimetry using automated research readers," *Radiation Measurements*, vol. 94, pp. 27–34, 2016.

[40] E. G. Yukihara, "A review on the OSL of BeO in light of recent discoveries: The missing piece of the puzzle?," *Radiation Measurements*, vol. 134, p. 106291, 2020.

[41] A. Ozdemir, N. Can, K. Kurt, and Z. Yegingil, "Optically stimulated luminescence (OSL) dosimetric properties of $Li_2B_4O_7$:Ag,Gd and its relationship with thermoluminescence (TL) glow-curves," *Journal of Alloys and Compounds*, vol. 751, pp. 159–169, 2018.

[42] B. E. Kananen, E. S. Maniego, E. M. Golden, N. C. Giles, J. W. McClory, V. T. Adamiv, Y. V. Burak, and L. E. Halliburton, "Optically stimulated luminescence (OSL) from ag-doped $Li_2B_4O_7$ crystals," *Journal of Luminescence*, vol. 177, pp. 190–196, 2016.

[43] T. Aydn, H. Demirta, and S. Aydn, "TL/OSL studies of $Li_2B_4O_7$:Cu dosimetric phosphors," *Radiation Measurements*, vol. 58, pp. 24–32, 2013.

[44] N. S. Rawat, M. S. Kulkarni, M. Tyagi, P. Ratna, D. R. Mishra, S. G. Singh, B. Tiwari, A. Soni, S. C. Gadkari, and S. K. Gupta, "TL and OSL studies on lithium borate single crystals doped with Cu and Ag," *Journal of Luminescence*, vol. 132, no. 8, pp. 1969–1975, 2012.

[45] V. Altunal, W. Abusaid, V. Guckan, A. Ozdemir, and Z. Yegingil, "Luminescence characterization of Ce and Gd doped MgB_4O_7 phosphors," *Journal of Luminescence*, vol. 246, p. 118815, 2022.

[46] A. Ozdemir, V. Altunal, V. Guckan, K. Kurt, and Z. Yegingil, "Luminescence characteristics of newly-developed MgB_4O_7:Ce^{3+},Na^+ phosphor as an OSL dosimeter," *Journal of Alloys and Compounds*, vol. 865, p. 158498, 2021.

[47] L. F. Souza, A. M. B. Silva, P. L. Antonio, L. V. E. Caldas, S. O. Souza, F. dErrico, and D. N. Souza, "Dosimetric properties of MgB_4O_7:Dy,Li and MgB_4O_7:Ce,Li for optically stimulated luminescence applications," *Radiation Measurements*, vol. 106, pp. 196–199, 2017.

[48] Y. Kitagawa, E. G. Yukihara, and S. Tanabe, "Development of Ce^{3+} and Li^+ co-doped magnesium borate glass ceramics for optically stimulated luminescence dosimetry," *Journal of Luminescence*, vol. 232, p. 117847, 2021.

[49] J. V. B. Valença, A. C. A. Silva, N. O. Dantas, L. V. E. Caldas, F. dErrico, and S. O. Souza, "Optically stimulated luminescence of the [20% Li_2CO_3 +x% K_2CO_3 +(80 - x)% B_2O_3] glass system," *Journal of Luminescence*, vol. 200, pp. 248–253, 2018.

[50] Y. Isokawa, S. Hirano, N. Kawano, G. Okada, N. Kawaguchi, and T. Yanagida, "Dosimetric and scintillation properties of Ce-doped Li_3PO_4-B_2O_3 glasses," *Journal of Non-Crystalline Solids*, vol. 487, pp. 1–6, 2018.

[51] R. Hemam, L. R. Singh, A. I. Prasad, P. Gogoi, M. Kumar, M. P. Chougaonkar, S. D. Singh, and R. N. Sharan, "Critical view on TL/OSL properties of $Li_2B_4O_7$ nanoparticles doped withăCu, Ag and co-doping Cu, Ag: Dose response study," *Radiation Measurements*, vol. 95, pp. 44–54, 2016.

[52] R. Hemam, L. R. Singh, S. D. Singh, and R. Sharan, "Preparation of CaB_4O_7 nanoparticles doped with different concentrations of Tb^{3+}: Photoluminescence and thermoluminescence/optically stimulated luminescence study," *Journal of Luminescence*, vol. 197, pp. 399–405, 2018.

[53] C. L. Nielsen, R. M. Turtos, M. Bondesgaard, J. S. Nyemann, M. L. Jensen, B. B. Iversen, L. P. Muren, B. Julsgaard, and P. Balling, "A Novel Nanocomposite Material for Optically Stimulated Luminescence Dosimetry," *Nano Letters*, vol. 22, pp. 1566–1572, Feb 2022.

[54] P. Dorenbos, "f $\rightarrow$ d transition energies of divalent lanthanides in inorganic compounds," *Journal of Physics: Condensed Matter*, vol. 15, no. 3, pp. 575–594, 2003.

[55] P. Dorenbos, "Systematic behaviour in trivalent lanthanide charge transfer energies," *Journal of Physics: Condensed Matter*, vol. 15, no. 49, pp. 8417–8434, 2003.

[56] P. Dorenbos, "Locating lanthanide impurity levels in the forbidden band of host crystals," *Journal of Luminescence*, vol. 108, no. 1, pp. 301–305, 2004.

[57] P. Dorenbos, "Lanthanide charge transfer energies and related luminescence, charge carrier trapping, and redox phenomena," *Journal of Alloys and Compounds*, vol. 488, no. 2, pp. 568–573, 2009.

[58] P. Dorenbos, "Charge transfer bands in optical materials and related defect level location," *Optical Materials*, vol. 69, pp. 8–22, 2017.

[59] T. Lyu, P. Dorenbos, P. Xiong, and Z. Wei, "$LiTaO_3$:Bi^{3+},Tb^{3+},Ga^{3+},Ge^{4+}: A Smart Perovskite with High Charge Carrier Storage Capacity for X-ray Imaging, Stress Sensing, and Non-Real-Time Recording," *Advanced Functional Materials*, vol. 32, no. 39, p. 2206024, 2022.

[60] T. Lyu, P. Dorenbos, C. Li, and Z. Wei, "Wide Range X-ray to Infrared Photon Detection and Energy Storage in LiTaO3:Bi^{3+},Dy^{3+} Perovskite," *Laser & Photonics Reviews*, vol. 16, no. 9, p. 2200055, 2022.

[61] T. Lyu and P. Dorenbos, "Vacuum-Referred Binding Energies of Bismuth and Lanthanide Levels in $LiTaO_3$ Perovskite: Toward Designing Energy Storage Phosphor for Anti-Counterfeiting, X-Ray Imaging, and Mechanoluminescence," *Laser & Photonics Reviews*, vol. n/a, no. n/a, p. 2200304, 2022.

[62] L. C. Oliveira, E. G. Yukihara, and O. Baffa, "Lanthanide-doped MgO: A case study on how to design new phosphors for dosimetry with tailored luminescent properties," *Journal of Luminescence*, vol. 209, pp. 21–30, 2019.

[63] E. D. Milliken, L. C. Oliveira, G. Denis, and E. G. Yukihara, "Testing a model-guided approach to the development of new thermoluminescent materials using yag:ln produced by solution combustion synthesis," *Journal of Luminescence*, vol. 132, no. 9, pp. 2495–2504, 2012.

[64] X. Mi, D. Sheng, Y. Yu, Y. Wang, L. Zhao, J. Lu, Y. Li, D. Li, J. Dou, J. Duan, and S. Wang, "Tunable Light Emission and Multiresponsive Luminescent Sensitivities in Aqueous Solutions of Two Series of Lanthanide Metal-Organic Frameworks Based

on Structurally Related Ligands," *ACS Applied Materials & Interfaces*, vol. 11, no. 8, pp. 7914–7926, 2019.

[65] B. Shao, J. Huo, and H. You, "Prevailing Strategies to Tune Emission Color of Lanthanide-Activated Phosphors for WLED Applications," *Advanced Optical Materials*, vol. 7, no. 13, p. 1900319, 2019.

[66] N. Kerbellec, D. Kustaryono, V. Haquin, M. Etienne, C. Daiguebonne, and O. Guillou, "An Unprecedented Family of Lanthanide-Containing Coordination Polymers with Highly Tunable Emission Properties," *Inorganic Chemistry*, vol. 48, no. 7, pp. 2837–2843, 2009.

[67] A. Meijerink, M. M. E. van Heek, and G. Blasse, "Luminescence of Ag^+ in crystalline and glassy SrB_4O_7," *Journal of Physics and Chemistry of Solids*, vol. 54, no. 8, pp. 901 – 906, 1993.

[68] P. Boutinaud and H. Bill, "Optical centers related to silver in Ag^+ -doped strontium fluoride crystals," *Journal of Physics and Chemistry of Solids*, vol. 57, no. 1, pp. 55–64, 1996.

[69] C. Pedrini and B. Jacquier, "Luminescence analysis of licl: Ag single crystal using synchrotron radiation," *Physics Letters A*, vol. 69, no. 6, pp. 457–459, 1979.

[70] A. Ozdemir, V. Altunal, V. Guckan, N. Can, K. Kurt, I. Yegingil, and Z. Yegingil, "Characterization and some fundamental features of Optically Stimulated Luminescence measurements of silver activated lithium tetraborate," *Journal of Luminescence*, vol. 202, pp. 136–146, 2018.

[71] L. Nascimento, F. Vanhavere, E. Boogers, J. Vandecasteele, and Y. De Deene, "Medical dosimetry using a RL/OSL prototype," *Radiation Measurements*, vol. 71, pp. 359–363, 2014.

[72] R. Gaza, S. McKeever, M. Akselrod, A. Akselrod, T. Underwood, C. Yoder, C. Andersen, M. Aznar, C. Marckmann, and L. Bøtter-Jensen, "A fiber-dosimetry method based on OSL from Al_2O_3:C for radiotherapy applications," *Radiation Measurements*, vol. 38, no. 4, pp. 809–812, 2004.

[73] C. W. E. van Eijk, "Neutron detection and neutron dosimetry," *Radiation Protection Dosimetry*, vol. 110, pp. 5–13, 08 2004.

[74] M. Kulkarni, M. Luszik-Bhadra, K. Muthe, R. Behrens, N. Rawat, A. Soni, D. Mishra, S. Gadkari, S. Gupta, and D. Sharma, "New OSL detector combination for albedo neutron dosimetry," *Radiation Measurements*, vol. 71, pp. 505–508, 2014.

Paper I

II. Boosted UV emission on the optically and thermally stimulated luminescence of CaB_6O_{10}:Gd,Ag phosphors excited by X-rays

Leonardo V. S. França[*]*, Oswaldo Baffa*

Departamento de Física, FFCLRP, Universidade de São Paulo, Av. Bandeirantes, 3900, 14040-900, Ribeirão Preto, Brazil.

[*] Email: leofranca@usp.br

Abstract

The luminescent properties of X-ray phosphors based on optically stimulated luminescence (OSL) are quite fortuitous, since it demands the existence of both trapping and recombination (luminescent) centers. Nevertheless, lanthanide-doped materials have changed this paradigm by two main reasons: lanthanide doping provides the development of high efficient phosphors and allows for a relatively easy prediction of the energy-levels of the trapping centers involved in OSL phenomena. In view of that, this work reveals some luminescent and dosimetric properties of a phosphor never reported before, i.e., gadolinium and silver doped CaB_6O_{10} polycrystalline samples. The phosphor synthesis followed a solid state reaction method and was optimized regarding the concentration of dopants for a better OSL response. Comparing to non-doped samples, the OSL showed an enhancement of ~140x when doped with gadolinium and silver. The phosphor exhibited a high UV emission under blue stimulation (475 nm), with a linear dose-response for the range

analyzed (1 mGy up to 2 Gy) and a minimum detectable dose of ∼40 μGy. The material exhibited a fading of ∼30% within the first 24 h after irradiation, which is attributed to shallow traps created by Ag^+ incorporation. Wavelength-resolved thermoluminescence (TL) and OSL spectra revealed a sharp 317 nm emission, which is ascribed to ${}^6P_J \rightarrow {}^8S_{7/2}$ transition of Gd^{3+} centers, indicating that the Gd^{3+} has a crucial role in the luminescence mechanisms. In addition, the OSL spectrum exhibited also a broad emission at 350 nm attributed to ${}^3D_J$, ${}^1D_2 \rightarrow {}^1S_0$ transitions of Ag^+ centers. Insights on the luminescent processes are given, including the role of Gd^{3+} and Ag^+ centers in the trapping and recombination processes responsible for the TL and OSL. New mechanisms of luminescent enhancement by silver incorporation are suggested.

Introduction

Estimating the energy deposited in matter by ionizing radiations is essential in several contexts, i.e., irradiation facilities for diagnosis and cancer therapy, synchrotron radiation facilities, nuclear reactors, food industry and even in radiation accidents. One of the techniques for dose estimation is based on optically stimulated luminescence (OSL). The OSL is the anti-Stokes emission by a previously irradiated material when optically stimulated. It takes place with the participation of two different centers in semiconductor or insulator materials: trapping and recombination centers. When given enough energy, the electrons are promoted to the conduction band and holes are freed to move in the valence band. Eventually these charge carriers can be captured in the trapping and the recombination centers. If the material is heated, the charge carriers may escape from the trapping centers and eventually recombine with the opposite charge carriers radiatively, i.e., in the recombination centers. This emission of light is the well known thermoluminescence (TL). The OSL occurs when the stimulation is by light, rather than heat. In a quantitative approach, as needed in dosimetry, the luminescence of the material is collected during a controlled stimulation, i.e, with a heating temperature ramp or with a continuous (or pulsed) light stimulation. TL dosimetry is a well established technique, being part of the daily routine of many irradiation facilities worldwide.

On the other hand, OSL dosimetry has received growing attention in the last years. Depending on the detector used, OSL can be a hypersensitive technique with wide dose

ranges, allowing applications in several types of dosimetry, i.e., personal, medical, retrospective and space dosimetry [1,2]. It is not destructive as TL, allowing repeated measurements and re-evaluation of the results, versatile regarding the choice of excitation sources and filters, which implies a higher efficiency in light detection, among other advantages over TL. [3–5]. However there is a high demand for alternative materials for OSL dosimetry. Currently, for X and gamma-rays there are only two commercially available materials, namely carbon doped aluminum oxide (Al_2O_3:C) and beryllium oxide (BeO), which have demonstrated prominence over other materials [6–8].

A potential phosphor to be used in dosimetry needs to fulfill a set of requirements, i.e., high sensitivity, synthesis-reproducibility, readout-repeatability, linear dose-response and dose storage after irradiation, to name a few. However, attending all these requirements is the main challenge for the establishment of an OSL dosimeter. In view of that, several works have presented dosimetric investigations of novel phosphors, including boron-based materials.

For the last ten years, lithium tetraborate ($Li_2B_4O_7$) crystals have been the most explored boron-based material, since it is tissue equivalent (Z_{eff}=7.3), possesses chemical stability and it is the host matrix of a thermoluminescent dosimeter (TLD-800, $Li_2B_4O_7$:Mn), with well known luminescent and dosimetric properties. However, there are only preliminary studies using the OSL of the manganese doped material [9, 10]. OSL studies of $Li_2B_4O_7$ with other dopants, such as copper only, copper codoped with silver and gadolinium codoped with silver have been reported as well. However, these phosphors exhibited either low sensitivity (non-distinguishable OSL from background instrument for a 15 mGy dose) [11], a relatively high minimum detectable dose (10 mGy) [12] or dose-range linearity limited to high doses (> 6 Gy), with OSL fading of 27% within the first 24 h [13].

Besides the lithium tetraborate, other borate type materials have been investigated. Yukihara et al. presented OSL studies using polycrystalline samples of cerium and lithium doped magnesium tetraborate (MgB_4O_7) for gamma-neutron dosimetry. The phosphor exhibited an OSL sensitivity of ∼50% of Al_2O_3:C using Hoya U-340 filters, with no saturation up to almost 1 kGy [14]. Using the same chemical compounds, Souza et al. reported that the samples presented a good signal stability, exhibiting a negligible fading (<1%) within 40 days after irradiation with beta particles [15]. In addition to samples in crystalline form, there are also preliminary studies using borate glasses, which have shown an

increasing OSL with dose, with restriction to low doses (<100 mGy) or limited to high doses (>250 Gy) [16,17]. Moreover, even different nanosized borates have been explored, i.e., lithium and calcium tetraborates nanoparticles were investigated using OSL. Silver doped lithium borate exhibited a linear dose-response (20 mGy - 50 Gy) with a strong fading of ∼30% in the first 24 h after irradiation and terbium activated calcium borate presented a similar fading pattern within the first 24 h storage time [18, 19].

The phosphor in which this report is based on is a new compound, i.e., gadolinium and silver doped calcium hexaborate (CaB_6O_{10} - CBO as an acronym hereinafter). To the best of our knowledge, this host matrix has been poorly explored. It has a relatively low effective atomic number (Z_{eff}=11.5) and there are only two reports on the luminescence of lanthanide doped CBO samples [20, 21] and two preliminary dosimetric studies, i.e., one using lead as dopant and another one with cerium and lithium doped [22, 23]. The use of lanthanides as dopants is desirable since the new energy levels and the role of the lanthanides on luminescent processes (specially TL and OSL) are easily predicted [24,25]. Furthermore, the combination of dopants (including lanthanides) may improve luminescent response of some materials [26–28]. In these cases, the co-doping ion in the host matrix acts in a energy-transfer process, enhancing the luminescent efficiency of the phosphor.

Several works have presented the use of transition-metal ions doped materials for luminescence dosimetry applications, covering all types of dosimetry. Depending on the host matrix used, they may act as activators in TL and OSL phenomena. More specifically, using silver as dopant in tetraborate lithium single crystals, some reports have shown that they are sensitive to X-rays and neutrons under light stimulation [29, 30]. In addition to single crystals form, polycrystalline samples exhibited OSL after exposure to beta particles, with enhancement of the OSL and the TL by increasing silver molar concentrations [31, 32]. Not restricting to lithium tetraborate host matrix, silicon dioxide doped with silver was found to have an OSL response comparable to that of commercial Al_2O_3:C (Landauer), suggesting the application in real-time in vivo OSL dosimetry [33].

In this work, we present some luminescent and dosimetric properties of Gd- Ag-doped CBO polycrystalline samples. As far as we know, there is no reports showing a clear role of the trivalent Gd in trapping processes following radiative recombination (OSL). In addition, mechanisms of the OSL enhancement in lanthanide- doped compounds by ionic

silver incorporation have not been proposed yet. Regarding structural and morphological aspects, samples were characterized using powder X-ray diffraction (XRD) and scanning electron microscopy (SEM). The dopant concentrations were optimized for a better efficiency on OSL response. TL glow curves were obtained to give information about the nature of the trapping centers involved and correlate to OSL results. Dose-response and fading studies were carried out for the optimized phosphor. Diffuse reflectance spectra were collected for verifying the presence of the surface plasmonic band the silver nanoparticles, formed or not during syntheses. Radioluminescence (RL or XEOL - X-ray Excited Optical Luminescence) and wavelength-resolved TL/OSL were acquired for enlightening about the luminescent centers that take part in TL and OSL processes. Insights on TL and OSL mechanisms are given, including possible structural defects responsible for the trapping processes. In addition, recombination mechanisms in which Gd^{3+} takes part are proposed, which can push forward in the understanding of the trapping mechanisms involving the trivalent Gd in other compounds. Lastly, a new mechanism of luminescent enhancement by silver incorporation involving trapping and recombination processes is suggested.

Materials and Methods

Materials syntheses

The syntheses of non-doped and doped CBO polycrystalline samples followed the solid state reaction method. For the preparation of non-doped calcium hexaborate samples, the precursors used, i.e., calcium carbonate (1.09 g of $CaCO_3$, ACS, 99.0% min, Sigma-Aldrich, Japan) and boric acid (3.71 g of H_3BO_3, BioReagent, 99.5% min, Sigma-Aldrich, USA) were mixed in an agate mortar and pestle. After mixing, the mixture of the reagents was placed in an alumina crucible and annealed in air, in a muffle furnace (EDG model EDG10P-S) following the pattern: temperature ramp (3 °C min^{-1} rate) from room temperature up to 400 °C, followed by a plateau over 1 h; the plateau at 400 °C follows another temperature ramp up to 800 °C, ending with another plateau over 3 h. The thermal treatment of the precursors was expected to produce the following reaction:

$$CaCO_3(s) + 6H_3BO_3(s) \rightarrow CaB_6O_{10}(s) + 9H_2O + CO_2(g).$$

Afterwards, the mixture was cooled down naturally inside the furnace and crushed with

agate mortar and pestle.

For the syntheses of doped samples, solutions of gadolinium nitrate hexahydrate (99.9% min, Sigma-Aldrich, USA) and silver nitrate (99.8% min, Cennabras, Brazil) were prepared. The precursors were mixed with Milli-Q water, producing solutions of 0.04 and 0.002 M for gadolinium and silver, respectively. For doping the calcium hexaborate, different amounts of the solutions prepared (gadolinium nitrate: from 0 to 3% and/or silver nitrate: from 0 to 0.5% molar concentrations) were added to the initial mixture in a glass beaker and placed in a magnetic stirrer hot plate (∼150 °C) with a stir bar. The mixture was allowed to heat and agitate until the solute evaporates completely (≥ 20 min). Then, the resultant powder followed the same annealing, cooling and crushing processes described for the non-doped samples preparation.

Instrumentation - characterization techniques

Both non-doped and doped samples were investigated regarding crystalline structure, dosimetric response and luminescent properties. To verify the crystalline phases of the synthesized powder samples, powder X-ray diffraction (XRD) measurements were carried out. In view of that, an XRD system (model D2 PHASER, Bruker-AXS) with Cu K-α radiation (X-ray tube operated at 30 kV and 10 mA) and scanning with a 0.02° step size was used. The X-ray diffractograms were matched to powder pattern calculation performed with PowderCell software (version 2.4) [34]. For that, crystallographic data for CBO were extracted from the original paper [35]. Furthermore, morphologic studies were performed with a Scanning Electron Microscope (SEM, model EVO 50, Carl Zeiss) with a 20 kV accelerating voltage and using the secondary electrons detector under high vacuum. Before scanning, samples were prepared by coating sputtering with gold during 120 s with a Cressington 108 sputter coater.

Diffuse reflection spectra were acquired using a 500 W Hg-Xe light source (model 6295ns, Newport) with an optical fiber spectrometer (model USB4000, Ocean Optics) in a 150 mm diameter integrating sphere with barium sulfate coating. For the dosimetric characterization, continuous wave OSL measurements were performed. The home-made system used consists of a photomultipler (model 9250B04, Thorn-EMI electron tube) coupled to two UV band-pass filters (model U-340, 3 mm - Hoya) and two blue LEDs (475 nm) for stimulation of the samples. The signal from the photomultiplier is digitized by

a photon counting unit (model C3866, Hamamatsu) and transmitted to a data acquisition board. All OSL measurements were performed using a 200 ms sampling time. Due to the phenomenological similarities between OSL and TL and to gain complementary informations, TL measurements were carried out. The glow curves were acquired with a TL reader (model 3500, Harshaw) using a 3 °C s^{-1} heating rate and in the presence of nitrogen gas flow.

The luminescent properties of the samples were explored by analyses of radioluminescence, OSL emission and TL emission spectra. Both RL and TL spectra acquisitions were obtained using a low-cost TL-RL spectrometer. This system contains a compact X-ray tube (operated at 50 kV and 0.2 mA) for RL measurements, delivering a dose rate of ∼ 5.5 Gy min^{-1} and a heating system for the TL spectra measurements. Light from the samples is collected by an optical fiber spectrometer (model USB2000, Ocean Optics), which presents a maximum responsivity at 500 nm and 10% of response at 300 and 730 nm. For further details the reader is referred to the TL-RL spectrometer report [36]. For the wavelength-resolved OSL acquisition, the same setup was used, but replacing the X-ray tube for an LED (475 nm) for stimulation. In addition, a UV band-pass filter was coupled to the optical fiber, allowing detection only between 280 and 390 nm. For all OSL and TL measurements, powder samples of 50 mg were previously placed in capsules, irradiated and immediately stored in black plastic bags for avoiding exposure to environmental light. For all measurements, powder samples of 10 mg uniformly dispersed on rounded metal cups were used, with exception for XRD analyses.

All irradiation of the samples were performed using two X-ray sources. The first one, a compact X-ray tube (model Magnum, Moxtek) with tungsten target operated at 50 kV and 0.2 mA was used for studies of dependence of OSL response on gadolinium/silver molar concentrations, comparison of OSL response for several samples, OSL fading and TL glow curves. The second one, an Isovolt Titan source (model E-160M-2 GE with a 0.8 mm beryllium window and a 2 mm aluminum filter) maximum energy and current of 160 kV and 10 mA, respectively, was used for studies of dose response (OSL) and TL/OSL spectra. For dose-response measurements, the electric current of the X-ray source (1 - 10 mA) and distance source-samples (0.3 - 1.5 m) were adjusted for allowing the measurements in the specified dose range. Furthermore, for assuring the desired doses, an ionizing chamber (34069 SFD mammo chamber, 6 cm^3 sensitive volume, PTW) was used

for measuring the air kerma before irradiation of the samples. From now on the reader should interpret "dose" as air kerma unless otherwise specified.

Results

Structural and morphological analyses

Both non-doped and doped synthesized samples were expected to possess the crystallographic phase of the calcium hexaborate, as originally reported by Chen et al. [35]. To verify that, the powder samples were analyzed by XRD and matched to a powder pattern calculation based on data of the reference crystallographic phase (space group, lattice parameters and atomic coordinates). Figure 1 shows the results for the non-doped and CBO doped samples with different molar concentrations of gadolinium and silver. By comparison with reference data, the synthesized samples confirmed the expected phase and matches with XRD exhibited on the original paper [35]. Furthermore, the diffractograms from non-doped and doped samples are in good agreement, suggesting that gadolinium and silver contents did not change the crystallographic phase and thus they were successfully incorporated in the CBO lattice structure.

In addition, scanning electron microscopy images were obtained for the gadolinium and silver doped samples. The samples were previously submitted to a gold sputter coating for enhancing the signal to noise ratio. Since samples were not sieved after the crushing process, they did not exhibit regular grain sizes, ranging from ∼1 up to 150 μm, as depicted in Figure 2. Besides, the crystallites showed to be highly agglomerated, as seen in Figure 2b. SEM images for higher magnifications were obtained for verifying the presence of silver nanoparticles, possibly formed during annealing processes. Even analyzed with different samples, the presence of Ag nanoparticles was not detected.

Enhancing the luminescent response

The sample of CBO doped with gadolinium showed to be sensitive to light, when previously irradiated with X-rays. To find the most efficient molar concentration of gadolinium on OSL response, six different amounts of gadolinium nitrate (between 0 and 3% molar concentrations) were chosen and syntheses were made according to the experimental protocol already described. As can be seen in Figure 3a (data points in black) the OSL

emission increased ~9x with 0.5% molar concentration of gadolinium nitrate with respect to the non-doped sample. The 1.5% sample did not exhibit a significant OSL enhancement but reached the maximum with 2.0% molar concentration. For the most concentrated sample (3%), OSL emission decreased almost 40% compared to the most efficient sample. This effect is expected since the probability of energy migration to quenching sites increases as the average distance between Gd ions is reduced [37].

Furthermore, for enhancing the OSL from CBO:$Gd_{2\%}$, new phosphors codoped with silver were produced. Samples were synthesized using five different molar concentrations of silver nitrate (between 0 and 0.5%) and OSL measurements were carried out. As depicted in Figure 3a (data points in red), the 0.05% sample increased the OSL luminescence by 3x with respect to the sample with gadolinium only. Doubling the concentration, no enhancement was noticed, but achieved a better response with the 0.2% molar concentration sample. Moreover, when a 0.5% molar concentration was used, the OSL response decreased by 50% compared to the most efficient sample. Therefore, the CBO doped with

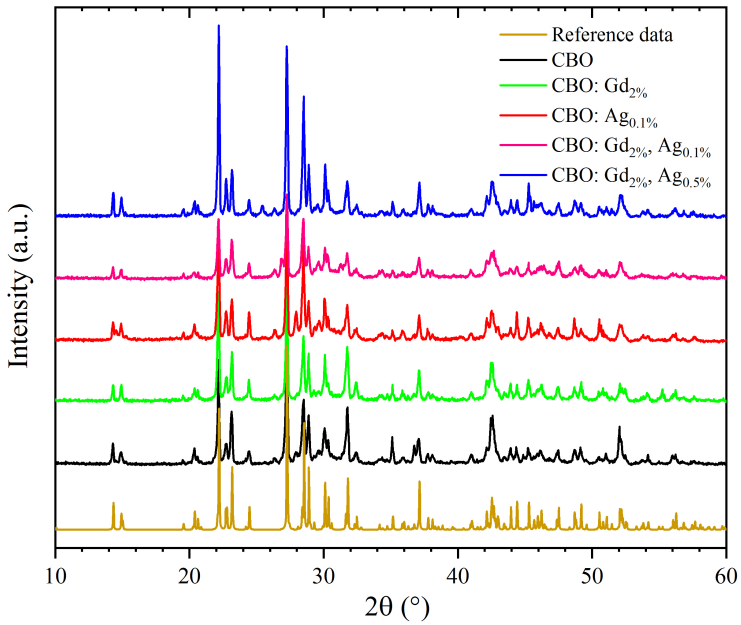

Figure 1: X-ray diffractograms from non-doped CBO and doped with gadolinium and silver samples. The diffractograms from the samples were matched to a powder pattern calculation of the CBO (Reference data on graph).

2% of (nitrate) gadolinium and 0.2% of (nitrate) silver was found to be the most promising material to be investigated.

Figure 3b shows the comparison of the OSL decay curves for different molar concentrations of gadolinium and silver. The non-doped sample showed a weak OSL signal. However when doped with gadolinium, the initial OSL intensity enhanced by 27x.

(a)

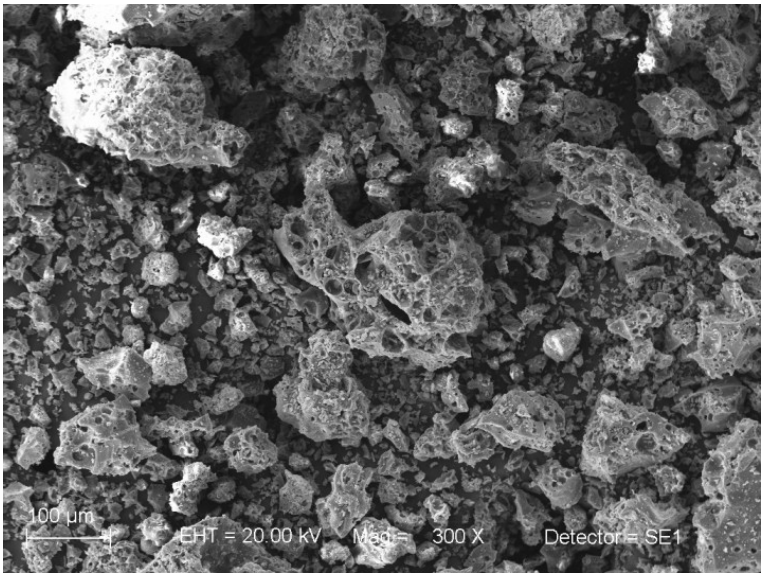

(b)

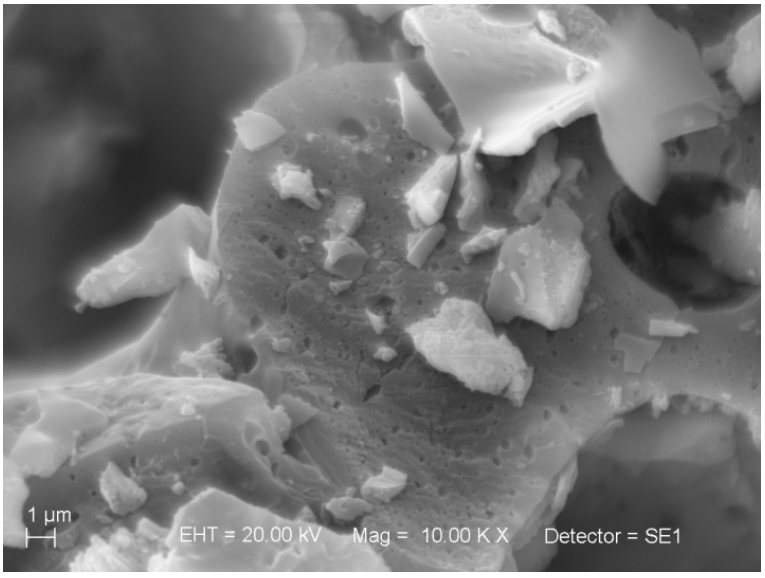

Figure 2: SEM images of CBO:$Gd_{2\%}$, $Ag_{0.2\%}$ polycrystalline samples obtained with 300 X (a) and 10,000 X (b) magnifications.

(a)

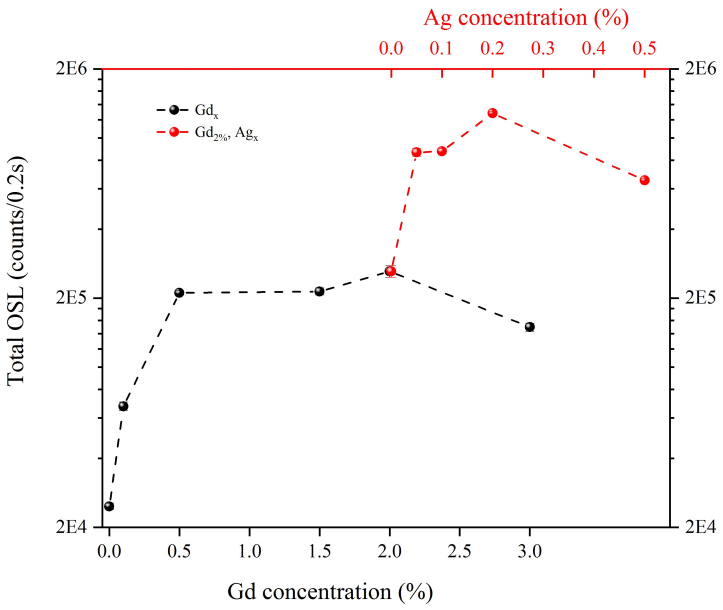

(b)

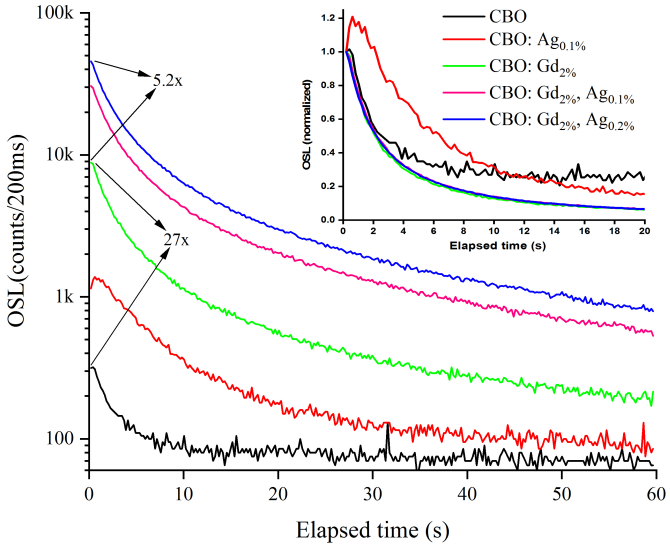

Figure 3: (a) Dependence of molar concentration of gadolinium and silver nitrates on the OSL emission (total emission during 60 s). Data points must be related to the coordinates with the respective color. Each point with bars represents the average and standard deviation for three OSL measurements. (b) Comparison of OSL for different combination of dopants. The OSL curves are shown in a semi-log plot for a better comparison of the relative decaying curves. The inset shows the normalized by initial OSL intensity curves for the first 20 s. Dose delivered = 200 mGy.

In addition, the sample co-doped with silver (0.2% molar concentration) increased the OSL intensity even more, exhibiting an enhancement of 5x compared to the sample with gadolinium only. Furthermore, the sample doped only with silver presented an OSL much less intense than sample with gadolinium only, which suggests that the silver may take part in a sensitization process, transferring energy to gadolinum. Thus, the silver acts as a booster in the luminescence response of the material. The inset shows the normalized OSL curves for the first 20 s. Clearly, the Ag-doped sample exhibited the presence of an initial increasing signal followed by the OSL decay, as well as, a delay in the detrapping process compared to gadolinium co-doped samples. These features suggest the presence of shallow traps, as mentioned by Yukihara and McKeever [2], and hence the silver incorporation is responsible for the creation of shallow traps in the CBO host matrix.

In addition, the synthesis of the most sensitive phosphor demonstrated to be reproducible regarding the OSL response. Using samples from three different syntheses and nine aliquots (three per different synthesis) with a 100 mGy dose, the relative standard deviation was 4.3% using the initial OSL intensity and 6.6% using the total OSL over 90 s (results not shown here).

To verify the influence of the dopants on the thermoluminescence and to compare with OSL results, TL glow curves of the samples were obtained. As we can see in Figure 4, the silver codoped samples exhibited the most intense peaks, with distinction for the 0.2% silver sample. This effect on the TL enhancement is in agreement with the OSL results. Comparing the 0.2% silver codoped with the non-doped sample, the main peak ($\sim$ 300 °C) was $\sim$7x more intense. The other samples, i.e., non-doped, silver only and gadolinium only doped samples showed a much less sensitivity compared to the silver codoped ones. Furthermore, the gadolinium doped sample did not present the same sensitivity pattern as that of OSL, i.e., more sensitive than non-doped and Ag doped CBO samples. This feature will be explained in the discussion section.

In addition to the relative TL intensity aspects, the samples exhibited significant differences in the shape of glow curves. The non-doped sample exhibited a very broad peak ranging from 60 up to 420 °C, with maximum intensity at 280 °C and a small shoulder at 140 °C. These two peaks are in agreement with the results of non-doped samples presented in a previous work on characterization of CBO: Ce, LiCl, considering the differences in the heating rates used [23]. In addition, the sample doped only with silver

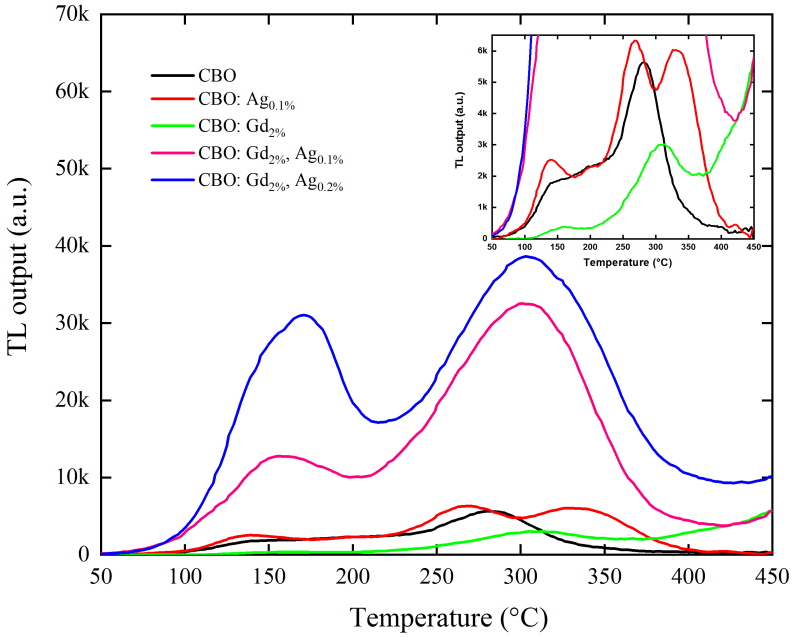

Figure 4: Comparison of the glow-curves for different combination of dopants. The curves were corrected by the response of non-irradiated samples. The inset depicts the curves in a larger scale for better discrimination. Three measurements were carried out for each sample. Heating rate used: 3 °C s^{-1}. Dose delivered: 500 mGy.

presented a more complex set of peaks, i.e., one at 140 °C and a partially overlapped double peak centered at 260 and 330 °C. Although not discriminated, all silver doped samples exhibited the presence of shallow traps indicated by the emission starting at ∼ 60 °C. These results agree with the OSL results for the Ag-doped CBO sample. Moreover, the sample doped with gadolinium only presented a secondary peak at 160 °C and a main peak at around 300 °C. The main peak is shifted only by 10 °C compared to the main peak of cerium doped CBO [23], which suggests that the main peak is associated with defects in the CBO structure. As indicated by the emission at temperatures above 400 °C, the gadolinium doped sample exhibited an atypical background, which may be related to a non-optimized annealing. Besides the component generated by shallow traps, the samples co-doped with silver exhibited the same peaks of the sample with gadolinium only but with higher relative intensities, which suggests that silver incorporation did not change the depth of traps responsible for the TL glow curves.

Dosimetric properties

Using the material that showed to be the most sensitive among the synthesized samples, dose-response studies were carried out. Samples were irradiated with doses ranging from 1 to 2000 mGy according to the protocol: two samples irradiated following an immediate OSL readout each time until all samples were irradiated and analyzed. As can be seen in Figure 5a, the dose-response is seen to be linear in the dose range analyzed, as indicated by the fitting parameters and also the slope is seen to be in good agreement to what is expected for a log-log plot, i.e., slope equal to 1. Moreover, the minimum detectable dose was determined using the background (BG) from three non-irradiated samples and the sensitivity (S) of the material for the OSL reader used (MDD = 3σ/S, where σ represents the standard deviation from BG and S represents the OSL response divided by the dose). The minimum detectable doses evaluated were ∼40.0 μGy using the initial OSL intensity and ∼67.9 μGy using the total OSL (for 30 s integration). Measurements using higher doses could not be performed due to the saturation limit of the photomultiplier response, which was verified by the initial OSL intensity of the samples irradiated with high doses.

As part of the dosimetric characterization, the ability of storing the luminescent response after irradiation was quantified. For that, the measurements were performed in two stages, in a short period, i.e., within 48 h after irradiation and another one in a longer period, i.e., up to 9 days after irradiation. To take into account the high number of irradiations and OSL measurements to be performed, the short and long fadings were carried out separately and data were joined for analysis. For both studies, the irradiations were carried out so that the OSL measurements could be performed sequentially, increasing the time after irradiation. Figure 5b depicts the results obtained and as can be seen from the curve fitting in red, the material exhibited a decrease of ∼30% of total OSL during the first 24 h after irradiation with stabilization of the signal up to 9 days after irradiation. This reduction of the OSL signal can be attributed to the presence of shallow trapping centers, which were indicated by the emission starting at ∼60 °C of the glow curves. These results match with dosimetric studies of gadolinium and silver doped $Li_2B_4O_7$ polycrystalline powder. In this report, the material exhibited a fading of nearly 27% during the first 24 h and was assigned to trap centers associated with a TL peak at ∼ 80 °C [13]. The strong agreement of these results may be attributed to the similarity of the materials, which are both gadolinium and silver doped borates.

(a)

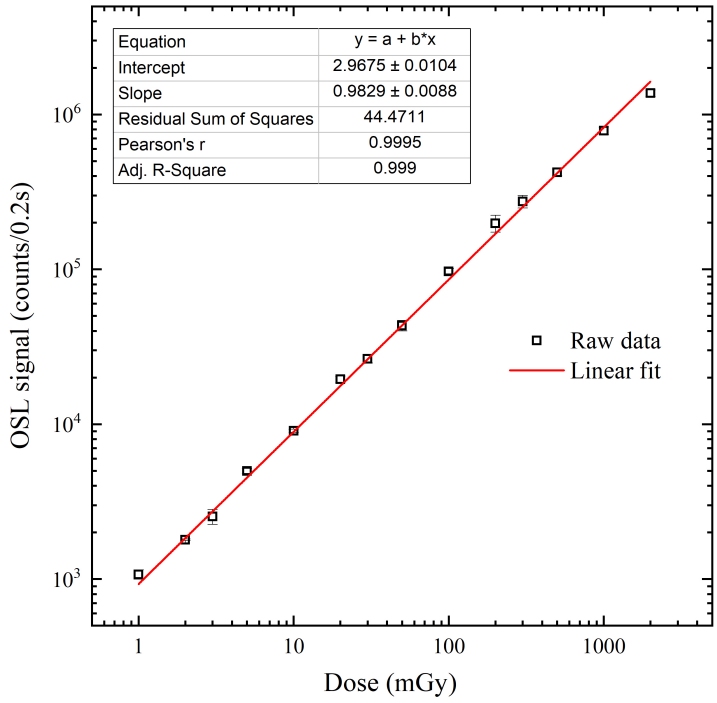

(b)

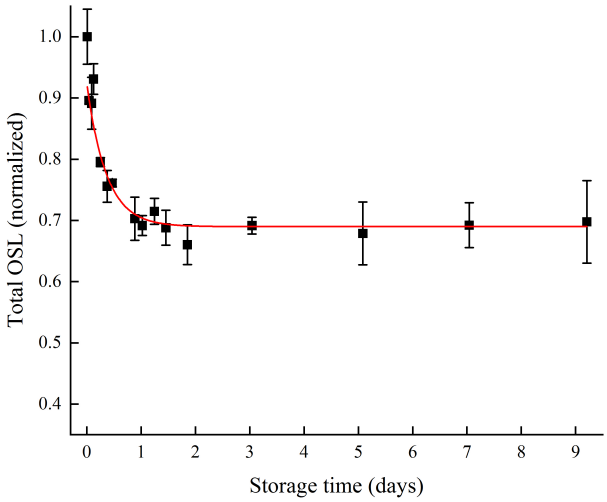

Figure 5: (a) Dose response using samples of CBO:$Gd_{2\%}$, $Ag_{0.2\%}$. Each point with bars represents the average of the initial OSL intensity and standard deviation for three measurements. (b) OSL fading for the CBO:$Gd_{2\%}$, $Ag_{0.2\%}$. Each point with bars represents the average and standard deviation for three measurements of total OSL over 90 s. Dose delivered = 100 mGy.

Luminescent properties

The synthesized phosphors were investigated regarding the nature of the luminescence and the role of the dopants on the enhancement of the dosimetric response. Firstly, diffuse reflection spectra of the samples were obtained. As shown in Figure 6, the presence of silver gave rise to a broad absorption band starting at $\sim$ 400 nm, with maximum at 470 nm and decreasing at higher wavelengths. On the other hand, the presence of gadolinium did not show any significant changes in the absorption spectra. As reported by studies with silver doped strontium borate crystalline samples, non-luminescent Ag^0 centers are responsible for an absorption band at 430 nm, which is indicated by the yellow colour of the samples [38]. The short mismatch between the absorption bands may be assigned to the different host matrixes used. Nevertheless, it is well known that silver nanoparticles exhibit a surface plasmon absorption band at ~410 nm, with variation depending on nanoparticles size. As a result, a luminescence enhancement of radiative centers may take place [39–41]. In spite of these two possible origins of the absorption band, the presence of silver nanoparticles was not detected, as already reported. Therefore we attribute the blue optical absorption to non-luminescent Ag^0 centers formed during syntheses. Using the Tauc plot,

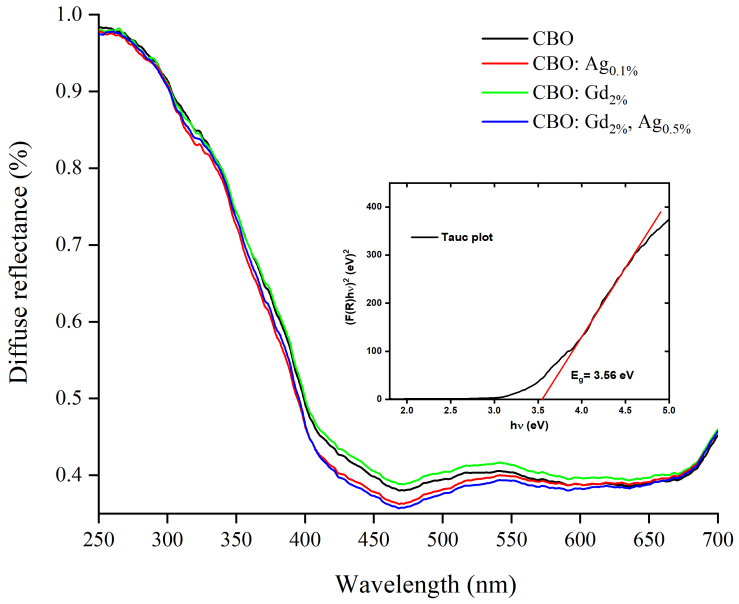

Figure 6: Diffuse reflectance spectra of the samples. The inset shows the tauc plot for the CBO.

the band-gap for the CBO was estimated as 3.56 eV, as depicted in the inset of the figure.

Furthermore, to investigate about the nature of the luminescent centers formed, radioluminescence emission spectra of the samples were acquired. As shown in Figure 7, the non-doped sample is dominated by a broad emission between 260 and 630 nm centered at 390 nm. The addition of silver to the host material did not show significant changes, with exception of a smooth decreasing on the emission intensity. However, for the sample

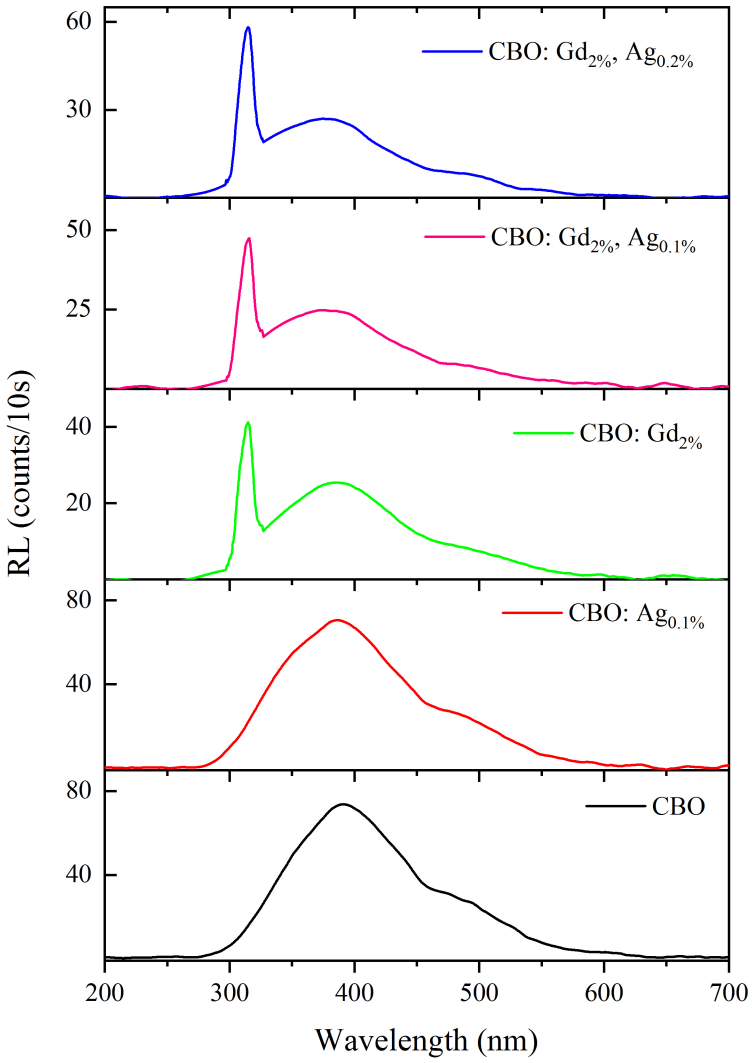

Figure 7: Influence of the dopants on the radioluminescence emission of the samples. Each spectrum represents the average of three spectra. The spectra were not corrected by the responsivity of the system.

doped with gadolinium only, the radioluminescence exhibited a sharp emission at ~317 nm, which can be ascribed to the transition $^6P_J \rightarrow {}^8S_{7/2}$ of Gd^{3+} [42], besides a significant reduction of the overall spectrum intensity. Moreover, with the addition of silver to gadolinium doped samples, there was a slight increase on the broad emission, besides the enhancement of ~75% on the sharp emission (0.2% silver sample).

In addition to the RL measurements, OSL spectra of the samples were acquired. As depicted in Figure 8, the gadolinium doped sample exhibited its UV characteristic emission only (~ 317 nm), whereas the silver doped sample presented a broad and weak emission between 290 and 380 nm. Furthermore, the silver codoped samples exhibited an intense broad band centered at 350 nm, which clearly shows an efficient interaction between gadolinium and silver contents. We attribute this broad emission to ^3D_J, $^1D_2 \rightarrow {}^1S_0$ transitions of Ag^+ ions [43]. It is important to point out that the Ag^+ centers were only efficiently activated in the presence of Gd^{3+} centers. In terms of the relative intensities, all the OSL spectra are in agreement with the OSL decay curves, including the OSL for the non-doped sample.

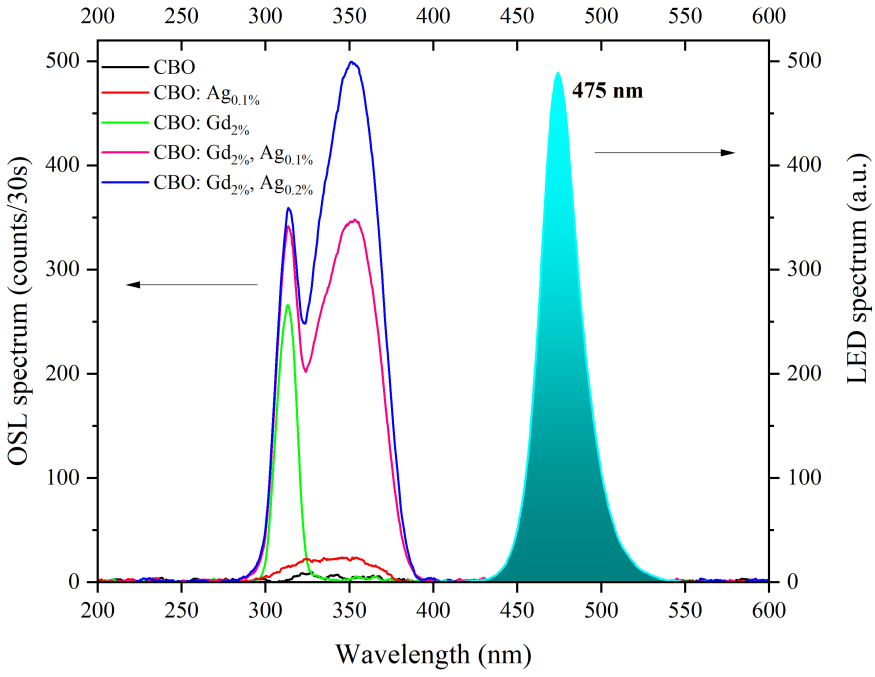

Figure 8: Comparison of the OSL emission spectra of samples. The spectrum of the LED used for excitation is shown as reference (475 nm). Dose delivered ~250 Gy.

Besides the RL and OSL spectra, a wavelength-resolved TL spectrum was obtained for the CBO doped with gadolinium and silver. A high dose had to be deposited in the sample for taking into account the low sensitivity of the detector used (CCD spectrometer). As can be seen in Figure 9, the material exhibited a single emission primarily (~ 317 nm), which is the same sharp emission verified by radioluminescence and OSL spectra. However the intense emission at 350 nm presented in the OSL spectra was not detected. Thus, that indicates that the emission due to the intrinsic gadolinium transition has an important role in the thermoluminescence of the material. Furthermore, by fixing the wavelength at the UV emission, one can see the reconstruction of a wavelength-fixed glow curve, which presented a broad peak at 290 °C overlapped with another peak at lower temperatures. Whereas the main peak confirms the results obtained by the glow curves, the emission attributed to the shallow traps could not be detected. In addition, the second

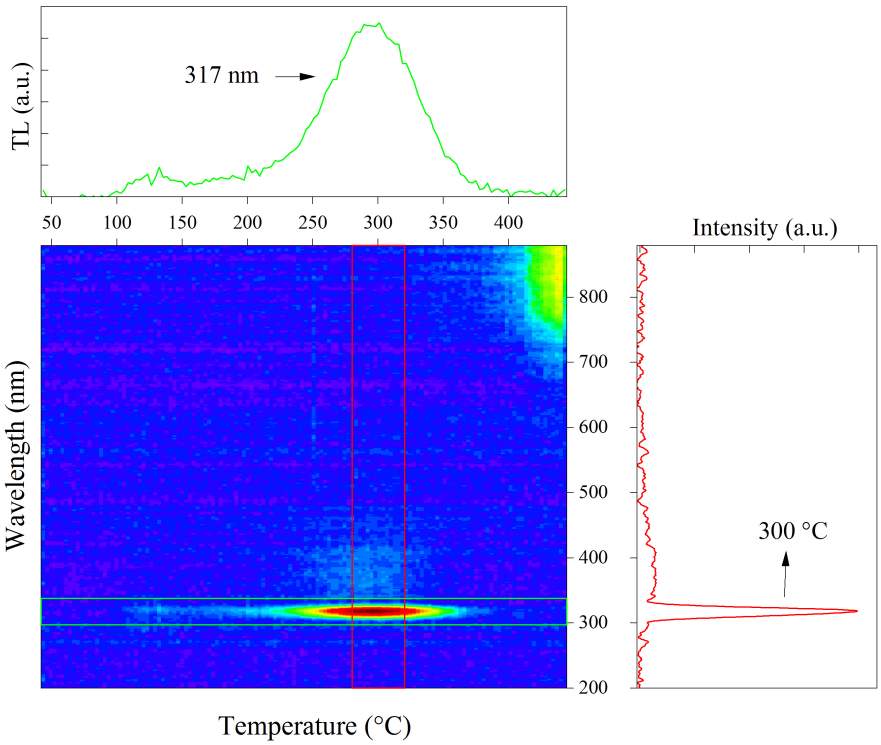

Figure 9: Wavelength-resolved TL spectra for the CBO:$Gd_{2\%}$, $Ag_{0.2\%}$ shown as a contour plot. The upside graph represents a wavelength-fixed glow curve centered at 317 nm and the graph on right part shows the overall emission at ~300 °C. The spectra were not corrected by the responsivity of the system. Heating rate: 3 °C/s. Dose delivered: ~1 kGy.

peak did not seem to be well defined and this may be due to the sensitivity limitation of the system used. The emission above 400 °C is assigned to blackbody light emission from the heating planchet.

Discussion

A model for the luminescent processes involving the phosphor proposed in this work must take into account some aspects: several TL peaks between 60 and 400 °C; characteristic emission of the Gd^{3+} as seen by RL and wavelength-resolved TL/OSL, including the 350 nm emission (OSL) of the silver co-doped samples; fast fading within the first 24 h and the enhancement on the luminescent response by silver codoping. Considering the aspects cited above, as well as the complexity of the TL and the OSL mechanisms and the limitations of this work, we give some insights for the trapping and recombination mechanisms involving the luminescence of the phosphors under study.

As reported by the XRD results, the dopants incorporation did not change the crystallographic phase of the host matrix. Besides, the CBO presents a crystallographic structure with boron and oxygen ions mostly tied by strong covalent bonds, i.e., with BO_3 and BO_4 groups and Ca^{2+} ions as the largest ions in the lattice [35]. The ionic radius for a seven coordinated Ca^{2+} ion, as in the CBO structure, is around 1.06 Å, which is comparable to ionic radii of Gd^{3+} and Ag^{+} ions, i.e., 1.00 and 1.22 Å, respectively for the same coordination number [44]. Nevertheless the boron ions present in the host matrix have a small ionic radius of 0.01 and 0.11 Å, for three and four coordination numbers, respectively [44]. Therefore, we suggest the Gd^{3+} and Ag^{+} substitute for different Ca^{2+} sites, with some distortion in the lattice for the case of the silver incorporation. In addition, we speculate that the valence state mismatch between Gd^{3+} and Ca^{2+} ions can be partially compensated by the substitution of Ag^{+} in other Ca^{2+} sites.

For allowing the trapping of electrons and holes freed through irradiation, we consider some types of defects that may be present in the crystal. Whereas trivalent Nd, Sm, Eu, Dy, Ho, Er, Tm usually act as electron trapping centers in wide band gap compounds and trivalent Ce, Pr, Tb, as hole trapping centers [45, 46], there is a lack of reports showing the role of the trivalent Gd in trapping processes. Guo et al. reported that Gd^{3+} act as electron-trapping centers in the persistent luminescence of the $Ca_6BaP_4O_{17}$:Eu^{2+},

Gd^{3+} [47]. Regarding electron or hole trapping processes, no other reports have been found for trivalent Gd^{3+} centers.

It turns out that according to Dorenbos' models for the energy levels of divalent and trivalent lanthanides in wide band-gap materials, the shape of the zigzag curves do not change significantly for different hosts [48–50]. In addition, the energy levels for Gd^{3+} and Gd^{2+} exhibit the lowest and the highest defect levels, respectively, among the lanthanides. To the best of our knowledge, for the most of inorganic compounds these defect levels lie on the valence and conduction bands, which means that they are not stable as charge carrrier traps. However, since the defect level of the lanthanides are highly dependent on the host compounds, we consider the possibility of Gd^{2+} in CBO to present a defect energy level right below the conduction band, i.e., Gd^{3+} acting as an electron trapping center.

A typical defect found in boron-based materials is the generated by oxygen vacancies (V_o). These defects act as electron trapping centers and there are several works reporting the presence of these defects in borates, including $Li_2B_4O_7$ and MgB_4O_7 [51–53]. Furthermore, another electron trapping center that may be present in the CBO lattice is that created by interstitial Ag_I^+ ions. These defects under irradiation at room temperature capture electrons forming Ag_I^0, as indicated by electron paramagnetic resonance studies on Ag-doped $Li_2B_4O_7$ crystals [29,54]. Therefore, it is expected for the CBO to present these different electron trapping centers, since its chemical composition and structural features are similar to those of the reported compounds. The Equation 1 sums up some possible electron trapping processes that may take place following irradiation.

$$\left.\begin{aligned} Gd^{3+} + e^- &\rightarrow Gd^{2+} \\ Ag_I^+ + e^- &\rightarrow Ag_I^0 \\ V_o + e^- &\rightarrow V_o^- \end{aligned}\right\} \text{ (electron trapping)} \qquad (1)$$

Besides the electron trapping centers, we suggest two different hole trapping centers that may be present in the CBO lattice. The presence of these defects is supported by the similarities between CBO and $Li_2B_4O_7$ host compounds. One is that originated by substitution of Ag^+ for Ca^{2+} ions. By replacing Li^+ ions, Ag^+ ions can act as hole trapping centers as presented by some reports on Ag-doped $Li_2B_4O_7$ [29,54]. In addition, since the host compound is characterized by BO_3 and BO_4 groups, another hole trapping center is

likely to be generated. This center known as boron-oxygen hole center (BOHC) is created by the oxygen ligand that bridges a BO_3 and a BO_4 or two BO_4 groups [10,55–58]. Hence, we suggest that substitutional Ag_S^+ and BOHC centers are responsible for the creation of two different hole trapping centers, which take part in the latency period between the irradiation and the excitation (heat or light) of the material. These hole trapping processes are represented in Equation 2.

$$\left.\begin{aligned} Ag_S^+ + h^+ &\rightarrow Ag_S^{2+} \\ BOHC + h^+ &\rightarrow BOHC^+ \end{aligned}\right\} \quad \text{(hole trapping)} \tag{2}$$

As indicated by the glow curves, the Ag- doped material exhibited the presence of shallow traps. In addition, the initial OSL increasing of the Ag-doped CBO samples suggested that silver incorporation promoted the creation of shallow traps. These results are confirmed by the fading results. As already mentioned, the same fading pattern, i.e., the reduction of $\sim 30\%$ in the OSL intensity within the first 24 h and the presence of shallow traps were reported by studies with Gd- and Ag- doped $Li_2B_4O_7$ samples [13]. Therefore, the shallow traps can be associated with substitutional Ag_S^+ hole trapping centers or interstitial Ag^+ electron trapping centers. Regarding BOHC trapping centers, we suggest that they can be responsible for the generation of the second and third peaks of the glow-curves. However we do not exclude the possibility of charge retrapping.

For modelling possible mechanisms for the radiative recombinations in the OSL and TL processes, we consider the presence of two different luminescent centers. As shown by the wavelength resolved TL and OSL spectra, the material exhibited an emission at 317 nm which is assigned to an intrinsic transition of Gd^{3+} centers. Furthermore, the broad emission at 350 nm in the OSL of the Ag- codoped samples is attributed to Ag^+ ions. Therefore we consider that Ag^+ luminescent centers take part only in the OSL, whereas Gd^{3+} luminescent centers play a role in both TL and OSL processes. Considering that trivalent Gd does not have a clear role in trapping processes, we suggest two different possibilities for the radiative processes to occur: one with Gd^{3+} acting as an electron trapping-recombination center and another one without taking part in the trapping process, just acting as a luminescent center.

In the first case, the trapped-electron Gd^{3+} center (Gd^{2+}) captures a hole, leading

to the radiative recombination, as represented by Equation 3. We suggest that this process can be responsible for the sharp emission (317 nm) of the OSL. For the second case, another electron trapping center should take part in an intermediate process, where interstitial Ag^+ or oxygen vacancies V_o centers may take place. As a result, a non-radiative recombination process occurs, as represented by Equation 4, following the excitation of the Gd^{3+} center by an energy-transfer process, represented by Equation 5. We suggest that the energy-transfer process between activated Ag^+ and Gd^{3+} can be the cause of the TL response of the material. This explains the similar TL sensitivity of the gadolinium doped sample compared to that of the non-doped sample, since the silver substantially enhanced the TL emission of the material. Moreover, it is known that Ag^+ and Gd^{3+} satisfy the resonance conditions for energy-transfer, making $P_J \rightarrow {}^8S_{7/2}$ transition possible [43, 59]. For simplicity, we do not consider that oxygen vacancies take place in the trapping processes leading to the radiative recombination. However, these defects may compete with the other electron trapping centers reported.

$$h^+ + Gd^{2+} \rightarrow (Gd^{3+})^* \rightarrow Gd^{3+} + h\nu \quad \text{(radiative recomb.)} \tag{3}$$

$$\left.\begin{aligned} h^+ + Ag_I^0 &\rightarrow (Ag_I^+)^* \\ h^+ + V_o^- &\rightarrow (V_o)^* \end{aligned}\right\} \quad \text{(non-radiative recomb.)} \tag{4}$$

$$(Ag_I^+)^* \rightarrow (Gd^{3+})^* \rightarrow Gd^{3+} + h\nu \quad \text{(radiative energy-transfer)} \tag{5}$$

For the broad emission centered at 350 nm in the OSL of the material, another mechanism is proposed. By the OSL spectra of samples, we can see that the Ag- doped sample exhibited a weak emission. However, when codoped with gadolinium a broad emission ascribed to Ag^+ centers appeared, besides the intrinsic emission of Gd^{3+} centers. Therefore, we suggest that a coupling between Gd^{3+} and Ag^+ centers takes place, which makes the Ag^+ emission possible. This is represented by Equation 6.

$$(Gd^{3+})^* \rightarrow (Ag_I^+)^* \rightarrow Ag^+ + h\nu \quad \text{(radiative coupling)} \tag{6}$$

It is noteworthy that there are three different mechanisms for luminescent enhancement by silver incorporation reported so far: the first one is that generated by the

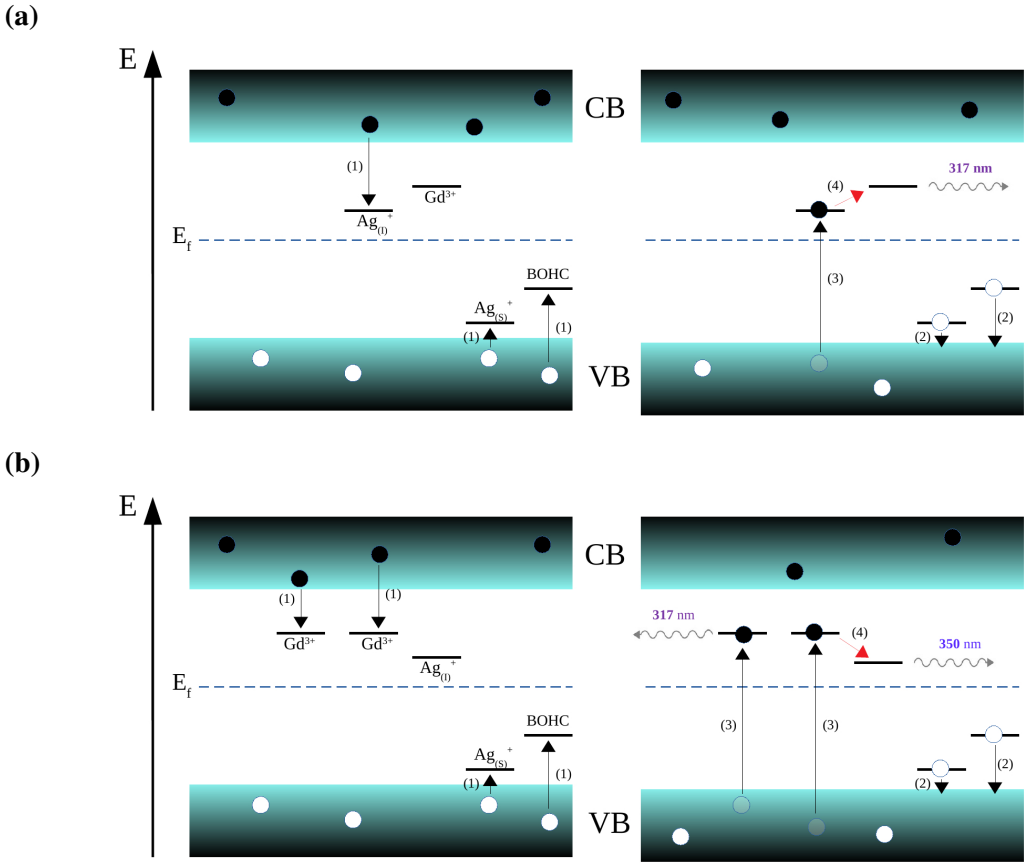

Figure 10: Diagram representation of possible TL (a) and OSL (b) mechanisms for CBO:Gd^{3+}, Ag^{+} samples. (1) represents the trapping of charges; (2) represents the optical or heat stimulation; (3) represents the recombination processes and (4) represents an energy-transfer to a luminescent center (in the TL) or a radiative coupling (in the OSL). E_f stands for fermi level. Black and white circles represent electrons and holes, respectively.

surface plasmon resonance of the silver nanoparticles [39, 40], including OSL enhancement [60,61], a second one is that generated by an energy-transfer from Ag^{+} centers in conventional down-conversion photoluminescence (high-energy photon absorption following a lower-energy photon emission) [43,59] and the third one is that caused by molecule-like non plasmonic silver particles [41]. The mechanisms suggested here are the first ones involving ionic silver contents on the enhancement of an anti-Stokes emission, more specifically TL and OSL.

Therefore, to summarize the TL and OSL processes that take place, when the material is irradiated with sufficient energy, electron-hole pairs are formed. Eventually, the electrons can be trapped at Gd^{3+}, interstitial Ag_I^+ centers or both. Similarly, the freed holes can be trapped at substitutional Ag_S^+ and BOHC centers. After stimulation with heat or

light, the trapped holes can return to the valence band and eventually recombine with the electrons trapped at the recombination centers, following a direct or an indirect emission of light. Figure 10 sums up all trapping, detrapping and recombination mechanisms that may take place in the material investigated.

We consider that additional spectroscopic analyses are necessary to lead us to a more complete model, including the determination of the depth of traps, attribution of the traps responsible for the second and third peaks of the glow-curves and if charge retrapping takes place. Furthermore, other analyses are necessary for validating the proposed mechanisms for the TL and OSL emissions.

Conclusions

The silver incorporation appeared to have an important role in the enhancement of the OSL and the TL of the phosphor, which suggests the possibility of enhancement by addition of the transition metal in other compounds. The material presented two different luminescent centers, i.e., Gd^{3+} and Ag^{+} centers, where the former plays a central role in both TL and OSL and the latter takes part only in the OSL processes. The wavelength resolved OSL spectra indicate that the OSL enhancement takes place by means of a coupling between Gd^{3+} and Ag^{+} centers. Furthermore, possible defects responsible for the charge trapping in the latency period between irradiation and stimulation were proposed: substitutional Ag_S^+ centers and boron-oxygen- hole-center (BOHC), i.e, a defect created in an oxygen that bridges a BO_3 and a BO_4 or two BO_4 groups, both acting as hole-trapping centers. The luminescence mechanisms suggest that Gd^{3+} centers act by two different means, i.e., as an electron trap-recombination center and as a luminescent center only, activated through a sensitization process from the excited recombination center, i.e., interstitial Ag_I^+ centers. This second mechanism is suggested as the responsible for the enhancement of the TL emission of the material. Both mechanisms for enhancement of the TL and the OSL are the first reports involving the participation of ionic silver contents. The material proposed in this work has shown very promising features, including ease to manufacture, synthesis reproducibility, whole OSL response at the optimum window of the majority of the PMT tubes and a good dose linearity response, with the possibility to surpass the limits of the dose range analyzed. There is still potential for optimization and this material can be a

useful phosphor in OSL dosimetry applications.

Acknowledgements

This research was partially funded by Brazilian agencies Fundação de Amparo à Pesquisa do Estado de São Paulo (FAPESP CEPID-NEUROMAT 13/07699-0), Coordenação de Aperfeiçoamento de Pessoal de Nível Superior (CAPES, Finance Code 001) and Conselho Nacional de Desenvolvimento Científico e Tecnológico (CNPq Grant 304107/2019-0). We are grateful to Luiz C. Oliveira and Éder J. Guidelli for the relevant comments and suggestions for this work. The technical support of Eldereis de Paula, Lourenço Rocha and Carlos R. da Silva is also appreciated.

References

[1] E. B. Podgoršak, *Radiation Physics for Medical Physicists*. Springer, 2006.

[2] E. G. Yukihara and S. W. S. McKeever, *Optically Stimulated Luminescence - Fundamentals and Applications*. Wiley, 2011.

[3] L. Bøtter-Jensen, S. W. S. McKeever, and A. G. Wintle, *Optically Stimulated Luminescence Dosimetry*. Elsevier, 2003.

[4] L. Bøtter-Jensen, "Luminescence techniques: instrumentation and methods," *Radiation Measurements*, vol. 27, no. 5, pp. 749 – 768, 1997.

[5] S. W. S. McKeever and M. Moscovitch, "On the advantages and disadvantages of optically stimulated luminescence dosimetry and thermoluminescence dosimetry," *Radiation Protection Dosimetry*, vol. 104, pp. 263–270, 2003.

[6] E. G. Yukihara, S. W. S. McKeever, and M. S. Akselrod, "State of art: Optically stimulated luminescence dosimetry - frontiers of future research," *Radiation Measurements*, vol. 71, pp. 15 – 24, 2014.

[7] V. Schembri and B. J. M. Heijmen, "Optically stimulated luminescence (OSL) of carbon-doped aluminum oxide (Al_2O_3:C) for film dosimetry in radiotherapy," *Medical Physics*, vol. 34, pp. 2113–2118, 2007.

[8] A. Jahn, M. Sommer, W. Ullrich, M. Wickert, and J. Henniger, "The BeOmax system - Dosimetry using OSL of BeO for several applications," *Radiation Measurements*, vol. 56, pp. 324 – 327, 2013.

[9] M. Danilkin, I. Jaek, M. Kerikmae, A. Lust, H. Mandar, L. Pung, A. Ratas, V. Seeman, S. Klimonsky, and V. Kuznetsov, "Storage mechanism and OSL-readout possibility of $Li_2B_4O_7$:Mn (TLD-800)," *Radiation Measurements*, vol. 45, no. 3, pp. 562 – 565, 2010.

[10] A. Ratas, M. Danilkin, M. Kerikmae, A. Lust, H. Mandar, V. Seeman, and G. Slavin, "$Li_2B_4O_7$:Mn for dosimetry applications: Traps and mechanisms," *Proceedings of the Estonian Academy of Sciences*, vol. 61, p. 279, 01 2012.

[11] K. J. Kearfott, W. G. West, and M. Rafique, "The optically stimulated luminescence (OSL) properties of LiF:Mg,Ti, $Li_2B_4O_7$:Cu, $CaSO_4$:Tm, and CaF_2:Mn thermoluminescent (TL) materials," *Applied Radiation and Isotopes*, vol. 99, pp. 155 – 161, 2015.

[12] N. S. Rawat, M. S. Kulkarni, M. Tyagi, P. Ratna, D. R. Mishra, S. G. Singh, B. Tiwari, A. Soni, S. C. Gadkari, and S. K. Gupta, "TL and OSL studies on lithium borate single crystals doped with Cu and Ag," *Journal of Luminescence*, vol. 132, no. 8, pp. 1969 – 1975, 2012.

[13] A. Ozdemir, N. Can, and K. K. Z. Yegingil, "Optically stimulated luminescence (OSL) dosimetric properties of $Li_2B_4O_7$:Ag,Gd and its relationship with thermoluminescence (TL) glow-curves," *Journal of Alloys and Compounds*, vol. 751, pp. 159 – 169, 2018.

[14] E. G. Yukihara, B. A. Doull, T. Gustafson, L. C. Oliveira, K. Kurt, and E. D. Milliken, "Optically stimulated luminescence of MgB_4O_7:Ce,Li for gamma and neutron dosimetry," *Journal of Luminescence*, vol. 183, pp. 525 – 532, 2017.

[15] L. F. Souza, A. M. B. Silva, P. L. Antonio, L. V. E. Caldas, S. O. Souza, F. d'Errico, and D. N. Souza, "Dosimetric properties of MgB_4O_7:Dy,Li and MgB_4O_7:Ce,Li for optically stimulated luminescence applications," *Radiation Measurements*, vol. 106, pp. 196 – 199, 2017.

[16] J. V. B. Valenca, A. C. A. Silva, N. O. Dantas, L. V. E. Caldas, F. d'Errico, and S. O. Souza, "Optically stimulated luminescence of the [20% Li_2CO_3 + x% K_2CO_3 +(80 - x)% B_2O_3] glass system," *Journal of Luminescence*, vol. 200, pp. 248 – 253, 2018.

[17] V. Hegde, N. Chauhan, V. Kumar, C. S. D. Viswanath, K. K. Mahato, and S. D. Kamath, "Effects of high dose gamma irradiation on the optical properties of Eu^{3+} doped zinc sodium bismuth borate glasses for red LEDs," *Journal of Luminescence*, vol. 207, pp. 288 – 300, 2019.

[18] R. Hemam, L. R. Singh, A. I. Prasad, P. Gogoi, M. Kumar, M. P. Chougaonkar, S. D. Singh, and R. N. Sharan, "Critical view on TL/OSL properties of $Li_2B_4O_7$ nanoparticles doped withăCu, Ag and co-doping Cu, Ag: Dose response study," *Radiation Measurements*, vol. 95, pp. 44 – 54, 2016.

[19] R. Hemam, L. R. Singh, S. D. Singh, and R. N. Sharan, "Preparation of CaB_4O_7 nanoparticles doped with different concentrations of Tb^{3+}: Photoluminescence and thermoluminescence/optically stimulated luminescence study," *Journal of Luminescence*, vol. 197, pp. 399 – 405, 2018.

[20] L. Zhao, D. Wang, C. Chen, and Y. Wang, "Synthesis and photoluminescence properties of novel CaB_6O_{10}:RE^{3+} (RE=Ce, Tb, Dy, Eu) phosphors under ultraviolet excitation," *Materials Research Bulletin*, vol. 70, pp. 817 – 821, 2015.

[21] K. Lemański, M. Stefański, D. Stefańska, and P. J. Dereń, "Luminescent properties of Eu^{3+} ions in CaB_6O_{10} polycrystals," *Journal of Luminescence*, vol. 159, pp. 219 – 222, 2015.

[22] L. C. Oliveira and O. Baffa, "A new luminescent material based on CaB_6O_{10}:Pb to detect radiation," *Journal of Luminescence*, vol. 181, pp. 171 – 178, 2017.

[23] L. C. Oliveira and O. Baffa, "Optically and thermally stimulated luminescence of CaB_6O_{10}:Ce,LiCl: Basic properties," *Journal of Luminescence*, vol. 188, pp. 180 – 187, 2017.

[24] P. Dorenbos, "Lanthanide charge transfer energies and related luminescence, charge carrier trapping, and redox phenomena," *Journal of Alloys and Compounds*, vol. 488, no. 2, pp. 568 – 573, 2009.

[25] P. Dorenbos and A. J. J. Bos, "Lanthanide level location and related thermoluminescence phenomena," *Radiation Measurements*, vol. 43, no. 2, pp. 139 – 145, 2008.

[26] V. Orante-Barrón, L. C. Oliveira, J. B. Kelly, E. D. Milliken, G. Denis, L. G. Jacobsohn, J. Puckette, and E. G. Yukihara, "Luminescence properties of MgO produced by solution combustion synthesis and doped with lanthanides and Li," *Journal of Luminescence*, vol. 131, pp. 1058 – 1065, 05 2011.

[27] E. G. Yukihara, E. D. Milliken, L. C. Oliveira, V. R. Orante-Barrón, L. G. Jacobsohn, and M. W. Blair, "Systematic development of new thermoluminescence and optically stimulated luminescence materials," *Journal of Luminescence*, vol. 133, pp. 203 – 210, 2013.

[28] L. C. Oliveira, O. Baffa, and E. G. Yukihara, "MgO:Li,Ce,Sm as a high-sensitivity material for Optically Stimulated Luminescence dosimetry," *Scientific Reports*, vol. 6, no. 24348, 2016.

[29] B. E. Kananen, B. E. Kananen, E. S. Maniego, E. M. Golden, N. C. Giles, J. W. McClory, V. T. Adamiv, Y. V. Burak, and L. E. Halliburton, "Optically stimulated luminescence (OSL) from Ag-doped $Li_2B_4O_7$ crystals," *Journal of Luminescence*, vol. 177, pp. 190 – 196, 2016.

[30] G. D. Patra, S. G. Singh, B. Tiwari, A. K. Singh, D. G. Desai, M. Tyagi, S. Sen, and S. C. Gadkari, "Optically stimulated luminescence in Ag doped $Li_2B_4O_7$ single crystal and its sensitivity to neutron detection and dosimetry in OSL mode," *Radiation Measurements*, vol. 88, pp. 14 – 19, 2016.

[31] A. Ozdemir, V. Altunal, V. Guckan, N. Can, K. Kurt, I. Yegingil, and Z. Yegingil, "Characterization and some fundamental features of Optically Stimulated Luminescence measurements of silver activated lithium tetraborate," *Journal of Luminescence*, vol. 202, pp. 136 – 146, 2018.

[32] E. Pekpak, A. Yilmaz, and G. Ozbayoglu, "The effect of synthesis and doping procedures on thermoluminescent response of lithium tetraborate," *Journal of Alloys and Compounds*, vol. 509, no. 5, pp. 2466 – 2472, 2011.

[33] R. R. Patil, R. Barve, S. V. Moharil, M. S. Kulkarni, and B. C. Bhatt, "Development of Ag doped crystalline SiO_2 for possible applications in real-time in-vivo OSL dosimetry," *Radiation Measurements*, vol. 71, pp. 208 – 211, 2014.

[34] W. Kraus and G. Nolze, "*POWDER CELL* – a program for the representation and manipulation of crystal structures and calculation of the resulting X-ray powder patterns," *Journal of Applied Crystallography*, vol. 29, no. 3, pp. 301–303, 1996.

[35] X. Chen, M. Li, X. Chang, H. Zang, and W. Xiao, "Synthesis and crystal structure of a new calcium borate, CaB_6O_{10}," *Journal of Alloys and Compounds*, vol. 464, no. 1, pp. 332 – 336, 2008.

[36] L. V. S. França, L. C. Oliveira, and O. Baffa, "Development of a thermoluminescence and radioluminescence integrated spectrometer," *Measurement*, vol. 134, pp. 492 – 499, 2019.

[37] G. Blasse and B. C. Grabmaier, *Luminescent Materials*. Springer, 1994.

[38] A. Meijerink, M. M. E. van Heek, and G. Blasse, "Luminescence of Ag^+ in crystalline and glassy SrB_4O_7," *Journal of Physics and Chemistry of Solids*, vol. 54, no. 8, pp. 901 – 906, 1993.

[39] T. Hayakawa, S. T. Selvan, and M. Nogami, "Field enhancement effect of small Ag particles on the fluorescence from Eu^{3+}-doped SiO_2 glass," *Applied Physics Letters*, vol. 74, no. 11, pp. 1513–1515, 1999.

[40] L. P. Naranjo, C. B. de Araujo, O. L. Malta, P. A. S. Cruz, and L. R. P. Kassab, "Enhancement of Pr^{3+} luminescence in $PbOGeO_2$ glasses containing silver nanoparticles," *Applied Physics Letters*, vol. 87, no. 24, p. 241914, 2005.

[41] M. Eichelbaum and K. Rademann, "Plasmonic enhancement or energy transfer? On the luminescence of gold-, silver-, and lanthanide-doped silicate glasses and its potential for light-emitting devices," *Advanced Functional Materials*, vol. 19, no. 13, pp. 2045–2052.

[42] W. T. Carnall, P. R. Fields, and K. Rajnak, "Electronic Energy Levels of the Trivalent Lanthanide Aquo Ions. II. Gd^{3+}," *The Journal of Chemical Physics*, vol. 49, no. 10, pp. 4443–4446, 1968.

[43] J. A. Jimenez, "Enhanced UV emission of Gd^{3+} in glass by Ag^{+} co-doping," *Materials Letters*, vol. 159, pp. 193 – 196, 2015.

[44] R. D. Shannon, "Revised effective ionic radii and systematic studies of interatomic distances in halides and chalcogenides," *Acta Crystallographica Section A*, vol. 32, pp. 751–767, Sep 1976.

[45] E. D. Milliken, L. C. Oliveira, G. Denis, and E. G. Yukihara, "Testing a model-guided approach to the development of new thermoluminescent materials using YAG:Ln produced by solution combustion synthesis," *Journal of Luminescence*, vol. 132, no. 9, pp. 2495 – 2504, 2012.

[46] H. Luo and P. Dorenbos, "The dual role of Cr^{3+} in trapping holes and electrons in lanthanide co-doped $GdAlO_3$ and $LaAlO_3$," *Journal of Materials Chemistry C*, vol. 6, pp. 4977–4984, 2018.

[47] H. Guo, Y. Wang, W. Chen, W. Zeng, S. Han, G. Li, and Y. Li, "Controlling and revealing the trap distributions of $Ca_6BaP_4O_{17}$:Eu^{2+}, R^{3+} (R = Dy, Tb, Ce, Gd, Nd) by codoping different trivalent lanthanides," *Journal of Materials Chemistry C*, vol. 3, pp. 11212–11218, 2015.

[48] P. Dorenbos, "f → d transition energies of divalent lanthanides in inorganic compounds," *Journal of Physics: Condensed Matter*, vol. 15, no. 3, pp. 575–594, 2003.

[49] P. Dorenbos, "Systematic behaviour in trivalent lanthanide charge transfer energies," *Journal of Physics: Condensed Matter*, vol. 15, no. 49, pp. 8417–8434, 2003.

[50] P. Dorenbos, "Charge transfer bands in optical materials and related defect level location," *Optical Materials*, vol. 69, pp. 8 – 22, 2017.

[51] M. W. Swinney, J. W. McClory, J. C. Petrosky, S. Yang, A. T. Brant, V. T. Adamiv, Y. V. Burak, P. A. Dowben, and L. E. Halliburton, "Identification of electron and hole traps in lithium tetraborate ($Li_2B_4O_7$) crystals: Oxygen vacancies and lithium vacancies," *Journal of Applied Physics*, vol. 107, no. 11, p. 113715, 2010.

[52] E. Pekpak, A. Yilmaz, and G. Ozbayoglu, "An Overview on Preparation and TL Characterization of Lithium Borates for Dosimetric Use," *The Open Mineral Processing Journal*, vol. 3, pp. 14–24, 05 2010.

[53] O. Annalakshmi, M. T. Jose, U. Madhusoodanan, J. Sridevi, B. Venkatraman, G. Amarendra, and A. B. Mandal, "Thermoluminescence mechanism in rare-earth-doped magnesium tetra borate phosphors," *Radiation Effects and Defects in Solids*, vol. 169, no. 7, pp. 636–645, 2014.

[54] A. T. Brant, B. E. Kananan, M. K. Murari, J. W. McClory, J. C. Petrosky, V. T. Adamiv, Y. Burak, P. A. Dowben, and L. E. Halliburton, "Electron and hole traps in Ag-doped lithium tetraborate ($Li_2B_4O_7$) crystals," *Journal of Applied Physics*, vol. 110, no. 9, p. 093719, 2011.

[55] S. Watanabe, E. F. Chinaglia, M. L. F. Nascimento, and M. Matsuoka, "Thermoluminescence Mechanism In $Li_2B_4O_7$:Cu," *Radiation Protection Dosimetry*, vol. 65, no. 1-4, pp. 79–82, 1996.

[56] A. V. Porotnikov, I. N. Ogorodnikov, S. V. Kudyakov, A. V. Kruzhalov, and S. L. Votyakov, "EPR of hole centers in nonlinear $LiBO_3$ crystals," *Physics of the Solid State*, vol. 39, pp. 1224 – 1227, 1997.

[57] I. N. Ogorodnikov, L. I. Isaenko, A. V. Kruzhalov, and A. V. Porotnikov, "Thermally stimulated luminescence and lattice defects in crystals of alkali metal borate LiB_3O_5 (LBO)," *Radiation Measurements*, vol. 33, no. 5, pp. 577 – 581, 2001.

[58] M. Kerikmae, M. Danilkin, A. Lust, V. Nagirnyi, L. Pung, A. Ratas, I. Romet, and V. Seeman, "Hole traps and thermoluminescence in $Li_2B_4O_7$:Be," *Radiation Measurements*, vol. 56, pp. 147 – 149, 2013.

[59] B. V. Padlyak, A. Drzewiecki, T. B. Padlyak, V. T. Adamiv, and I. M. Teslyuk, "Resonant excited UV luminescence of the Gd^{3+} centres in borate glasses, co-doped with Gd and Ag," *Optical Materials*, vol. 79, pp. 302 – 309, 2018.

[60] E. J. Guidelli, O. Baffa, and D. R. Clarke, "Enhanced UV emission from silver/ZnO and gold/ZnO core-shell nanoparticles: Photoluminescence, radioluminescence, and optically stimulated luminescence," *Scientific Reports*, vol. 5, no. 14004, 2015.

[61] E. J. Guidelli, A. P. Ramos, and O. Baffa, "Optically stimulated luminescence under plasmon resonance conditions enhances X-ray detection," *Plasmonics*, vol. 9, p. 10491056, 2014.

Paper II

III. Swiss-cheese like Structure in a Borate-Based Compound Forms a High Sensitive X-ray, Gamma-ray and Neutron Luminescence Detector

Leonardo V. S. França[a,], Elisabeth Müller[b], Eduardo G. Yukihara[c], Oswaldo Baffa[a]*

[a] Departamento de Física, FFCLRP, Universidade de São Paulo, Av. Bandeirantes, 3900, 14040-900, Ribeirão Preto, Brazil.

[b]Electron Microscopy Facility, Paul Scherrer Institute, Forschungsstrasse 111, 5232, Villigen PSI, Switzerland.

[c]Department of Radiation Safety and Security, Paul Scherrer Institute, Forschungsstrasse 111, 5232, Villigen PSI, Switzerland.

* Email: leofranca@usp.br

Abstract

Space, radiotherapy, X-ray imaging/screening, nuclear reactors, large research facilities (linear accelerators and synchrotron radiation facilities), nuclear accidents. All these examples are associated to the need of monitoring high-energy radiation. Herein, we report the luminescent and dosimetric properties of a radiation detector based on CaB_6O_{10}: Tb^{3+}, Ag^{+} phosphors obtained through the solid-state reaction method. The operation principle here is the optically stimulated luminescence (OSL), which is the luminescence of a previous irradiated material after optical stimulation. The phosphor, whose grains formed a Swiss-cheese like structure, presented strong UV-OSL under blue stimulation (minimum

detectable dose of 2.3 μGy), with dose linearity in the whole dose range analysed and no signs of saturation (up to 20 Gy). The thermoluminescence (TL) of the phosphor featured mainly a peak at 275 °C, whose trapping center showed to be associated to the main OSL component. Furthermore, TL and OSL processes exhibited different recombination pathways, i.e., one that leads to TL (Tb^{3+} emission) and another one that leads to OSL (Ag^{+}-transferred energy emission). In addition, OSL was observed after neutron irradiation, with neutron-gamma ratio 1.3 times superior than that of neutron-sensitive Luxel-N detectors (Al_2O_3 mixed with $^{6}Li_2CO_3$). Also, the phosphor exhibited a fading of 10% after 5.3 h and 32% after 10 days, reaching stability. Both OSL and TL showed to be reproducible and repeatable, confirming the correlations between the luminescent processes and validating the synthesis protocol used. Besides of reporting outstanding features of a radiation detector with stimulation-dependent tunable emission, this work paves the way for the development of new charge storage phosphors.

Introduction

High-energy radiation detection has revealed to be a ubiquitous necessity owing to applications, such as X-ray imaging, radiotherapy, medical, personal, space and accidental dosimetries and even food preservation [1–7]. Herein, the luminescence dosimetry, i.e., the assessment of radiation dose by correlation with the luminescence intensity of a phosphor, seizes the opportunity. Specifically the Optically Stimulated Luminescence (OSL), also known as Photostimulated Luminescence, has emerged as a reliable and non-destructive tool for dose evaluation [8, 9], which has also shown to be useful in anticounterfeiting, optical data storage and bioimaging applications [10–15]. The OSL is the light emission of a previous irradiated material when optically stimulated with wavelength-specific light source. Here, the luminescence is usually of anti-stokes type, i.e., its wavelength emission is shorter than excitation wavelength. It is the previous irradiation and the forbidden energy levels within band-gap promoted by defects in the crystal structure that allow for this anti-stokes emission.

Similar in nature to the well known persistent luminescence, the OSL requires two types of defects in compounds, i.e., one that generates trapping centers and another one that generates recombination (luminescence) centers, the latter being more energetic

stable. In practice, the difference of OSL and persistent luminescence lies in the stimulation source: whereas the ambient thermal energy releases the trapped charges in the persistent luminescence, wavelength-specific light releases the trapped charges in OSL. For both phenomena, thermoluminescence (TL) can be used to probe the energy depth of the corresponding trapping center.

By exploiting the systematic energy levels of divalent and trivalent lanthanides within the band-gap, predicted by Dorenbos [16–18], several inorganic compounds have been engineered for charge-carrier storage dependent applications [19–21], including luminescence dosimetry [22,23]. However, in the case of OSL dosimetry applications, most of the new proposed phosphors have been obtained through a trial-and-error approach, and they are either part of a preliminary study, lacking more in-depth considerations or have presented one or more undesirable features. For instance, Mn^{2+}-doped $ZnGa_2O_4$ phosphor showed full fading after two weeks, with no report of its dose-response [24]; β-$Na(Gd,Lu)F_4:Tb^{3+}$ nanophosphors showed a dominating TL peak at 65 °C, which is very unstable for dosimetric purposes [25]; Nanocrystalline $BaLiF_3:Sm^{3+}$ phosphors showed a saturating exponential response for doses higher than 1 Gy [26]; Nanocubes of Cu-doped LiF presented sensitivity adequate for high-doses (radiotherapeutic window), but not suitable low-doses as needed in personal dosimetry [27]. Although there are many other reports on the development of new OSL detectors showing other undesirable features, to present a systematic review on these materials is out of scope of the present work. To date, only two phosphors are commercially available for OSL dosimetry applications, namely, Al_2O_3:C (Landauer) and BeO (Dosimetrics), which demonstrate the demand for new phosphors with suitable properties.

In view of this, we have recently reported a borate-based compound, i.e., CaB_6O_{10}: Gd^{3+}, Ag^+ (CaB_6O_{10} = CBO hereinafter), which presented a resonant effect of Gd^{3+} and Ag^+ conjugated ions on boosting its OSL response under blue stimulation [28]. This phosphor exhibited high sensitivity to X-rays, with a minimum detectable dose of ∼40 μGy. However, to the best of our knowledge, Gd^{3+} energy level is not predictable using the zig-zag curves of the Dorenbos model, since the trivalent $4f$ ground state lies well below the top of the valence band. That is undesirable since it hinders the trap depth design, and therefore, the optimization potentialities of the phosphor. In addition, one of the advantages of CBO compared to the gold-standard Al_2O_3:C is the high amount of boron contents

in its structure, which would in principle improve its sensitivity to neutrons. However, the OSL of that compound was not evaluated after neutron irradiation.

A trivalent lanthanide that has presented a systematic role as hole trapping center in a variety of compounds is the Tb^{3+}. That is due to the fact that Tb^{3+} ground state energy level usually lies above the top of the valence band, which provides it the ability to work as either a hole trapping center or a hole recombination center [29–31]. On the other hand, Ag^{+} is known to act as either an electron trapping center or a hole trapping center, depending on the type of the defect in the host (interstitial or substitutional) []. Considering the introduction in CBO host, the similarities of the seven-coordinated ionic radii of both Tb^{3+} and Ag^{+} (0.98 Å and 1.22 Å, respectively) compared to that of Ca^{2+} (1.06 Å) for the same coordination number [32] suggest an aliovalent substitution in CBO. As a result, Tb^{3+} introduction would lead to an inward crystal dislocation, whereas Ag^{+} substitution would lead to an outward crystal dislocation. Although the interplanar distances in CBO may accommodate interstitial Ag^{+}, Tb^{3+} interstitial incorporation is not expected due to its high charge. In addition to the extrinsic defects, the CBO host is likely to possess intrinsic defects, as suggested by the TL and OSL of the compound with different single dopants, such as Pb, Ce, Gd or Ag [28, 33, 34]. This is in line with typical defects in borates such as oxygen vacancies [35, 36] and boron-oxygen-hole-center, i.e., a defect created by an oxygen that bridges two borate groups (BO_3 or BO_4) [37, 38].

In this work we have reported structural, luminescent and dosimetric investigations of the compound CaB_6O_{10}: Tb^{3+}, Ag^{+} obtained through a facile and low-cost synthesis method. This compound was recently reported in a systematic evaluation of OSL lifetimes of lanthanides and silver codoped CBO [39]. Besides of the nature of luminescence emission, i.e., lifetime and OSL emission spectrum, no other investigation was reported. In addition, no clear explanation was given for the redshift of the OSL emission of the Tb,Ag- codoped compound compared to that of Ag- doped compound. Neutron irradiations were particularly performed to test the OSL sensitivity of the compound to neutrons, which is one of the major drawbacks of OSL dosimeters based on Al_2O_3:C. This work reports not only outstanding features of the phosphor, such as wide dose range with no signs of saturation, minimum detectable dose of 2.3 μGy and sensitivity to neutrons, but also paves the way for exploiting the luminescent properties and charge storage capabilities of other lanthanide and silver codoped compounds.

Results and Discussion

Analyses of both transmission electron microscopy (TEM) and scanning TEM (STEM) images, as well as selected area electron difraction (SAED) and powder diffraction patterns were carried out in order to evaluate the crystallinity and structural properties of CBO: Tb^{3+}, Ag^{+} phosphors. **Figure 1a** depicts an example of small-sized grains of CBO (∼75 nm grain size), which appear as composing a Swiss-cheese like structure and the holes representing particles with regular arrangement in a low magnification. If the STEM mode is considered, both annular dark field (ADF) and bright field (BF) images highlight the contours of the grains (Figure S1, Supporting Information).

When a higher magnification is considered, as seen in the high-resolution TEM (HRTEM) image (**Figure 1b**), the specimen exhibited a high ordered structure in all directions, which makes evident the high cristallinity obtained through a facile synthesis method. The white spots shown in the inset represent the Ca ions as illustrated in the schematic of CBO phase (**Figure 1c**). Other regions of the specimen also presented regularity in their structure, sometimes seen as crystallographic planes without atomic contrast (Figure S2, Supporting Information). Identification of the other elements (boron and oxygen) may be achieved by means of high-resolution STEM in ADF and BF modes, which allows atomic discrimination via Z-dependent constrast. In ADF mode, high Z elements are depicted as bright spots as shown in **Figure 1d**. These ∼2 nm size spots are likely to be related to Ag nanoparticles hopping near crystal surface.

Figure 1e shows a typical SAED pattern of the especimen. The presence of dots instead of rings in the SAED pattern of the sample suggest that the compound is comprised mainly of single crystals. Some interplanar distances, whose miller indices are labelled in the SAED pattern, are in a good agreement with expected values for the CBO. In addition, the Rietveld refinement of powder diffration data (**Figure 1f**), represented by the difference between experimental data and expected values, confirmed the pure monoclinic phase as that of CBO (ICSD 161320) [42], with no clear influence of dopants.

The influence of dopants on the host was investigated by steady-state photoluminescence emission (PL) and photoluminescence excitation (PLE) spectra (**Figure 1g**). When excited at 240 nm, two main overlapped emission bands at 296 nm and 316 nm take place, the former ascribed to $^1D_2 \rightarrow {}^1S_0$ transitions of Ag^{+} ions and the latter related

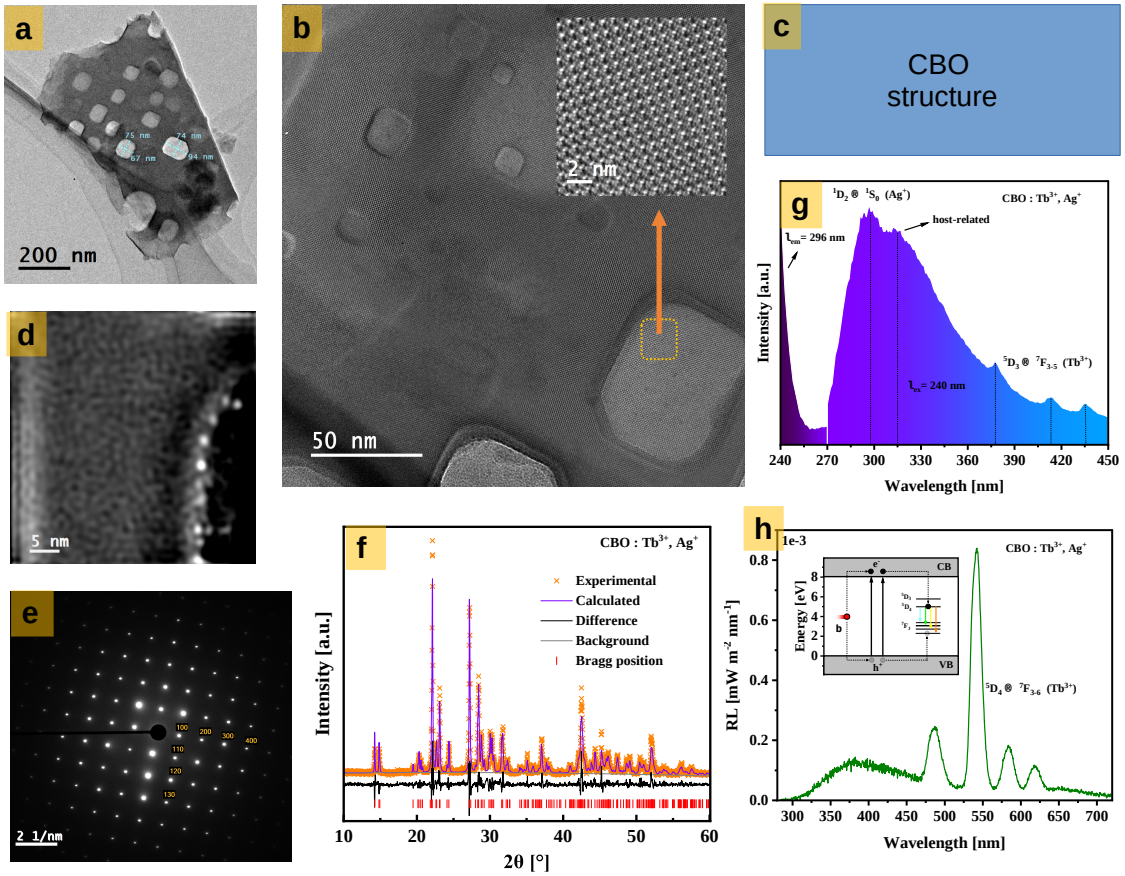

Figure 1: Structural and basic luminescent properties of CBO: Tb^{3+}, Ag^{+}. a) TEM image showing a Swiss-cheese like structure of particles (25,000 x). b) HRTEM image of a particle as exemplified in Fig. 1a (200,000 x). The zoomed in region in the inset shows the periodic arrangement as expected for a crystal. c) Schematic of CBO structure. d) STEM image in ADF-mode showing the presence of agglomerated nanoparticles on crystal surface (5,000,000 x). e) Example of a SAED pattern of sample. f) Rietveld refinement of powder diffraction pattern against CBO single phase. g) Steady-state PLE and PL spectra. h) RL under beta irradiation. The inset illustrates the excitation and recombination pathways leading to the prompt emission during exposure to beta irradiation.

to a host-related transition. Other three emissions centered at 378 nm, 413 nm and 435 nm, which originate from $^5D_3 \rightarrow {}^7F_{3-5}$ transitions of Tb^{3+} ions, are also present. Whereas Ag^{+} emission and Tb^{3+} emissions were detected in Ag- single doped and Tb- single doped compounds, respectively, the 316 nm emission was observed only in the Tb- doped compound (Figure S3, Supporting Information). This suggests that that emission stems from an interaction between the Tb^{3+} ions and the host. That is also suggested by an atypical excitation band at 278 nm of CBO: Tb^{3+} when probing the 316 nm emission (Figure S3, Supporting Information). The typical Tb^{3+} emissions between 450 nm and 650 nm

could not be observed since the window detection had to be set to avoid second harmonic components, even though the characteristic excitation bands from the lower ground level $^7F_6$ of Tb^{3+} promoted its typical 541 nm emission (Figure S4, Supporting Information). When the emission was set at 296 nm, an excitation band peaking towards <240 nm was detected (Figure 1g). Although partially detected due to the lack of corrections for the system responsivity in the region below 240 nm, that excitation band may be the same of Ag^+ ions in SrB_4O_7:Ag^+, which ranged from 200 nm to 260 nm [43].

Under beta irradiation, CBO: Tb^{3+}, Ag^+ exhibited radioluminescence (RL), with well defined emission lines due to $^5D_4 \rightarrow {}^7F_{3-6}$ transitions of Tb^{3+} (**Figure 1h**). The irradiation promotes the excitation of charges, which follows activation of luminescence centers by charge trapping and then emission of light after charge recombination (refer to the inset of Figure 1h). Hence, Tb^{3+} centers are potential candidates to act as recombination centers in the OSL and TL processes of CBO: Tb^{3+}, Ag^+ phosphors. The broad emission band which covered the whole detection window used, i.e., from 300 nm to 720 nm, originated from the host [28] had a minor role. Therefore the host-related radiative recombinations were not effective as those enabled by Tb- doping.

The OSL of CBO: Tb^{3+}, Ag^+ was evaluated using three different combinations of stimulation wavelengths and detection windows, i.e., IR stimulation (850 nm) with detection in the visible (320 nm to 670 nm), IR stimulation with detection in the UV (260 nm to 390 nm) and blue stimulation (470 nm) with detection in the UV. Refer to Figure S5 (Supporting Information) for a comparison of the detection windows used. As shown in **Figure 2a**, the compound showed a strong BSL with initial OSL intensity near the Risø cut-off limit for the PMT ($5x10^6$ counts - units equivalent to the arbitrary units on y-axis). BSL showed to be more efficient than IR stimulated luminescence (IRSL), which means that IR does not provide resonant energy to stimulate the optically active UV-emitting centers. Furthermore, IRSL was more efficient with detection in the visible than in the UV, possibly with the visible-emitting Tb^{3+} luminescence centers taking part in the process (Figure 1h). The y-offset background in the first and last 10 s of the IRSL in the visible indicates that the compound presented some persistent luminescence (spontaneous emission after irradiation), even though not present in UV. This suggests that the compound possesses some shallow trapping centers, which is confirmed by the TL curves further presented.

As recently reported, CBO: Tb^{3+}, Ag^+ phosphor presents a broad UV emission

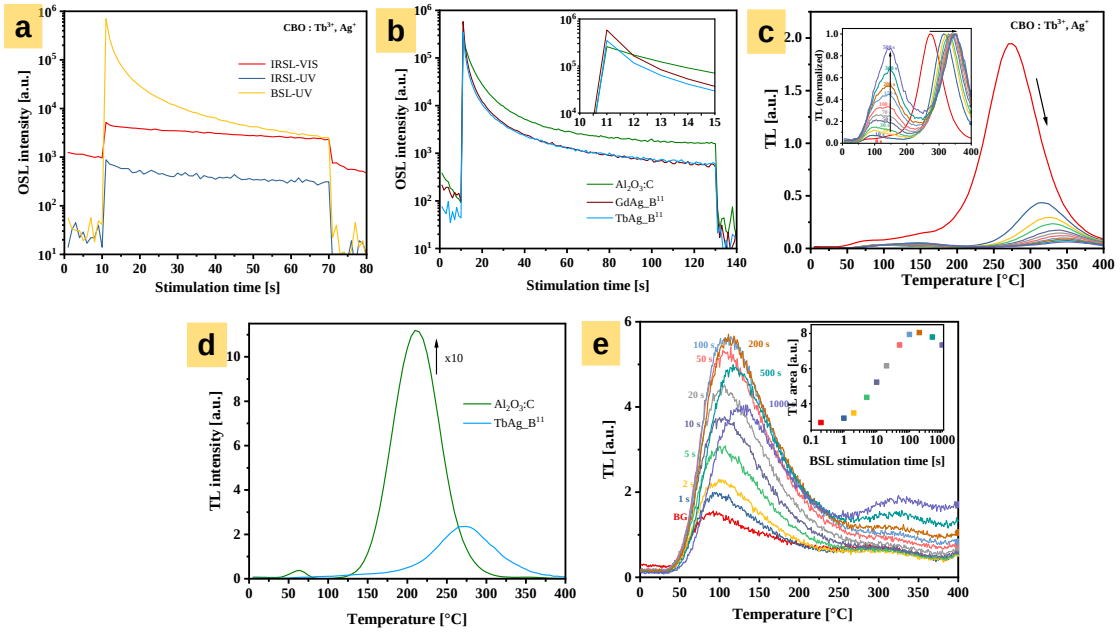

Figure 2: Typical OSL/TL curves and influence of blue stimulation on TL of CBO: Tb^{3+}, Ag^{+}. a) OSL comparison at different stimulation and detection window combinations. b) BSL sensitivity of CBO: Tb^{3+}, Ag^{+} against that of a standard phosphor (Al_2O_3:C thin powder (grains size < 38 µm, Landauer Inc.). The inset highlights the comparison of the initial OSL intensities (dose = 37 mGy). c) Effect of increasing blue stimulation times on TL (heating rate = 5 °C s^{-1}). The inset depicts the TL curves normalized by the maximum TL intensity. d) TL comparison against that of Al_2O_3:C (heating rate = 5 °C s^{-1}; dose = 37 mGy). The signal from Al_2O_3:C sample was reduced 10 x for better comparison. e) Blue-excited TL performed at increasing optical stimulation times (no previous irradiation; heating rate = 5 °C s^{-1}). The curve assigned as "BG" refers to the background. Inset: TL area integrated from 50 °C to 400 °C.

from 270 nm to 400 nm peaking at 330 nm under 430 nm stimulation, with a luminescence lifetime of 43 µs, owing to Ag^{+} luminescence centers [39]. That emission is an excellent match for the Hoya U340 filter, since it presents maximum transmission at 330 nm (Figure S5, Supporting Information). Comparing the phosphor BSL with that of a standard phosphor used in luminescence dosimetry, i.e., Al_2O_3:C, **Figure 2b** shows that they presented comparable sensitivities, although the standard phosphor features a more stable component. If blue stimulation is replaced with green stimulation and detection window enlarged towards blue, OSL of CBO: Tb^{3+}, Ag^{+} can be further optimized (enhancement of ~1.4 times comparing the OSL area - Figure S6, Supporting Information). It is worth mentioning that the Al_2O_3:C detectors can be found in different forms (disc pellets, thin films and powder, for instance), but the used here for comparison (powder) is

the most sensitive detector form and then allows for a more reliable comparison.

As shown in **Figure 2c**, TL of CBO: Tb^{3+}, Ag^{+} is composed of a main broad peak at 275 °C and minor components extending from 40 °C to 180 °C and peaks above 300 °C. In addition, the TL main peak and the lower temperature peaks showed to be strongly affected by blue light stimulation, although the higher temperature TL peaks showed harder depletion, as represented by the shift of the TL higher peaks (inset). Also, the TL curves normalized by the main TL peak intensity showed a relative increase of the lower temperature TL peaks (inset). One may claim that that is likely due to a phototransfer from deeper traps, but another possible cause is further presented. Conversely, it was observed that IR stimulation did not present significant influence on TL main peak or higher temperature peaks (Figure S7, Supporting Information), in compliance with the relatively weak IRSL (Figure 2a). These results suggest that the optical cross section of both TL and OSL recombination centers is relatively high for blue stimulation and relatively weak for IR stimulation. Regarding the TL emission, all TL curves reported here was collected in the visible window and the TL in the UV was at least 70 times less sensitive (Figure S8, Supporting Information). Therefore, the OSL and TL of CBO: Tb^{3+}, Ag^{+} phosphor present different recombination pathways, one that leads to UV emission (BSL) and another one that promotes the visible emission (TL). Blue stimulation may also lead to typical green emission of Tb^{3+} but that can not be verified since the anti-stokes arrangement of the OSL acquisition system restricts detection to higher energy photons.

Contrarily to OSL, the TL of the phosphor showed to be at least 50 times less sensitive than that of Al_2O_3:C (**Figure 2d**). At least three may be the possible causes for the discrepancy, i.e., OSL recombination more efficient than TL recombination, OSL enhancement by some intermediate process and thermal quenching. It was already pointed out that the BSL of CBO: Tb^{3+}, Ag^{+} stems from radiative recombination of UV-emitting Ag^{+} centers and its TL as related to some visible emission not yet identified. Since they correspond to different recombination pathways, there is no reason to assume that they would present comparable efficiencies (ratio of radiative recombination processes and non-radiative recombination processes). Furthermore, it is not clear if an intermediate process such as energy transfer triggered by optical stimulation takes place, which would enhance the OSL of the phosphor. At last, thermal quenching at temperatures corresponding to the TL peaks can significantly compromise the TL sensitivity. Other analyses and fur-

ther discussions will be provided to shed some light on this, even though the verification of the first aforementioned cause is out of scope of this work. It is also noteworthy that both reproducibility and repeatability tests for OSL/TL responses were performed: neither significant variations on the sensitivity of grains (different aliquots used) nor systematic changes under the same experimental conditions (same aliquot used) were observed (Figure S9, Supporting Information). Therefore, both OSL/TL shape and sensitivity features can be considered as consistently intrinsic to the phosphor under investigation.

The TL of CBO: Tb^{3+}, Ag^{+} was also measured after different optical stimulation times without prior irradiation. In this experiment the TL was performed after blue stimulation, cyclic repeated with increasing optical stimulation times. As depicted in **Figure 2e**, there is a clear increase in TL intensity with optical stimulation times, referred to here as blue-excited TL. Whereas the TL peak at 95-125 °C saturated after 100 s of blue stimulation, the TL peaks above 300 °C did not reach saturation. Considering the TL area from 50 °C to 400 °C as function of the optical stimulation times (inset), there is a linear dependence from 2 s to 100 s, which suggests that the trapping centers are increasingly filled during optical stimulation and then released after thermal stimulation. Provided that the band-gap energy of CBO is on the order of 7.8 eV by comparison to similar compounds [44], the blue-excited TL can be originated from an exciton recombination, where excitation here would require less energy than excitation across the band-gap. That may account for the relative increase of the TL peaks between 50 °C and 250 °C in the blue-stimulated sample after beta irradiation, as shown in Figure 2c. By exploiting blue excitation, an optical dosimeter based on a $SrAl_2O_4$:Eu^{2+},Sm^{3+} phosphor has been recently proposed, where optical dose, i.e., energy delivered by blue excitation, can be correlated with its OSL [45].

In order to verify if there is a correlation of OSL trapping centers with TL trapping centers of the phosphor under investigation, thermal stability of the BSL of CBO: Tb^{3+}, Ag^{+} was analysed. This experiment was carried out by repeating pre-annealed OSL over increasing annealing temperatures from 50 °C to 400 °C in 10 °C steps (step-annealing). **Figure 3a** shows a comparison of the step-annealed OSL against a typical TL curve of the phosphor. As can be seen, the OSL decrease rate followed the TL increase with temperature and the match of the inflection points of both curves suggests that the main trapping center of CBO is associated to both BSL and TL main components. Furthermore, the

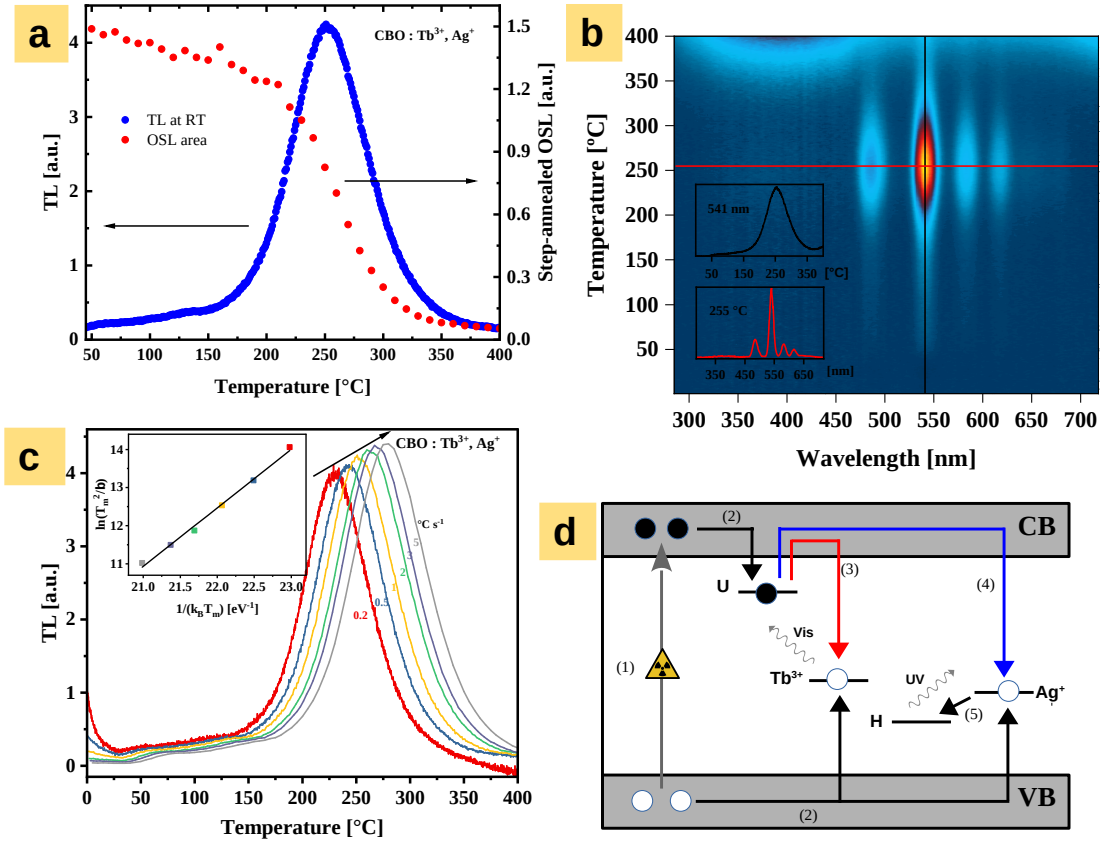

Figure 3: Mechanisms involving OSL and TL processes of CBO: Tb^{3+}, Ag^{+}. a) Step-annealed OSL against a typical TL curve (OSL area integrated over 120 s and dose = 37 mGy; TL heating rate = 1 °C s^{-1}). b) TL emission spectra depicted as a contour plot (heating rate = 0.5 °C s^{-1}; dose = 18.5 Gy). The insets show single plots of a TL curve with emission at 541 nm (top) and a TL emission with temperature at 255 °C (bottom). c) TL curves at increasing heating rates. The intensities were normalized by the corresponding heating rates. The inset shows the plot of $\ln(T_m^{\,2}/\beta)$ against $1/(k_B T)$ for determination of the trap depth corresponding to the main TL peak. d) Schematic diagrams of trapping and recombination mechanisms behind the TL and OSL processes: (1) represents the release of charges by a high-energy source, e.g., X-rays; (2) represents the trapping of charges; (3) represents the radiative recombination (Tb^{3+} emission) as a result of heating stimulation; (4) represents recombination as a result of blue stimulation and (5) represents an energy-transfer process leading to UV emission. Black and white circles represent electrons and holes, respectively.

systematic reduction of sensitivity as temperature is raised suggests that the TL suffers of thermal quenching. As a result, the TL sensitivity is compromised and thereby leads to a mismatch between OSL and TL sensitivities of the phosphor.

Although it is known that the TL main emission of CBO: Tb^{3+}, Ag^{+} lies in the visible region, it was not identified yet. **Figure 3b** shows the TL emission spectrum of the

phosphor plotted as a contour plot. The TL is characterized by the same emissions lines as seen through RL, i.e., Tb^{3+} emission associated to ${}^5D_4 \rightarrow {}^7F_{3-6}$ transitions, which are associated mainly to the TL peak centered at 255 °C. The shift of the main TL peak temperature compared to that shown in Figure 2c is due to the different heating rates used. In addition to Tb^{3+} emission lines, no other emission was observed, even though it is known that the phosphor exhibits a minor UV emission (Figure S8, Supporting Information) compared to the visible one. That emission may be too weak to be observed by the detection system used. The apparent emission from 300 nm to 500 nm at temperatures higher than 350 °C is due to the increased background of the EMCCD detector.

In order to evaluate the trap depth of the main TL peak with respect to the CBO band-gap energy, the heating-rate method was used, assuming that the TL of the phosphor is of first-order kinetics [46,47]. **Figure 3c** shows the TL curves normalized by the heating rate used. The TL temperature peaks ranged from 232 °C to 280 °C, as the heating rate increased from 0.2 °C s^{-1} to 5 °C s^{-1}. Considering the maximum TL intensities (T_m) and the heating rates (β) used, the plot of $\ln({T_m}^2/\beta)$ against $1/(k_B T)$ was performed (see inset) for determination of the trap depth (E). That can be estimated using the slope E/k_B of the linear fitting, where k_B is the Boltzmann constant (refer to the Experimental Section). The estimation of the trap depth and its escape frequency (s) were 1.53 eV and 3.1x10^{13} s^{-1}, respectively. This trap depth value is similar to that of Tb- singly doped CBO (1.51 eV, with $s = 7.0\text{x}10^{12}$ s^{-1}), suggesting that both compounds share a common trapping center (Figure S10, Supporting Information). Whereas Tb- singly doped CBO showed a decrease of the TL intensities with the heating rate (Figure S10), likely to be thermal-quenching-related, the Tb,Ag- codoped compound showed an increase (Figure 3c), which is possibly due to an anomalous inverse heating-rate effect as described by some reports [48–50].

Now it is important to draw a picture of how TL and OSL processes of CBO: Tb^{3+}, Ag^+ correlate with each other. Depending on the type of stimulation, radiative recombinations involving either Tb^{3+} emission centers (Figure 3b) or Ag^+ centers take place [39]. In the recent published work, we reported that Ag^+ is responsible for an asymmetric UV emission centered at 295 nm, associated to a 39 μs lifetime [39]. Although no clear explanation was given, that emission shifted to 332 nm and significantly broadened when Tb- codoping was present, in addition to a lifetime increase of 3.9 μs [39]. Furthermore, Tb- singly doped CBO exhibited a main component with a 4 μs lifetime. These results

suggest that an energy transfer process from Ag^+ centers to those responsible for the Tb-doped compound emission takes place. It was also shown that the nature of this broad emission is likely to be associated to intrinsic defects in the host (H), since the UV emission associated to $^5D_3 \rightarrow {}^7F_6$ transitions of Tb^{3+} was not verified neither by their emission lines nor by their typical lifetimes (415-970 μs) [51, 52]. The match of the host-related excitation band of the Tb- singly doped compound with Ag^+ emission also supports that interpretation (Figure S3, Supporting Information).

Prior to the radiative recombinations, both OSL and TL processes require trapping of charges. As already mentioned, both Tb- singly doped and Tb,Ag- codoped CBO exhibited a trapping center with a trap depth of 1.55 eV. In addition, Ag- singly doped CBO does not show significant radiative recombinations after heating stimulation [28]. Since Tb^{3+} acts as recombination (luminescence) centers (Figure 3b), it is likely that host-related unindentified centers act as trapping centers. Furthermore, trivalent Tb usually acts as hole trapping centers [30,53], which implies that their charge trapping counterparts in CBO act as electron trapping centers. It is known that a typical electron trapping center in borate compounds is the one originated from oxygen vacancies [54, 55] and likely to be present in CBO (ten oxygen atoms for each calcium atom). Therefore, we assume that unindentified centers (U), possibly oxygen vacancies in CBO act as electron trapping centers, which are responsible for the TL peak at 270 °C (Figure 2c). **Figure 3d** sums up the possible trapping and recombination pathways involving the OSL/TL of CBO: Tb^{3+}, Ag^+.

The dosimetric features in terms of the BSL of CBO: Tb^{3+}, Ag^+ phosphor were evaluated. **Figure 4a** shows the dose-response for two filter combinations, i.e., one that maximizes the range for high doses (neutral density - ND filter used) and another one restricted to lower doses. For both experiments, the maximum dose was set according to the detection limits of the system used. In the wider dose range, the phosphor showed a linear dose-response between 30 mGy and 20 Gy and did not reach saturation. Considering the lower dose range experiment, the dose-response was also linear and the estimated minimum detectable dose was 2.3 μGy. That is at least 170 times more sensitivity than that of a proposed neutron OSL dosimeter, i.e., MgB_4O_7:Ce,Li (minimum detectable dose = 0.4 mGy) [56].

In addition, the stability of OSL over storage time was measured for a period of 28 days. As depicted in **Figure 4b**, the OSL faded ~22% after the first day and ~32%

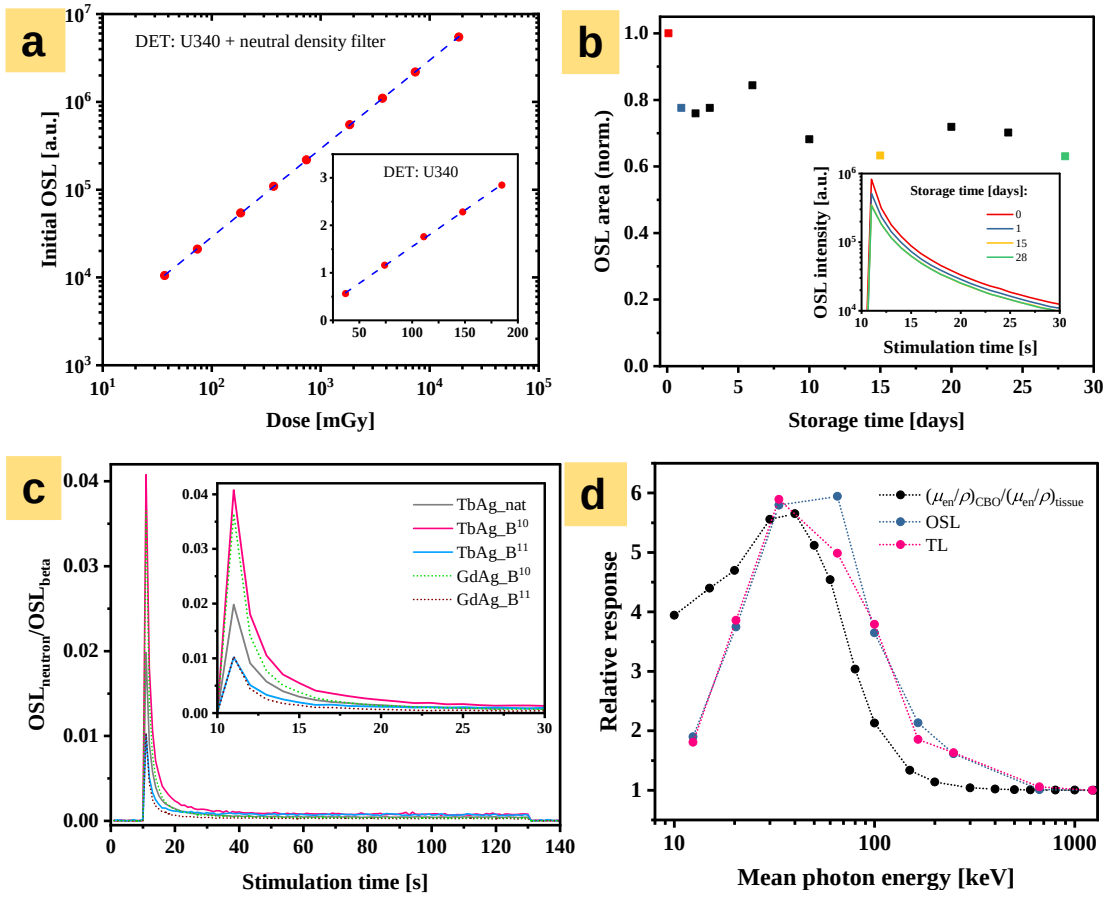

Figure 4: Dosimetric features in terms of the OSL of CBO: Tb^{3+}, Ag^{+}. a) Dependence of the OSL response on increasing doses optimized for high doses. The inset shows the dose response obtained with the detection system for lower doses (x- and y- units are the same as for higher doses). b) Stability of OSL signal over storage times (OSL area integrated over 120 s; dose = 37 mGy). The inset depicts typical OSL curves within the first 20 s of stimulation. c) Neutron induced OSL of CBO: Tb^{3+}, Ag^{+} for different isotopic boron compositions. The OSL response was normalized by a reference dose measurement - 37 mGy under beta irradiation. d) Dependence of OSL/TL response on photon energy (OSL area integrated over 120 s; TL area integrated from RT to 370 °C).

after ten days, following stability. It is worth mentioning that a pre-heating at 100 °C was applied between irradiation and OSL detection to ensure depletion of shallow trappping centers. That means that the shallow trapping centers associated to the TL peaks below 100 °C are not responsible for the fading. This thermal instability may be due to tunnelling recombination between an electron trapping center and Tb^{3+} excited state, as reported by Bos and Dobrowolska [48,57]. Considering a shorter range, the sample exhibited a fading of ∼10% after 5.3 h (Figure S11, Supporting Information). OSL fading of CBO: Tb^{3+},

Ag^+ needs to be taken into account for applications that require readout in a short storage time after irradiation.

Sensitivities of CBO: Tb^{3+}, Ag^+ phosphor to neutron irradiation were evaluated. To accomplish this, an ^{241}AmBe neutron source was used, and samples with natural boron composition as well as isotopically enriched ^{10}B and ^{11}B samples were used for comparison. **Figure 4c** shows that the samples exhibited OSL under neutron irradiation, which is more evident for the enriched ^{10}B sample, as expected. However, the signal of ^{11}B enriched sample is mostly originated from gamma radiation, as it is leaked from neutron source (neutron-gamma mixed field) and the sample with natural boron composition had an intermediate sensitivity. By taking the ratio of the neutron response of ^{10}B enriched sample to that of ^{11}B enriched sample and considering their gamma sensitivities, the neutron-gamma ratio of CBO sample was estimated as ~5.2, which is superior to that of neutron sensitive Luxel-N detectors (Al_2O_3:C mixed with $^6Li_2CO_3$ - neutron-gamma ratio ~4) [56]. The neutron induced TL of the samples followed a similar dependence on relative amounts of ^{10}B (Figure S12, Supporting Information).

Estimating the dependence of a phosphor response on different photon energies is of high importance in dosimetry, since the phosphor-based dosimeter must not compromise the energy estimation in the required applications. In view of this, the TL/OSL responses of CBO: Tb^{3+}, Ag^+ over a wide range of photon energies was evaluated. Also the ratio between mass-energy absorption coefficients of the phosphor and soft tissue (ICRU-44) was determined for comparison (See the Experimental Section for more details). **Figure 4d** depicts the OSL and TL responses normalized by dose and ^{60}Co reference measurement. Both OSL and TL showed a similar overresponse for photon energies below 300 keV, which stems from the high effective atomic number of CBO (Z_{eff}=11.5) compared to that of water (Z_{eff}=7.4, similar to that of tissue). This overresponse is in agreement with the mass-energy absorption coefficient of CBO: Tb^{3+}, Ag^+, which accounts for the high cross-section for photoelectric effect compared to that of water. As for the case of Al_2O_3:C (Z_{eff}=11.3) in personal and medical dosimetry, corrections need to be performed to bypass the overresponse of the phosphor to low energies in the applications on demand.

The reproducibility and Repeatability tests should be mentioned again here!

Conclusion

The dosimetric properties of CBO: Tb^{3+}, Ag^{+} phosphors, namely, high sensitivity to X-ray and gamma-rays, which is comparable to that of the gold-standard in OSL dosimetry (Al_2O_3:C), dose range window adequate for personal dosimetry and high-doses needed applications (< 20 Gy, no signs of saturation), neutron sensitivity, good reproducibility and repeatality have demonstrated the potentialities of a new OSL dosimeter. Furthermore, the emission tunability of the phosphor, i.e., either UV broad band centered at 330 nm (the highest trasmission wavelength of conventional U340 Hoya filters) or visible (Tb^{3+} characteristic lines, main emission at 541 nm), depending on the stimulation source (blue light or heating), demonstrates its versatility. However, optimizations are needed in order to reduce the fading features of the compound and the effective atomic number of the host (Z_{eff}=11.5), similar to that of Al_2O_3:C (Z_{eff}=11.3), should be taken into account in the envisioned applications. Regarding the nature of the luminescent processes, both TL and OSL were shown to share the same trapping centers, even though different recombination pathways take place during thermal and optical stimulations. This work is not only a report on the dosimetric features of a high sensitive radiation detector, but also provides a better grasp on the charge storage pathways in borate-based compounds.

Experimental Section

Synthesis: Pollycrystalline samples of CBO: Tb^{3+}, Ag^{+} were synthesized via solid state reaction method. $CaCO_3$ (99.0%, Sigma-Aldrich) and H_3BO_3 (99.5%, Sigma-Aldrich) were the starting precursors used. For doping, aqueous solutions of $(TbNO_3)_3$ (99.9%, Sigma-Aldrich) and $AgNO_3$ (99.9999%, Sigma-Aldrich) were prepared (0.04 M and 0.002 M, respectively - Milli-Q water used) and then 0.5% of the dopant nitrates relative to $CaCO_3$ were added to the starting precursors in a glass beaker. The mixture was then pre-heated (∼150 °C) and agitated in a magnetic stirrer hot plate until evaporation of the solvent (∼20 min). Then, the resultant white powder was annealed at 800 °C over 3 h, cooled in air and crushed using agate mortar and pestle. Specifically for the neutron irradiation measurements, enriched ^{10}B and ^{11}B samples were synthesized by replacing H_3BO_3 (natural boron composition) with $H_3{}^{10}BO_3$ (99%, Cambridge Isotope Laboratories) and $H_3{}^{11}BO_3$ (99%, Sigma-Aldrich).

Structural characterization: X-ray powder diffraction pattern was collected in a diffractometer (D2 PHASER, Bruker-AXS) at RT with Cu K-α radiation (λ=1.54184 Å), X-ray tube operated at 30 kV and 10 mA) and a 0.02° step size scan. The XRD pattern of the codoped compound was matched to the CaB_6O_{10} phase (ICSD 161320) [42] and Rietveld refinement was applied using GSAS-II software [58]. High resolution TEM images and selected area electron diffraction (SAED) patterns were both collected with an aberration-corrected scanning transmission electron microscopy (NEOARM/JEM-ARM200F, JEOL) operated at 200 kV. Prior to analysis, the sample was mixed with ethanol to ensure imaging of a thin specimen.

Basic luminescent properties: Steady-state PL emission and excitation spectra were recorded with a Fluorolog 3 spectrofluorometer (FL3-22, Horiba Scientific) equipped with a 450 W Xe lamp and a photomultiplier tube (R928, Hamamatsu). Both PL and PLE spectra were corrected for the detection system responsivity. RL spectrum was collected by an iXon Ultra 888 EMCCD camera (Andor/Oxford Instruments) coupled to a Kymera 193i-A spectrograph (Andor/Oxford Instruments) with a 150 l/mm grating (blaze wavelength = 500 nm). For the sample excitation, the sample was irradiated with a $^{90}Sr/^{90}Y$ beta source (∼37 mGy/s, calibrated in ^{60}Co air kerma using Al_2O_3:C thin detectors) attached to a Risø reader (TL/OSL-DA-20, DTU Nutech). The RL spectrum was corrected for the detection system responsivity.

OSL and TL measurements: OSL and TL measurements were carried out using the Risø reader. LEDs with peak wavelengths at 470 nm (72 mW/cm^2) or 850 nm (270 mW/cm^2) were used as the stimulation sources during BSL and IRSL acquisitions, respectively. Luminescence was detected by a photomultiplier tube (9107QB, ET Enterprises) coupled to either U-340 filters (7.5 mm thickness, Hoya) for BSL or BG39 filters (5 mm, Schott) for IRSL and TL. For both TL and OSL, previous irradiation was performed using the beta source attached to the Risø reader (dose = 185 mGy, unless otherwise specified). Prior to all irradiations, a pre-heating (400 °C or 500 °C) was applied to ensure depletion of previous induced charges. Specifically the dose-response and fading studies were carried out with irradiation followed by a pre-heating at 100 °C, i.e., to prevent the contribution of shallow trapping centers on the luminescent response. The minimum detectable dose (MDD) was estimated by using MDD = $3\sigma/S$, where σ represents the standard deviation of the background for the five OSL curves (average of the signal before and after stim-

ulation) and S represents the sensitivity of the system (slope of the linear fitting of the dose response). All TL curves were background subtracted. TL emission spectra were collected using the same detection setup used for RL spectrum acquisition and were also corrected for the dectection system responsivity. In the step-annealing experiment, the sample followed a cyclic routine: irradiation, pre-heat at T_i for 10 s, pause of 60 s, OSL readout over 120 s, annealing at 400 °C for depletion of remaining charges and then pause of 120s. The routine repeated by steadily increasing the pre-heat temperature T_i, i.e., from 50 °C to 400 °C, in 10 °C steps (T_i reached at 5 °C s^{-1} from RT). The calculation of the trap depth by using the heating-rate method considered a first-order kinetics, which implies in $\beta E/k_B T_m^2 = s \exp(-E/k_B T_m)$ [46], where β, E, k_B, T_m and s are respectively the heating rate, the trap depth, the Boltzmann constant, the TL peak temperature and the escape frequency. By linearizing the equation and using the heating rates and TL peak temperatures of the TL curves one may find a linear relation between $\ln(T_m^2/\beta)$ and $1/k_B T$. If that fits, the trap depth (E) and the escape frequency (s) can be determined.

Photon energy response and neutron irradiations: For the photon energy response studies, free-in-air irradiation of samples using X-rays and gamma-rays were undertaken. Nine different radiation qualities were used, i.e., N-15, N-25, N-40, N-80, N-120, N-200, N-300, S-Cs and S-Co, with mean photon energies ranging from 12.4 keV to 1250 keV, as specified by the International Organization for Standardization (ISO 4037-1:2019) [59]. The kerma in air for the different radiation qualities were 81.16, 8.86, 4.16, 2.59, 2.70, 3.11, 3.45, ?? and ?? mGy, for increasing energies (from N-15 to S-Co). Kerma in air calibrations were performed by a secondary calibration ionization chamber, which was calibrated against to the standard at the Physikalisch-Technische Bundesanstalt (PTB). The mass-energy absorption coefficient of CBO: Tb^{3+}, Ag^{+} was calculated using the weighted fraction of each element (see the calculation for Al_2O_3:C, for example [60]), considering the coefficients extracted from NIST database [61]. The neutron irradiations were performed with an Am/Be source at a distance of 40 cm from samples (dose equivalent Hp(10) = 5.36 mSv, ∼ 7.5 h irradiation), also traceable to PTB standards.

Acknowledgements

This research was partially funded by Brazilian agencies Fundação de Amparo à Pesquisa do Estado de São Paulo (FAPESP CEPID-NEUROMAT 13/07699-0), Coordenação de Aperfeiçoamento de Pessoal de Nível Superior (CAPES, Finance Code 001) and Conselho Nacional de Desenvolvimento Científico e Tecnológico (CNPq Grant 304107/2019-0). We are grateful to Federico Geser for the technical support regarding the irradiation of samples and to Fernanda Hediger for collecting PL spectra. The Risø TL/OSL-DA-20 reader (DTU Nutech) was acquired with partial support from the Swiss National Science Foundation (R'Equip project 206021_177028).

References

[1] M. Spahn, "X-ray detectors in medical imaging," *Nuclear Instruments and Methods in Physics Research Section A: Accelerators, Spectrometers, Detectors and Associated Equipment*, vol. 731, pp. 57–63, 2013.

[2] B. Mijnheer, S. Beddar, J. Izewska, and C. Reft, "In vivo dosimetry in external beam radiotherapy," *Medical Physics*, vol. 40, no. 7, p. 070903, 2013.

[3] L. Xing, B. Thorndyke, E. Schreibmann, Y. Yang, T.-F. Li, G.-Y. Kim, G. Luxton, and A. Koong, "Overview of image-guided radiation therapy," *Medical Dosimetry*, vol. 31, no. 2, pp. 91–112, 2006.

[4] C. J. Martin, "Personal dosimetry for interventional operators: when and how should monitoring be done?," *The British Journal of Radiology*, vol. 84, no. 1003, pp. 639–648, 2011.

[5] E. Benton and E. Benton, "Space radiation dosimetry in low-earth orbit and beyond," *Nuclear Instruments and Methods in Physics Research Section B: Beam Interactions with Materials and Atoms*, vol. 184, no. 1, pp. 255–294, 2001.

[6] E. A. Ainsbury, E. Bakhanova, J. F. Barquinero, M. Brai, V. Chumak, V. Correcher, F. Darroudi, P. Fattibene, G. Gruel, I. Guclu, S. Horn, A. Jaworska, U. Kulka,

C. Lindholm, D. Lloyd, A. Longo, M. Marrale, O. Monteiro Gil, U. Oestreicher, J. Pajic, B. Rakic, H. Romm, F. Trompier, I. Veronese, P. Voisin, A. Vral, C. A. Whitehouse, A. Wieser, C. Woda, A. Wojcik, and K. Rothkamm, "Review of retrospective dosimetry techniques for external ionising radiation exposures," *Radiation Protection Dosimetry*, vol. 147, pp. 573–592, 12 2010.

[7] J. Farkas and C. Mohácsi-Farkas, "History and future of food irradiation," *Trends in Food Science and Technology*, vol. 22, no. 2, pp. 121–126, 2011.

[8] M. Akselrod, L. Bøtter-Jensen, and S. McKeever, "Optically stimulated luminescence and its use in medical dosimetry," *Radiation Measurements*, vol. 41, pp. S78–S99, 2006.

[9] E. G. Yukihara, S. W. McKeever, and M. S. Akselrod, "State of art: Optically stimulated luminescence dosimetry Frontiers of future research," *Radiation Measurements*, vol. 71, pp. 15–24, 2014.

[10] L. Yuan, Y. Jin, Y. Su, H. Wu, Y. Hu, and S. Yang, "Optically stimulated luminescence phosphors: Principles, applications, and prospects," *Laser & Photonics Reviews*, vol. 14, no. 12, p. 2000123, 2020.

[11] Z. Sun, J. Yang, L. Huai, W. Wang, Z. Ma, J. Sang, J. Zhang, H. Li, Z. Ci, and Y. Wang, "Spy Must Be Spotted: A Multistimuli-Responsive Luminescent Material for Dynamic Multimodal Anticounterfeiting and Encryption," *ACS Applied Materials & Interfaces*, vol. 10, no. 25, pp. 21451–21457, 2018.

[12] Z. Liu, L. Zhao, W. Chen, X. Fan, X. Yang, S. Tian, X. Yu, J. Qiu, and X. Xu, "Multiple anti-counterfeiting realized in $NaBaScSi_2O_7$ with a single activator of Eu^{2+}," *Journal of Materials Chemistry C*, vol. 6, pp. 11137–11143, 2018.

[13] S. Lin, H. Lin, C. Ma, Y. Cheng, S. Ye, F. Lin, R. Li, J. Xu, and Y. Wang, "High-security-level multi-dimensional optical storage medium: nanostructured glass embedded with $LiGa_5O_8$: Mn^{2+} with photostimulated luminescence," *Light: Science & Applications*, vol. 9, no. 22, 2020.

[14] Y. Zhuang, L. Wang, Y. Lv, T.-L. Zhou, and R.-J. Xie, "Optical Data Storage and Multicolor Emission Readout on Flexible Films Using Deep-Trap Persistent Luminescence Materials," *Advanced Functional Materials*, vol. 28, no. 8, p. 1705769, 2017.

[15] F. Liu, W. Yan, Y.-J. Chuang, Z. Zhen, J. Xie, and Z. Pan, "Photostimulated near-infrared persistent luminescence as a new optical read-out from Cr^{3+}-doped $LiGa_5O_8$," *Scientific Reports*, vol. 3, no. 1554, 2013.

[16] P. Dorenbos, "Systematic behaviour in trivalent lanthanide charge transfer energies," *Journal of Physics: Condensed Matter*, vol. 15, pp. 8417–8434, nov 2003.

[17] P. Dorenbos and A. Bos, "Lanthanide level location and related thermoluminescence phenomena," *Radiation Measurements*, vol. 43, no. 2, pp. 139–145, 2008.

[18] P. Dorenbos, "Lanthanide charge transfer energies and related luminescence, charge carrier trapping, and redox phenomena," *Journal of Alloys and Compounds*, vol. 488, no. 2, pp. 568–573, 2009. Proceedings of the 25th Rare Earth Research Conference, June 22-26, Tuscaloosa, Alabama, USA.

[19] T. Lyu and P. Dorenbos, "Vacuum-Referred Binding Energies of Bismuth and Lanthanide Levels in $LiTaO_3$ Perovskite: Toward Designing Energy Storage Phosphor for Anti-Counterfeiting, X-Ray Imaging, and Mechanoluminescence," *Laser & Photonics Reviews*, no. 2200304, 2022.

[20] T. Lyu and P. Dorenbos, "Vacuum-Referred Binding Energies of Bismuth and Lanthanide Levels in ARE(Si,Ge)O4 (A = Li, Na; RE = Y, Lu): Toward Designing Charge-Carrier-Trapping Processes for Energy Storage," *Chemistry of Materials*, vol. 32, pp. 1192–1209, Feb 2020.

[21] T. Lyu and P. Dorenbos, "Towards information storage by designing both electron and hole detrapping processes in bismuth and lanthanide-doped $LiRE(Si,Ge)O_4$ (RE = Y, Lu) with high charge carrier storage capacity," *Chemical Engineering Journal*, vol. 400, p. 124776, 2020.

[22] E. Milliken, L. Oliveira, G. Denis, and E. Yukihara, "Testing a model-guided approach to the development of new thermoluminescent materials using YAG:Ln produced by solution combustion synthesis," *Journal of Luminescence*, vol. 132, no. 9, pp. 2495–2504, 2012.

[23] L. Oliveira, E. Yukihara, and O. Baffa, "Lanthanide-doped MgO: A case study on how to design new phosphors for dosimetry with tailored luminescent properties," *Journal of Luminescence*, vol. 209, pp. 21–30, 2019.

[24] A. Luchechko, Y. Zhydachevskyy, S. Ubizskii, O. Kravets, A. I. Popov, U. Rogulis, E. Elsts, E. Bulur, and A. Suchocki, "Afterglow, TL and OSL properties of Mn^{2+}-doped $ZnGa_2O_4$ phosphor," *Scientific Reports*, vol. 9, p. 9544, Jul 2019.

[25] D. Van der Heggen, D. R. Cooper, M. Tesson, J. J. Joos, J. Seuntjens, J. A. Capobianco, and P. F. Smet, "Optically stimulated nanodosimeters with high storage capacity," *Nanomaterials*, vol. 9, no. 1127, 2019.

[26] N. Chowdhury, N. Riesen, and H. Riesen, "Efficient Generation of Stable Sm^{2+} in Nanocrystalline $BaLiF_3$:Sm^{3+} by UV- and X-Irradiation," *The Journal of Physical Chemistry C*, vol. 123, no. 41, pp. 25477–25481, 2019.

[27] C. L. Nielsen, R. M. Turtos, M. Bondesgaard, J. S. Nyemann, M. L. Jensen, B. B. Iversen, L. P. Muren, B. Julsgaard, and P. Balling, "A Novel Nanocomposite Material for Optically Stimulated Luminescence Dosimetry," *Nano Letters*, vol. 22, no. 4, pp. 1566–1572, 2022.

[28] L. V. S. França and O. Baffa, "Boosted UV emission on the optically and thermally stimulated luminescence of CaB_6O_{10}:Gd,Ag phosphors excited by X-rays," *Applied Materials Today*, vol. 21, p. 100829, 2020.

[29] T. Lyu and P. Dorenbos, "Designing thermally stimulated 1.06μm nd^{3+} emission for the second bio-imaging window demonstrated by energy transfer from Bi^{3+} in La-, Gd-, Y-, and $LuPO_4$," *Chemical Engineering Journal*, vol. 372, pp. 978–991, 2019.

[30] H. Luo and P. Dorenbos, "The dual role of Cr^{3+} in trapping holes and electrons in lanthanide co-doped $GdAlO_3$ and $LaAlO_3$," *Journal of Materials Chemistry C*, vol. 6, pp. 4977–4984, 2018.

[31] H. Luo, A. J. J. Bos, and P. Dorenbos, "Controlled Electron-Hole Trapping and Detrapping Process in $GdAlO_3$ by Valence Band Engineering," *The Journal of Physical Chemistry C*, vol. 120, pp. 5916–5925, Mar 2016.

[32] R. D. Shannon, "Revised effective ionic radii and systematic studies of interatomic distances in halides and chalcogenides," *Acta Crystallographica Section A*, vol. 32, pp. 751–767, Sep 1976.

[33] L. C. Oliveira and O. Baffa, "A new luminescent material based on CaB_6O_{10}:Pb to detect radiation," *Journal of Luminescence*, vol. 181, pp. 171–178, 2017.

[34] L. Oliveira and O. Baffa, "Optically and thermally stimulated luminescence of CaB_6O_{10}:Ce,LiCl: Basic properties," *Journal of Luminescence*, vol. 188, pp. 180–187, 2017.

[35] M. W. Swinney, J. W. McClory, J. C. Petrosky, S. Yang, A. T. Brant, V. T. Adamiv, Y. V. Burak, P. A. Dowben, and L. E. Halliburton, "Identification of electron and hole traps in lithium tetraborate ($Li_2B_4O_7$) crystals: Oxygen vacancies and lithium vacancies," *Journal of Applied Physics*, vol. 107, no. 11, p. 113715, 2010.

[36] G. O. E. Pekpak, A. Yilmaz, "An Overview on Preparation and TL Characterization of Lithium Borates for Dosimetric Use," *The Open Mineral Processing Journal*, vol. 3, pp. 14–24, 2010.

[37] M. Kerikmäe, M. Danilkin, A. Lust, V. Nagirnyi, L. Pung, A. Ratas, I. Romet, and V. Seeman, "Hole traps and thermoluminescence in Li_2B_4O7:Be," *Radiation Measurements*, vol. 56, pp. 147–149, 2013.

[38] A. Ratas, M. Danilkin, M. Kerikmäe, A. Lust, H. Mändar, V. Seeman, and G. Slavin, "$Li_2B_4O_7$:Mn for dosimetry applications: traps and mechanisms," *Proceedings of the Estonian Academy of Sciences*, vol. 61, no. 4, pp. 279–295, 2012.

[39] L. V. S. França, F. H. Borges, R. R. Gonçalves, O. Baffa, and E. G. Yukihara, "Influence of lanthanide (Gd, Tb or Ce) and silver doping on the luminescence lifetimes of calcium borate investigated by pulsed optically stimulated luminescence," *Journal of Luminescence*, vol. 248, p. 118809, 2022.

[40] T. D. Gustafson, B. E. Kananen, N. C. Giles, B. C. Holloway, V. T. Adamiv, I. M. Teslyuk, Y. V. Burak, and L. E. Halliburton, "Electron traps in Ag-doped $Li_2B_4O_7$ crystals: The role of Ag interstitial ions," *Journal of Applied Physics*, vol. 131, no. 17, p. 175106, 2022.

[41] B. Kananen, E. Maniego, E. Golden, N. Giles, J. McClory, V. Adamiv, Y. Burak, and L. Halliburton, "Optically stimulated luminescence (OSL) from Ag-doped $Li_2B_4O_7$ crystals," *Journal of Luminescence*, vol. 177, pp. 190–196, 2016.

[42] X. Chen, M. Li, X. Chang, H. Zang, and W. Xiao, "Synthesis and crystal structure of a new calcium borate, CaB_6O_{10}," *Journal of Alloys and Compounds*, vol. 464, no. 1, pp. 332–336, 2008.

[43] A. Meijerink, M. M. E. van Heek, and G. Blasse, "Luminescence of Ag^+ in crystalline and glassy SrB_4O_7," *Journal of Physics and Chemistry of Solids*, vol. 54, no. 8, pp. 901–906, 1993.

[44] P. Dorenbos, "The Eu^{3+} charge transfer energy and the relation with the band gap of compounds," *Journal of Luminescence*, vol. 111, no. 1, pp. 89–104, 2005.

[45] D. Van der Heggen, R. Zilenaite, E. Ezerskyte, V. Fritz, K. Korthout, D. Vandenberghe, J. De Grave, J. Garrevoet, L. Vincze, D. Poelman, J. J. Joos, and P. F. Smet, "A standalone, battery-free light dosimeter for ultraviolet to infrared light," *Advanced Functional Materials*, vol. 32, no. 14, p. 2109635, 2022.

[46] S. W. S. McKeever, *Thermoluminescence of Solids*. Cambridge University Press, 1985.

[47] R. Chen, J. Lawless, and V. Pagonis, "On the various-heating-rates method for evaluating the activation energies of thermoluminescence peaks," *Radiation Measurements*, vol. 150, p. 106692, 2022.

[48] A. J. J. Bos, "Thermoluminescence as a Research Tool to Investigate Luminescence Mechanisms," *Materials*, vol. 10, no. 12, 2017.

[49] R. Chen and V. Pagonis, "A model explaining the anomalous heating-rate effect in thermoluminescence as an inverse thermal quenching based on simultaneous thermal release of electrons and holes," *Radiation Measurements*, vol. 106, pp. 20–25, 2017.

[50] A. Mandowski and A. Bos, "Explanation of anomalous heating rate dependence of thermoluminescence in YPO_4:Ce^{3+},Sm^{3+} based on the semi-localized transition (SLT) model," *Radiation Measurements*, vol. 46, no. 12, pp. 1376–1379, 2011.

[51] J. F. M. dos Santos, I. A. A. Terra, N. G. C. Astrath, F. B. Guimarães, M. L. Baesso, L. A. O. Nunes, and T. Catunda, "Mechanisms of optical losses in the $^5D_4$ and $^5D_3$ levels in Tb^{3+} doped low silica calcium aluminosilicate glasses," *Journal of Applied Physics*, vol. 117, no. 5, p. 053102, 2015.

[52] B. Zhang, S. Ying, L. Han, J. Zhang, and B. Chen, "Color-tunable phosphor of $Sr_3YNa(PO_4)_3F$:Tb^{3+} via interionic cross-relaxation energy transfer," *RSC Advances*, vol. 8, no. 45, p. 25378 25386, 2018.

[53] P. Dorenbos, "The Pr^{3+} and Tb^{3+} ground state locations in compounds obtained from thermoluminescence and intervalence charge transfer studies," *Optical Materials*, vol. 91, pp. 333–337, 2019.

[54] M. W. Swinney, J. W. McClory, J. C. Petrosky, S. Yang, A. T. Brant, V. T. Adamiv, Y. V. Burak, P. A. Dowben, and L. E. Halliburton, "Identification of electron and hole traps in lithium tetraborate ($Li_2B_4O_7$) crystals: Oxygen vacancies and lithium vacancies," *Journal of Applied Physics*, vol. 107, no. 11, p. 113715, 2010.

[55] O. Annalakshmi, M. Jose, U. Madhusoodanan, J. Sridevi, B. Venkatraman, G. Amarendra, and A. Mandal, "Thermoluminescence mechanism in rare-earth-doped magnesium tetra borate phosphors," *Radiation Effects and Defects in Solids*, vol. 169, no. 7, pp. 636–645, 2014.

[56] E. G. Yukihara, B. A. Doull, T. Gustafson, L. C. Oliveira, K. Kurt, and E. D. Milliken, "Optically stimulated luminescence of MgB_4O_7:Ce,Li for gamma and neutron dosimetry," *Journal of Luminescence*, vol. 183, pp. 525–532, 2017.

[57] A. Dobrowolska, A. J. J. Bos, and P. Dorenbos, "Electron tunnelling phenomena in YPO:Ce,Ln (Ln = Er, Ho, Nd, Dy)," *Journal of Physics D: Applied Physics*, vol. 47, p. 335301, jul 2014.

[58] B. H. Toby and R. B. Von Dreele, "*GSAS-II*: the genesis of a modern open-source all purpose crystallography software package," *Journal of Applied Crystallography*, vol. 46, pp. 544–549, Apr 2013.

[59] "X and gamma reference radiation for calibrating dosemeters and doserate meters and for determining their response as a function of photon energy Part 1: Radiation characteristics and production methods. International Organization for Standardization," 2019.

[60] P. Gasparian, F. Vanhavere, and E. Yukihara, "Evaluating the influence of experimental conditions on the photon energy response of Al_2O_3:C optically stimulated luminescence detectors," *Radiation Measurements*, vol. 47, no. 4, pp. 243–249, 2012.

[61] J. H. Hubbell and S. Seltzer, "Tables of X-Ray Mass Attenuation Coefficients and Mass Energy-Absorption Coefficients from 1 keV to 20 MeV for Elements Z = 1 to 92 and 48 Additional Substances of Dosimetric Interest, http://physics.nist.gov/physrefdata/xraymasscoef/cover.html (Accessed July 1, 2022)," 1995.

Supporting Information

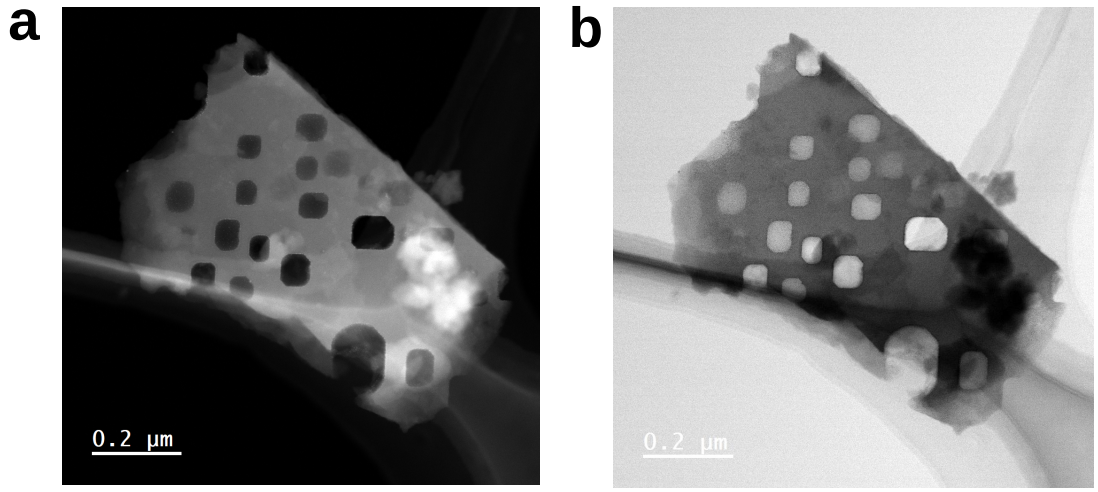

Figure S1: STEM images of Swiss-cheese like structure of grains obtained through a) annular dark field (ADF) and b) bright field (BF) modes.

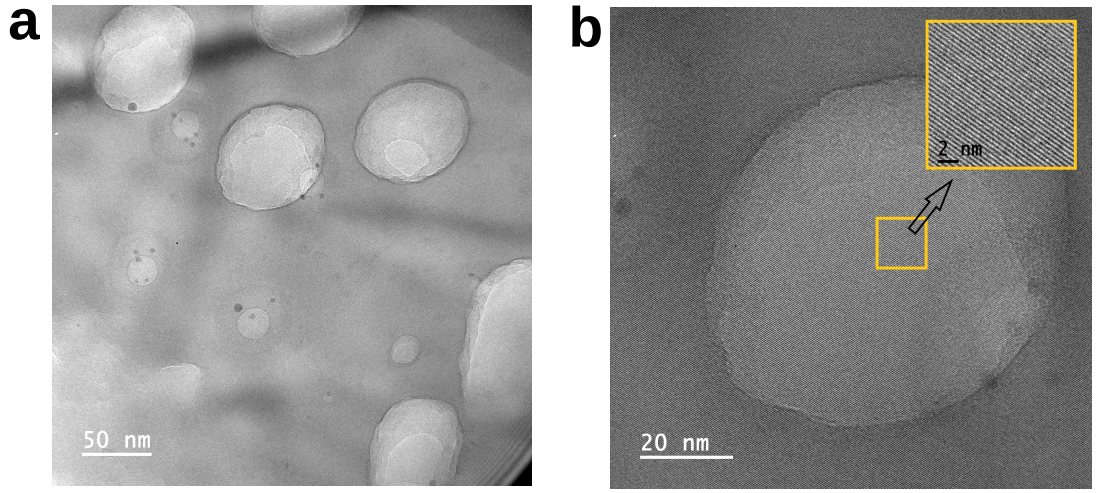

Figure S2: TEM images showing the regularities of the crystallographic planes. a) Lower magnification and b) Higher magnification images.

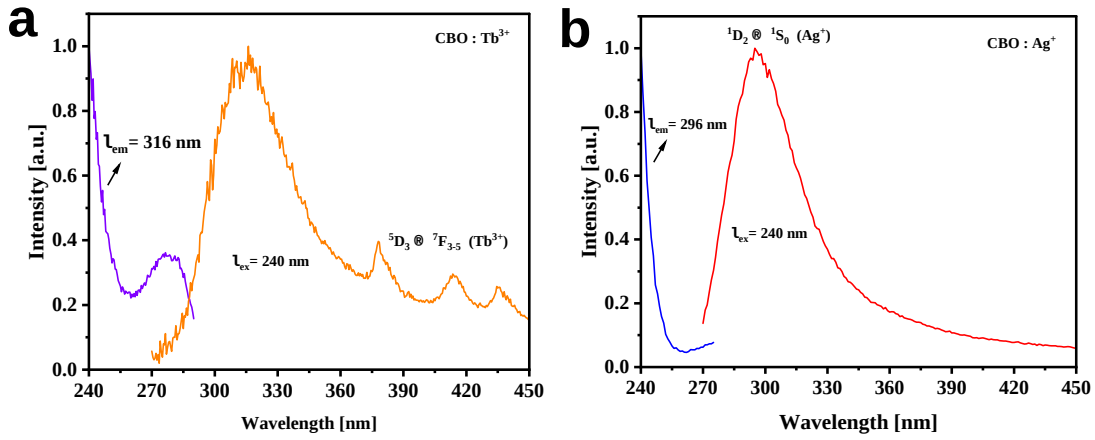

Figure S3: Steady-state PL and PLE spectra of singly-doped CBO: a) CBO: Tb^{3+} and b) CBO: Ag^{+}.

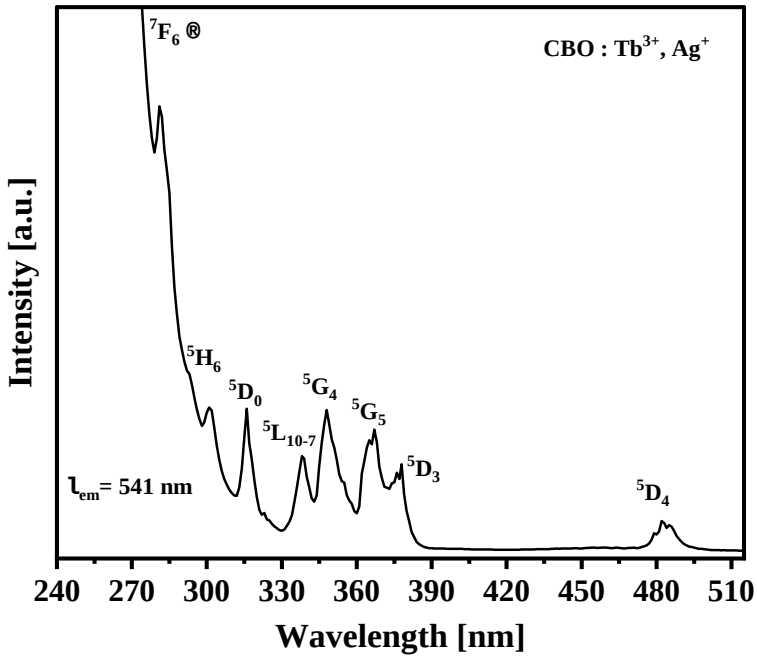

Figure S4: PLE spectra of CBO: Tb^{3+}, Ag+ by probing typical 541 nm emission of Tb^{3+}.

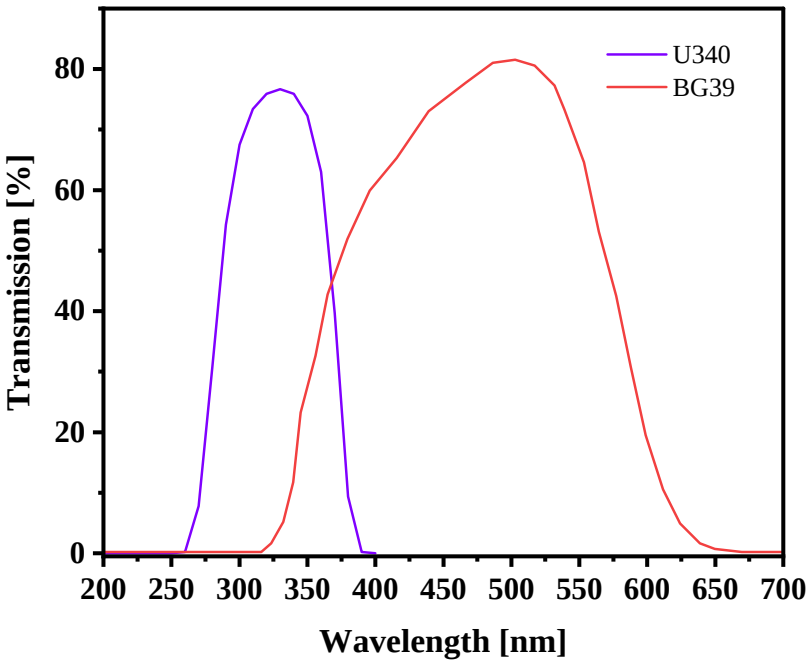

Figure S5: Comparison of the typical transmittance curves of the filters used for acquisition of the OSL and TL curves.

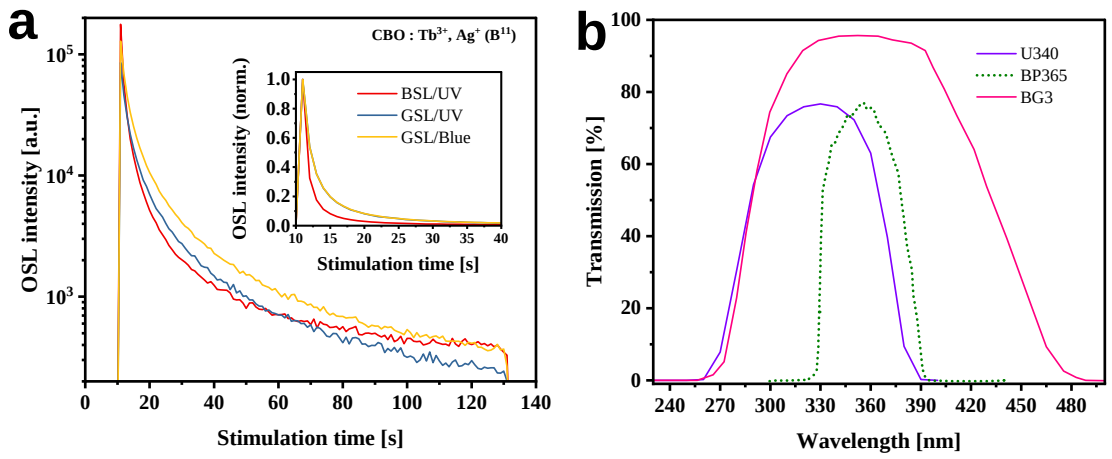

Figure S6: a) Comparison of OSL curves obtained using a Lexsyg reader using blue (458 nm) and green (525 nm) stimulations with detection at UV or UV-blue extended (m = 2.0 mg and dose = 1 s irradiation = ?? mGy). b) Comparison of the filters used: UV = U340 + BP365 filters; UV-Blue extended = BG3 + BP365 filters.

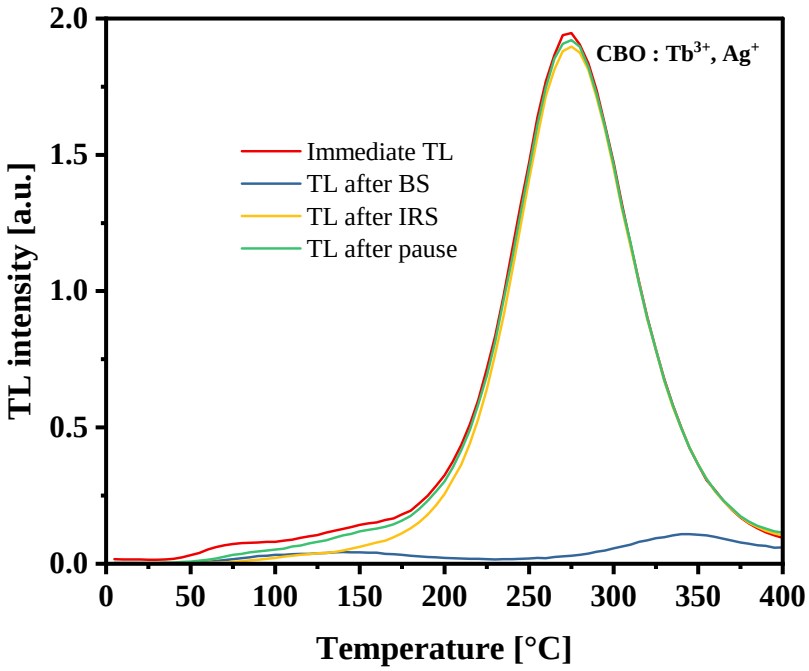

Figure S7: Comparison of TL curve right after irradiation (Immediate TL) with TL obtained after different conditions: after blue or IR stimulations (20 s without stimulation and 120 s of stimulation) and after pause (140 s). Dose = 185 mGy.

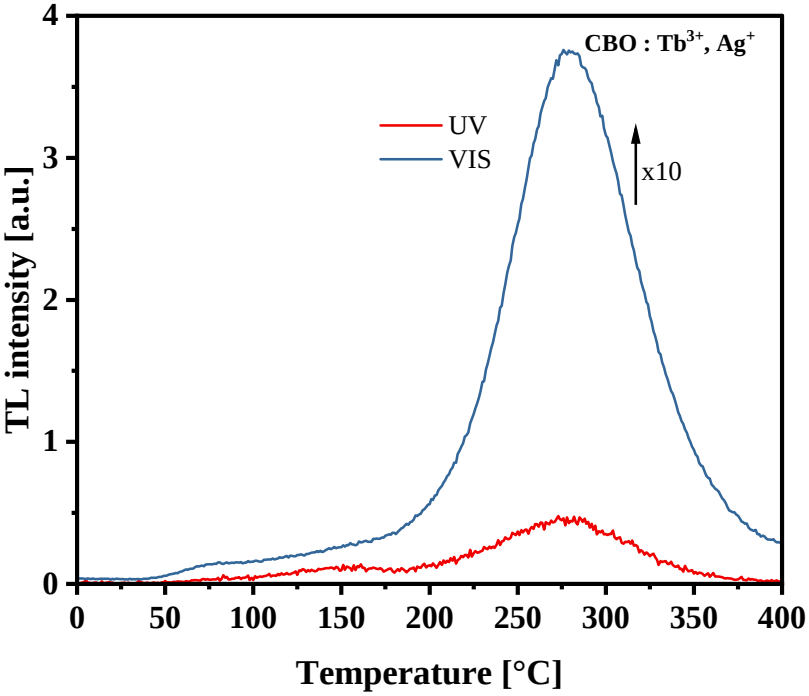

Figure S8: TL comparison recorded with UV and visible transmission filters. Dose = 185 mGy.

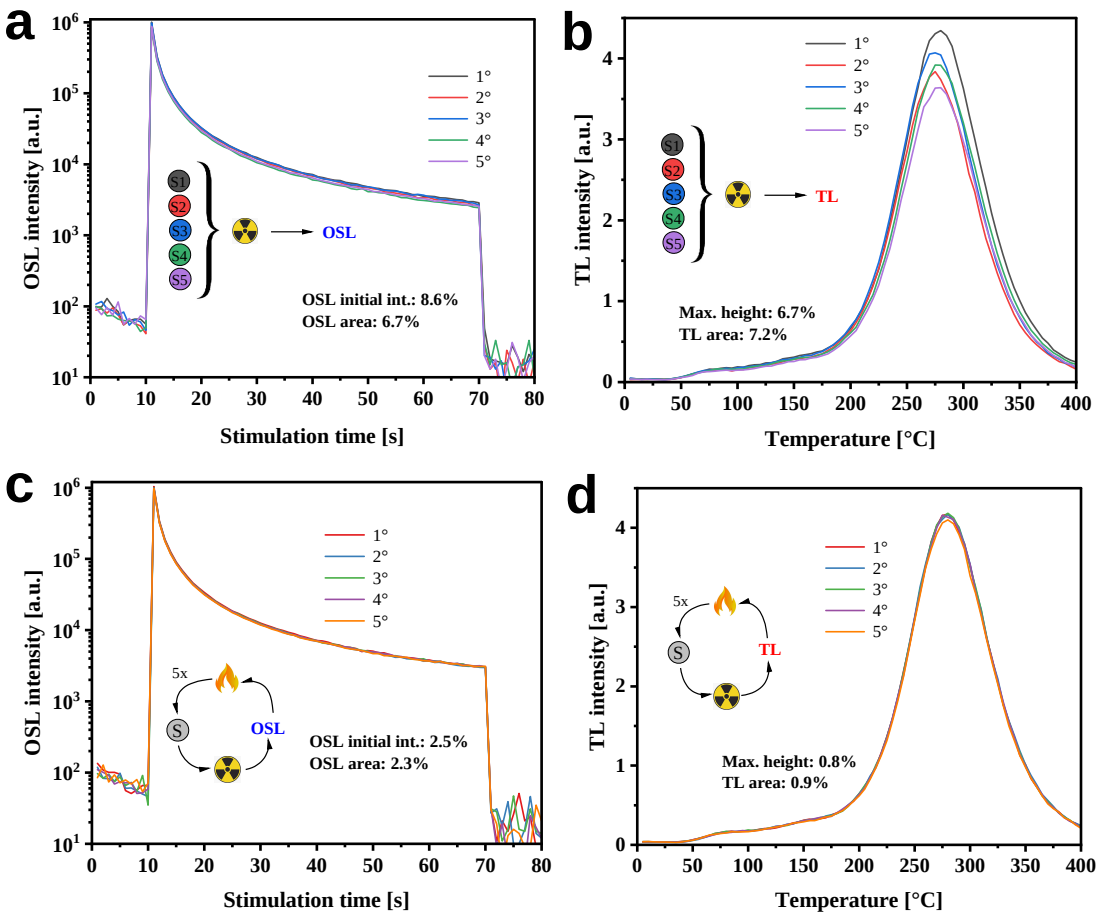

Figure S9: Reproducibility tests for five different aliquots for a) OSL and b) TL. Repeatability tests of the same aliquot (five times) for c) OSL and d) TL. OSL and TL areas were calculated during 60 s of stimulation and from 100 °C and 400 °C, respectively. Dose = 37 mGy.

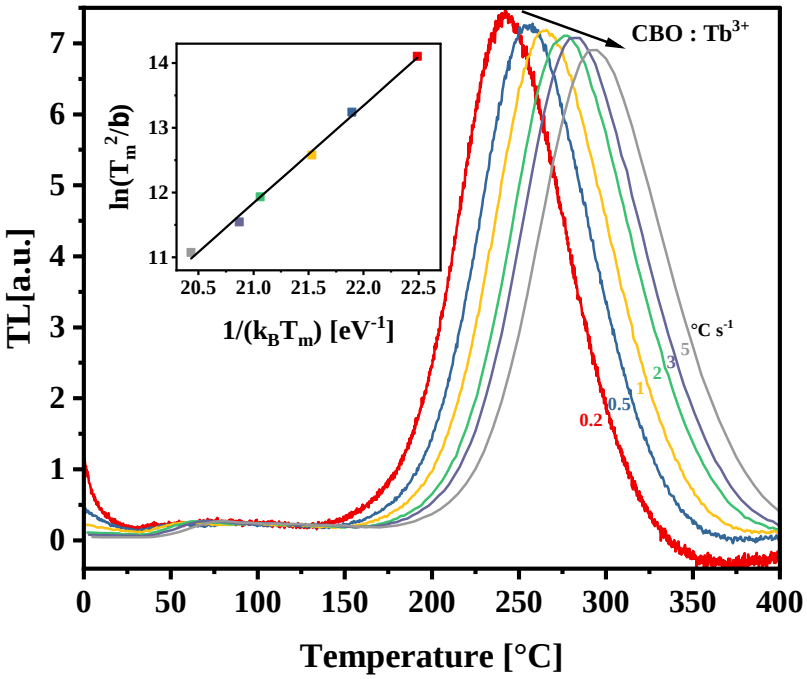

Figure S10: TL curves at increasing heating rates for the CBO: Tb^{3+} compound. The intensities were normalized by the corresponding heating rates. The inset shows the plot of $\ln(T_m{}^2/\beta)$ against $1/(k_B T)$ for determination of the trap depth corresponding to the main TL peak. The estimated values for the energy trap depth and frequency factor were: $E = 1.51$ eV and $s = 7.0\text{x}10^{12}\text{s}^{-1}$. Dose = 185 mGy.

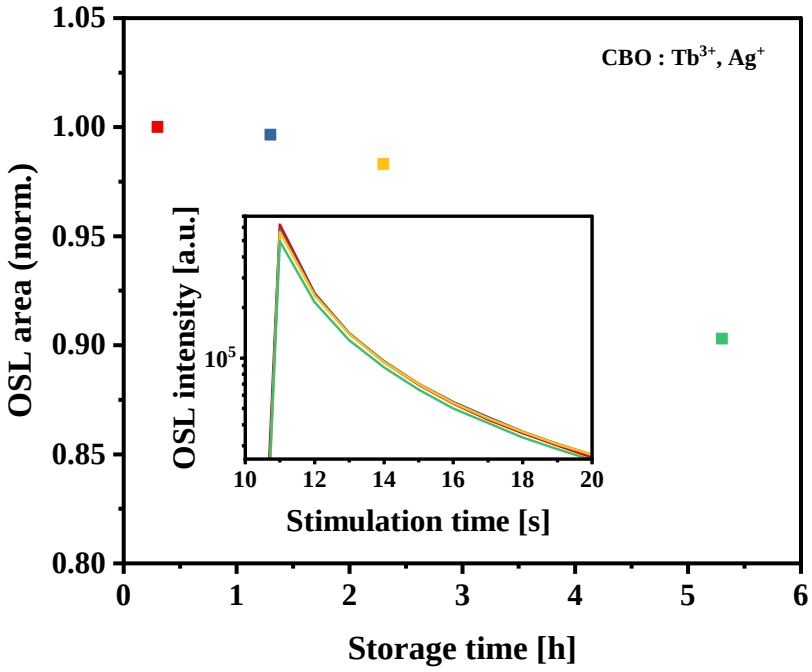

Figure S11: Short OSL fading within the first 5.5 h after irradiation. OSL area was calculated using 120 s of stimulation. The inset shows the OSL curves for the first 10 s of stimulation. Dose = 37 mGy.

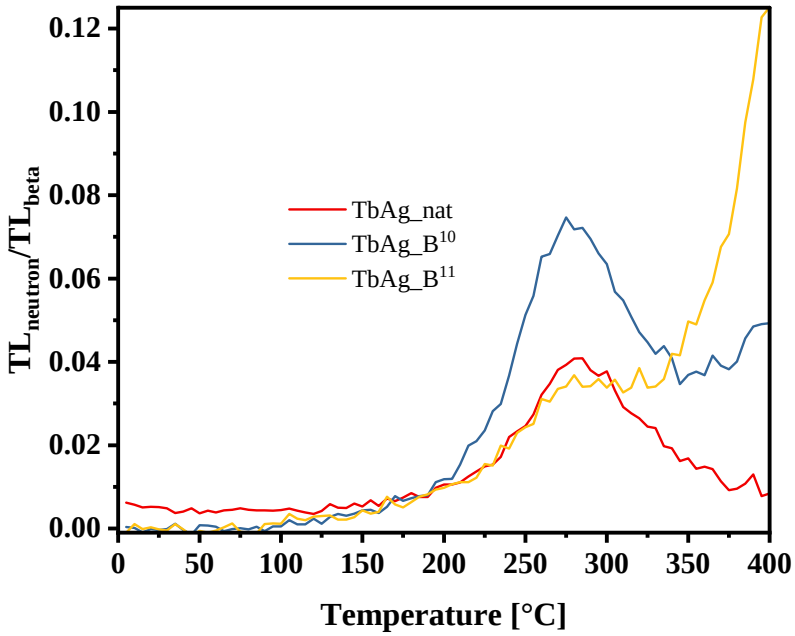

Figure S12: TL neutron response normalized by a reference beta dose (37 mGy) for different isotopic boron compositions of CBO: Tb^{3+}, Ag^{+}. VERIFY THIS!! The same neutron irradiation conditions for the OSL neutron tests apply.

Paper III

IV. Influence of lanthanide (Gd, Tb or Ce) and silver doping on the luminescence lifetimes of calcium borate investigated by pulsed optically stimulated luminescence

Leonardo V. S. França[a,c,], Fernanda H. Borges[b], Rogéria R. Gonçalves[b], Oswaldo Baffa[a], Eduardo G. Yukihara[c]*

[a] Departamento de Física, FFCLRP, Universidade de São Paulo, Av. Bandeirantes, 3900, 14040-900, Ribeirão Preto, Brazil.

[b]Departamento de Química, FFCLRP, Universidade de São Paulo, Av. Bandeirantes, 3900, 14040-900, Ribeirão Preto, Brazil.

[c]Department of Radiation Safety and Security, Paul Scherrer Institute, Forschungsstrasse 111, 5232, Villigen PSI, Switzerland.

* Email: leonardo.franca@psi.ch

Abstract

The objective of this work is to evaluate the optically stimulated luminescence (OSL) lifetimes of different polycrystalline CaB_6O_{10}:Ln, Ag_x (Ln = Gd, Tb and Ce; x: % molar concentration) compounds. For the determination of the luminescence lifetimes, time-tagged time-resolved (TTTR) data of the OSL under pulsed stimulation were analyzed. In addition, OSL emission spectra of the samples were recorded to correlate the emission

bands with the estimated lifetimes. Whereas single Ce-doped compound presented a fast dominant component ($\tau < 0.41$ μs, ∼63% of the signal), single Gd-doped compound exhibited a slow dominant component ($\tau = 2.3$ ms, ∼67% of the signal). All Ag-codoped compounds (except for the Ce-Ag-codoped compound) presented a common dominant component with a ∼43 μs lifetime, which is ascribed to a broad emission centered at ∼330 nm. Both lifetimes and OSL emission spectra for the Gd-Ag-codoped compounds suggest that two luminescent centers compete for the radiative recombinations, confirming previous reported results. The relative Gd and Ag molar concentrations also had a strong influence in the estimated luminescence lifetimes of the slow component, probably due to the introduction of shallow trapping centers by silver doping. Furthermore, the temperature dependence of the common luminescence from Ag-codoped compounds appeared to be in agreement with the Mott-Seitz model for the luminescence quenching. This work provides a better understanding of the physical processes and dynamics behind the radiative recombinations linked to OSL in borate compounds.

Introduction

Within the recombination processes responsible for the luminescence phenomenon, one of the physical parameters of main interest is the luminescence lifetime, which informs how fast the luminescence emission takes place after stimulation. The main factor governing the magnitude of the lifetime is the selection rules associated with the relaxation transition responsible for the emission of the luminescent center. Other factors such as the emission wavelength (for a given transition), temperature, luminescent center concentration and presence of shallow trapping centers may also influence the luminescence lifetimes [1–3]. In regard to the optically stimulated luminescence (OSL), which is the light emission of a prior irradiated material after light stimulation, two other factors may also influence the magnitude of the luminescence lifetime: the time needed to evict an electron from a trap and the time the electron takes to transition from the trap to the recombination center [4,5]. For a more in deep treatment on the principles of OSL lifetimes, one may consider the references hereinafter [4, 6–10].

One of the methods to determine the OSL lifetimes is based on time-tagged time-resolved (TTTR, or time-tagging) data of OSL under pulsed stimulation (POSL). POSL

in general is a useful technique, since it allows for time-resolved discrimination of the decay components and the elimination of undesirable components. Consequently, a higher signal-to-noise ratio can be achieved compared to continuous wave OSL [7]. In a TTTR-POSL experiment, the samples are stimulated with light pulses and the detected photons are time-stamped with respect to the light pulses [7, 11–14]. The data allows for the calculation of the so-called photon arrival time distributions (PATDs), which is the distribution of detected photons as a function of arrival time since the beginning of the stimulation pulse [15]. From the PATDs, the lifetime components of the OSL signal following a stimulation pulse can be determined. More details about this approach and similar techniques can be found in previous reports [7, 13, 15, 16].

Lifetime measurements not only can help in the identification of the luminescent centers present in a material, but can also reveal the presence of shallow trapping centers associated with thermoluminescence (TL) peaks below room temperature, having lifetimes in the order of microseconds to seconds at room temperature [7]. These shallow trapping centers may temporarily capture the released charges under optical stimulation, releasing them with a delay, which is characteristic of the trapping center lifetimes at room temperature. This effect may introduce additional lifetime components in the PATDs.

When analyzed at different temperatures, lifetime measurements can also be used to evaluate the thermal quenching of the luminescence, which is a decrease in luminescence efficiency with temperature. Considering the Mott-Seitz model of thermal quenching, in which the reduction in luminescence efficiency is caused by competing non-radiative relaxation routes whose probability increases with temperature [3], the temperature dependence of lifetime can be expressed as $\tau = \tau_0/(1 + \tau_0 \nu \exp(-E/kT))$, where ν and E represent the frequency factor and activation energy (energy-gap between ground and excited states to have non-radiative processes preferable) of the luminescent center, respectively. Additional information about thermal quenching of luminescence can be found elsewhere [6, 17, 18].

Lanthanide-doping has proven to be useful for the development of luminescent materials for a wide-range of applications, including LEDs, lasers, scintillators, storage and X-ray phosphors applications [1, 19–23]. This is due to the possibility of selecting wavelength emission and luminescence lifetimes, along with a relatively easy prediction of energy levels of the host. OSL dosimetry has benefited from lanthanide doping as

well. Several lanthanide-doped materials for OSL dosimetry applications can be found in the literature, including oxides, borates, aluminates, halides and sulphates [24–27]. In the case of OSL materials, it is important to determine whether the lanthanides act as recombination or as trapping centers, particularly in the presence of co-dopants [28].

Borate compounds typically present a defect created by oxygen vacancies, which act as electron trapping centers [29–31], as well as, a boron-oxygen hole center (BOHC), which is created by an oxygen that bridges a BO_3 and a BO_4 or two BO_4 groups [32–34]. These defects may have a special role on TL/OSL mechanisms of borate-based compounds.

In this context, a boron-based material, i.e., CaB_6O_{10} (hereinafter referred to as CBO), has revealed some interesting properties. For instance, Ce, Li-codoped CBO was shown to have a wide linear dynamic range (2 mGy - 300 Gy) and two luminescence lifetimes of 70 ns and 143 ns, which are suitable for 2D dose mapping applications [35]. Lanthanide-doping in CBO structure is suitable since the ionic radius of the seven coordinated calcium ions (1.06 Å) is comparable to that one of most Ln^{3+} ions [36], which then facilitates incorporation by ion substitution in the lattice. In addition, the combination of Gd and Ag as dopants led to the development of a high sensitive OSL phosphor (minimum detectable dose = 40 μGy), with silver showing a special role on the luminescence enhancement of the phosphor [37]. Nevertheless, the role of lanthanide dopants in the TL/OSL of this material has not been systematically investigated. In particular, for further material development it would be helpful to understand the recombination processes in lanthanide-doped CBO and the influence of co-dopants.

The main objective of the present study is to evaluate the OSL lifetime dependence on lanthanide (Gd, Ce or Tb) and silver-doped CBO compounds. Other Ln-doped CBO (Pr, Nd, Sm, Eu, Dy, Ho, Er, Tm and Yb) were previously investigated, but these compounds did not show significant OSL. Silver as dopant has demonstrated to enhance the luminescent response (intensity) of several phosphors, including that of Gd-doped CBO [37–39]. The use of different combination of dopants is desirable since they may introduce new energy levels in the band gap of the host, including trapping and recombination centers, as well as incorporation of charge compensators in the crystal. A correlation of the luminescence lifetimes with the OSL emission bands is presented. Also this work provides insights on the role of silver on the luminescence of the phosphors in-

volved. At last, the thermal quenching of the decay components associated with the main luminescence emission bands is presented, providing insights about the coupling between the luminescent centers and the surroundings in the lattice.

Materials and Methods

Material synthesis

All polycrystalline compounds used in this work were synthesized by solid state reaction. This method consists of mixing proper amounts of starting precursors and then exposing the mixture to high temperatures. Calcium carbonate ($CaCO_3$) and boric acid (H_3BO_3) were the precursors used for the growth of the host compound. For the lanthanides and silver doping, suitable amounts of lanthanide and silver nitrates were added to the starting mixture. Then, the resultant compound was placed in a muffle furnace and the temperature was increased up to 800 °C, followed by a plateau for 3 h. Table 1 presents all chemicals used for the syntheses of doped CBO as well as the molar concentrations of the dopants used. Specifically for the Gd-Ag-codoped compounds, three different combinations of molar concentrations were used, i.e., $Gd_{0.1\%}$-$Ag_{2\%}$, $Gd_{1\%}$-$Ag_{1\%}$ and $Gd_{2\%}$-$Ag_{0.2\%}$, represented in the text by Gd-Ag(1), Gd-Ag(2), Gd-Ag(3), respectively. It is worth mentioning that the percentages used for the dopants correspond to the relative amount of nitrate dopant used per amount of $CaCO_3$. A more detailed description of the synthesis procedure, including the amounts of the starting precursors used can be found in a previous work [37]. X-ray diffractograms for samples produced using the same method were also presented in this previous work. For the different combination of dopants used, with similar amounts of those reported here, the presented data showed that the expected phase for the CBO host was achieved.

OSL emission spectra acquisition

The OSL emission spectra were recorded with a Fluorolog 3 spectrofluorometer (FL3-22, Horiba Scientific) equipped with a double-grating monochromator at both excitation and emission positions. For excitation and light detection, a 450 W Xe lamp and a photomultiplier tube (R928, Hamamatsu) were used. For recording the spectra, the excitation was fixed at 430 nm and the detection range set between 270 to 400 nm. All entrance and exit

Table 1: Chemicals used in the syntheses of the samples. The codoped compounds are presented with a hyphen in between the dopants used. The Gd-Ag* represents the compounds with three different combinations of Gd and Ag molar concentrations: $Gd_{0.1\%}$-$Ag_{2\%}$, $Gd_{1\%}$-$Ag_{1\%}$ and $Gd_{2\%}$-$Ag_{0.2\%}$. The percentages used for the dopants correspond to the relative amount of dopant nitrate used per amount of $CaCO_3$.

Precursors		**Compounds**
Calcium carbonate ($CaCO_3$, ACS, 99.0% min., Sigma-Aldrich)		All compounds
Boric acid (H_3BO_3,	BioReagent, 99.5%, Sigma-Aldrich)	$Gd_{1\%}$, $Tb_{1\%}$, $Ag_{0.1\%}$, Gd-Ag*
	ACS, 99.5%, Sigma-Aldrich)	$Ce_{0.5\%}$, $Ce_{0.5\%}$-$Ag_{0.5\%}$, $Tb_{0.5\%}$-$Ag_{0.5\%}$
Gadolinium nitrate ($Gd(NO_3)_3{\cdot}6H_2O$, 99.9%, Sigma-Aldrich)		$Gd_{1\%}$, Gd-Ag*
Terbium nitrate ($Tb(NO_3)_3$	${\cdot}xH_2O$, 99.9%, Alfa-Aesar)	$Tb_{1\%}$
	${\cdot}5H_2O$, 99.9%, Sigma-Aldrich)	$Tb_{0.5\%}$-$Ag_{0.5\%}$
Cerium nitrate ($CeNO_3)_3{\cdot}6H_2O$, 99.9%, Alfa-Aesar)		$Ce_{0.5\%}$, $Ce_{0.5\%}$-$Ag_{0.5\%}$
Silver nitrate ($AgNO_3$,	99.8%, Cennabras)	$Ag_{0.1\%}$, Gd-Ag*
	99.9999%, Sigma-Aldrich)	$Ce_{0.5\%}$-$Ag_{0.5\%}$, $Tb_{0.5\%}$-$Ag_{0.5\%}$

slits of both excitation and detection was set as 5 nm. A longpass GG400 filter (Schott AG) was used on the excitation to avoid stimulation and detection of second-harmonic components. All spectra acquisitions were recorded using an increment of 1 nm per 0.1 s. Several sweeps had been carried out until the irradiation-induced signal was depleted significantly. All spectra were corrected by the detector system responsivity.

Prior to OSL measurements, the samples were irradiated using an Isovolt titan source model E-160 M2 (maximum energy and current of 160 kV and 10 mA, respectively) with a 0.8 mm beryllium window and a 2 mm aluminum filter. A dose of ∼100 Gy was used to ensure a reasonable signal-to-noise ratio in the spectra. The dose reported here is air kerma measured using a calibrated ionization chamber.

TTTR-POSL readout

TTTR-POSL measurements were carried out using a Risø TL/OSL reader (TL/OSL-DA-20, DTU Nutech) equipped with a time counter board (TimeHarp 260 NANO, PicoQuant). The TimeHarp board with a 0.25 ns base resolution and a deadtime < 2 ns enables recording individual photon events on its 32,768 channels. Details about the integration of a photon counting system with the Risø reader and signal data acquisition can be found in a previous report [15].

For each compound, 5 mg powder uniformly dispersed on steel cups was used. For stimulation of the samples, LEDs with peak wavelength at 470 nm and 72 mW/cm^2

irradiance (SMBB series, Ushio Europe B.V.) were used. As reported in a previous work, these LEDs present nominal rise and fall times of 133 ns and 474 ns, respectively, which restricts data acquisition to the microsecond timescale [16]. The luminescence was detected using a photomultiplier tube (9107QB, ET Enterprises) with two U-340 filters (2.5 and 5 mm thickness, Hoya) in front of it. In addition, a combination of the 5 mm thick U-340 with a 313 nm or a 330 nm narrow-band filters (both hard coated, OD 4.0, 10 nm FWHM, Edmund Optics) was used for some studies with a Gd-Ag-codoped compound.

Prior to TTTR-POSL measurements, the samples were irradiated with a $^{90}Sr/^{90}Y$ beta source (~37 mGy/s, calibrated in ^{60}Co air kerma using Al_2O_3:C thin detectors) attached to the Risø reader. Unless otherwise specified, a dose of ~37 mGy was used. During the sequence of measurements, all samples were heated up to 500 °C before irradiation to ensure depletion of previous trapped charges. For the study of the temperature dependence of the lifetimes, TTTR-POSL measurements were carried out at different temperatures (room temperature and 50 °C up to 150 °C, 25 °C step). An additional preheating at 200 °C in the Risø reader was carried out in between the irradiation and the TTTR-POSL measurements to empty the shallow traps and prevent overlapping of the OSL with TL.

For all compounds, three pulse periods in the TTTR-POSL measurements were used, i.e., 100 µs, 1000 µs and 10000 µs, with a pulse width of 10% relative to the pulse period used and bin widths of 0.512 µs, 4.096 µs and 32.768 µs, respectively. For the Ce-doped compounds, which presented a very fast decay component, the bin widths used were 0.128 µs, 1.024 µs and 16.384 µs, respectively. All TTTR-POSL measurements were carried out over 120 s and the PATDs were reconstructed by integrating the photon arrival times over the aforementioned period. For the study of the dependence of lifetimes with temperature, specific acquisition parameters were chosen, as reported on the captions of the corresponding figures.

PATDs analysis

PATDs were analyzed either individually or using a global fitting of the data for different pulse widths, with the lifetimes shared among different datasets. For the lifetime estimations, both rise and decay parts of the PATDs were taken into consideration, i.e., the recombination rates during the stimulation period (saturating exponential) and the recombination rates after the stimulation (exponential decay). The fitting was performed based

on the equations described in a previous report [16], which allow for the presence of multiple non-interacting recombination centers; see also Chithambo [7]. The integral of both rise and decay parts corresponds to the total luminescence during the pulse period. For practical purposes, the two main parameters taken into account were the estimated lifetimes and the pre-exponential factors (S_i), which are proportional to the intensity of the PATD individual components [16].

The instrumental background (including LED related effects) was measured for all samples and different pulse widths. The most significant backgrounds were for the Gd- and Tb-doped compounds, which corresponded to 2.5% (1000 μs pulse width) and 3.9% (100 μs pulse width) of the overall signal, respectively. For the other compounds, that showed to be lower than 1%. Therefore, the instrumental background was neglected in all analyses performed. As a result, the constant luminescence which appears as an offset in some of the PATDs is mostly associated with luminescence components with lifetimes much longer than the timescales in consideration.

In the reported results, the number in parentheses following the lifetimes is the numerical value of standard uncertainty referred to the corresponding last digits of the quoted result [40]. The different lifetime components for each compound are assigned as τ_1, τ_2 and τ_3, with the condition $\tau_1 < \tau_2 < \tau_3$. Only the most representative results are shown in the main text. The complementary data are presented in the Supplementary Materials.

Results

OSL emission spectra

In order to make a correlation with the luminescence lifetimes, the OSL emission spectra for the different compounds were previously collected. For singly-doped compounds, the OSL emission spectra provided clear results only for Gd- and Ag-doped samples. The Gd-doped compound exhibited a sharp emission centered at 311 nm (Figure 1a), which is attributed to the $^6P_J \rightarrow {}^8S_{7/2}$ transitions of Gd^{3+} centers [41]. The Ag-doped compound showed a broad emission at 295 nm (Figure 1b), probably associated to $4d^9 5s \rightarrow 4d^{10}$ transitions of Ag^+ luminescent centers. This emission is similar to that of isolated Ag^+ ions in Ag-doped SrB_4O_7 [42].

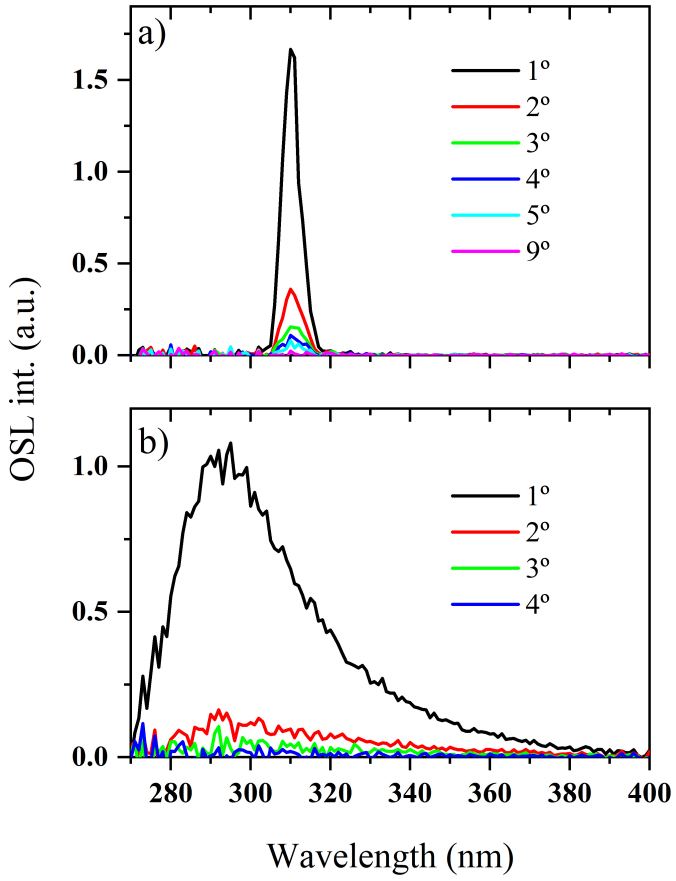

Figure 1: OSL emission spectra of a) Gd- and b) Ag-doped compounds. Several spectra in a row were collected to show the depletion of the OSL, with the order indicated by the graph legends. Only the first spectra and the last one are shown. The spectra were background subtracted, considering the last acquisition as the background.

For the other singly-doped compounds, the results were less conclusive. Ce-doped compound showed a strong phosphorescence after irradiation (room temperature emission followed by X-rays excitation, which takes place without light stimulation), with peaks at ~330 nm and ~360 nm likely due to 5d → 4f transitions of Ce^{3+} centers (see Figure S1). However, this emission could not be distinguished from the OSL emission. In addition, the OSL emission from Tb-doped compound could not be observed even using a higher prior dose (~500 Gy).

For the Gd-Ag-coped samples, the OSL emission spectra showed two distinct emissions: the sharp Gd^{3+} emission and a broad emission centered at ~330 nm (Figure 2). The ~330 nm-band intensity relative to the Gd^{3+} emission decreased with the relative Gd/Ag

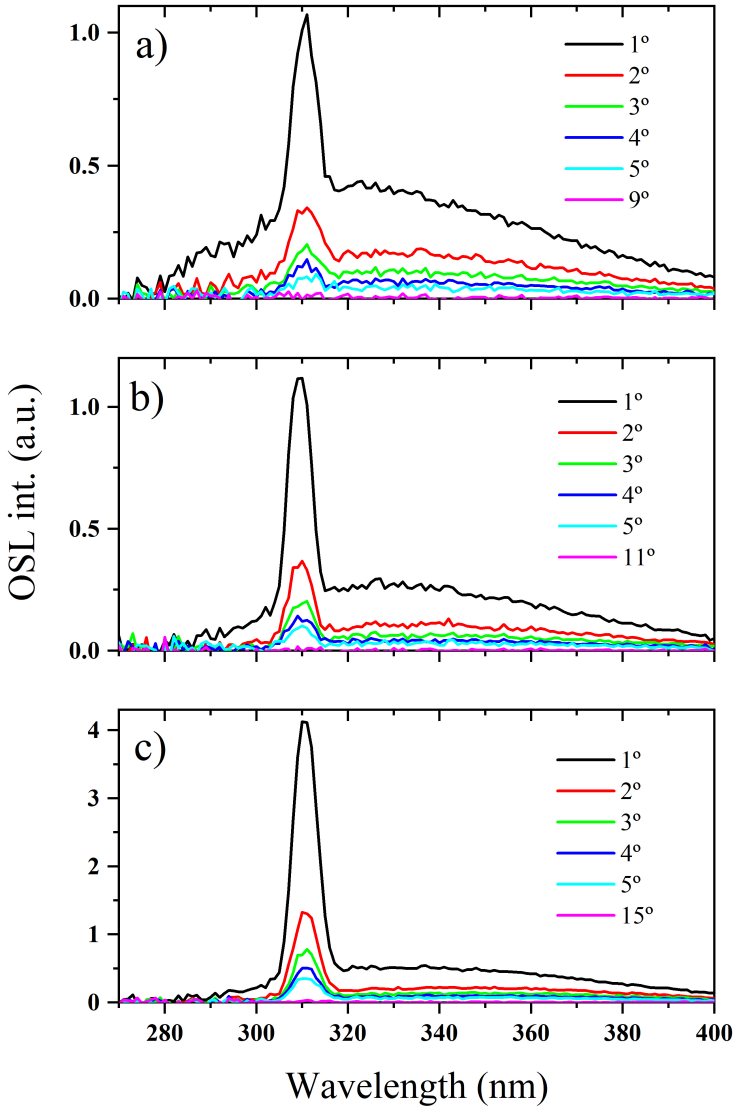

Figure 2: OSL emission spectra for the Gd-Ag-codoped compounds. a) Gd-Ag(1); b) Gd-Ag(2) and c) Gd-Ag(3). The same acquisition parameters and corrections of the OSL emission spectra for the single-doped compounds apply.

increase in the molar concentration, i.e. from sample Gd-Ag(1) to sample Gd-Ag(3) (Figure 2a to c). The Tb-Ag-codoped compound also exhibited a broad and intense emission band centered at 330 nm (Figure 3), similar to that one seen in the Gd-Ag-codoped compounds. These results suggest that the 330 nm emission is associated with Ag-doping, even though this emission is shifted compared to that observed in the single Ag-doped compound (295 nm). Although the reason for this shift is not clear, the luminescence life-

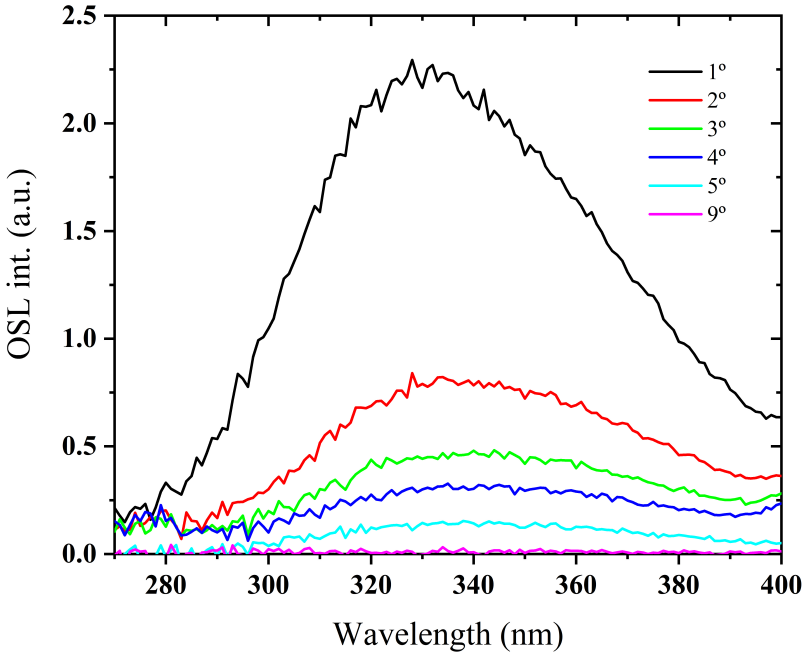

Figure 3: OSL emission spectra for the Tb-Ag-codoped compound. The same acquisition parameters and corrections of the OSL emission spectra for the single-doped compounds apply.

times of these compounds suggest that the different emission bands are associated with the same luminescent center, as later presented in this report.

The OSL emission spectra of single Gd- and Ag-doped as well as of the Gd-Ag(3)-codoped compounds were previously reported [37]. In that work, however, the spectra were recorded with a different detection system at different conditions and were not corrected for the detector system responsivity, which may account for the differences in comparison with the present work results.

The OSL emission spectra for the Ce-Ag-codoped compound were recorded as well. However, as for the Ce-doped compound, the sample exhibited a strong phosphorescence (see Figure S1), which could not be discriminated from the OSL. These results suggest that Ce-doping is responsible for the introduction of shallow trapping centers in the CBO host compound.

Luminescence lifetimes of singly-doped compounds

The PATDs from Gd-doped compound revealed two main components, with estimated lifetimes τ_1 = 4.3(2) µs (Figure 4a) and τ_2 = 2.263(20) ms (Figure 4b). The latter ac-

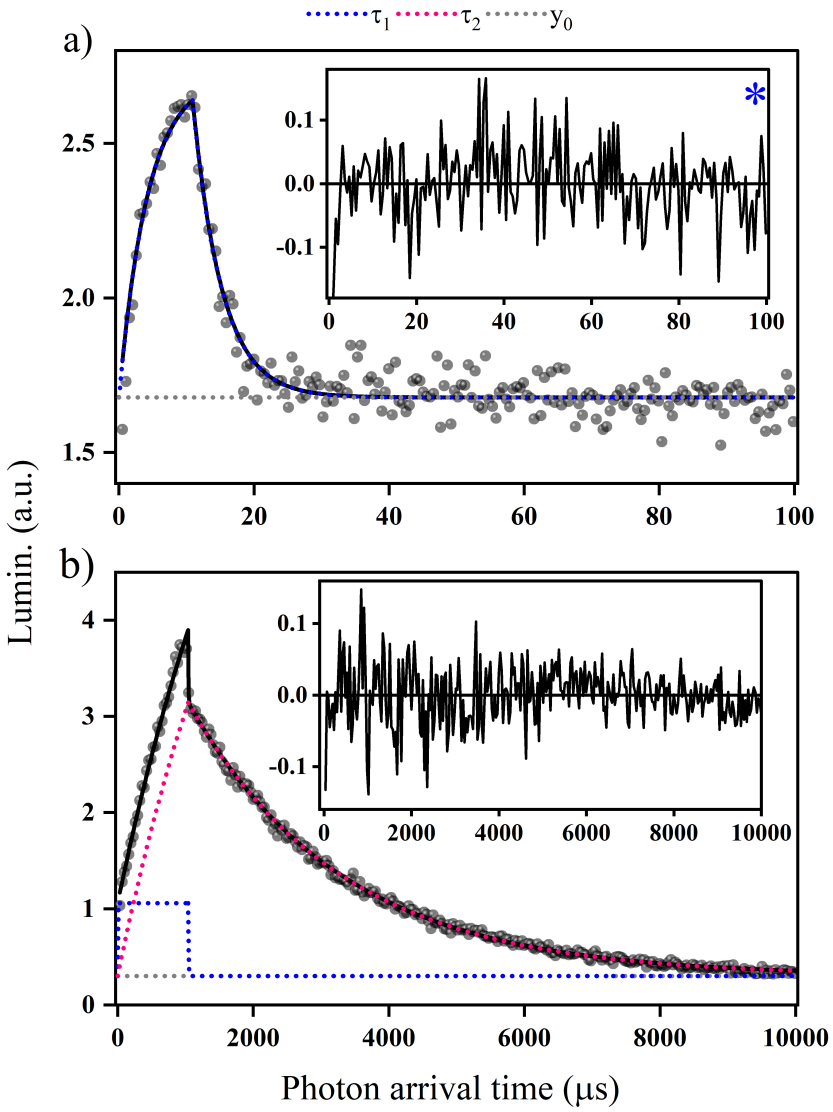

Figure 4: PATDs fitting for the Gd-doped compound using two pulse widths: a) 10 μs and b) 1000 μs. When the 1000 μs pulse width was used, the fast component was forced to be that one found with the 10 μs pulse width. The insets show the residuals from the exponential fitting and the blue star indicates that the y-axis was adjusted for better visualization of the overall residuals. Both individual components are y- shifted for better comparison with the fitted curves (solid black lines).

counts for almost 67% of the total signal (Figure 4b). The ~2.3 ms lifetime is in agreement with the expected lifetimes for the forbidden transition $^6P_J \rightarrow {}^8S_{7/2}$ of Gd^{3+}, as reported for Gd-doped borate glasses [43,44] and, therefore, we attribute it to the presence of Gd^{3+} centers. The analysis with the intermediate pulse width (100 μs) did not present additional components, but only showed the two components with either a poor resolution (fast component) or in a limited timescale (slow component) (see Figure S2). The source of the fast

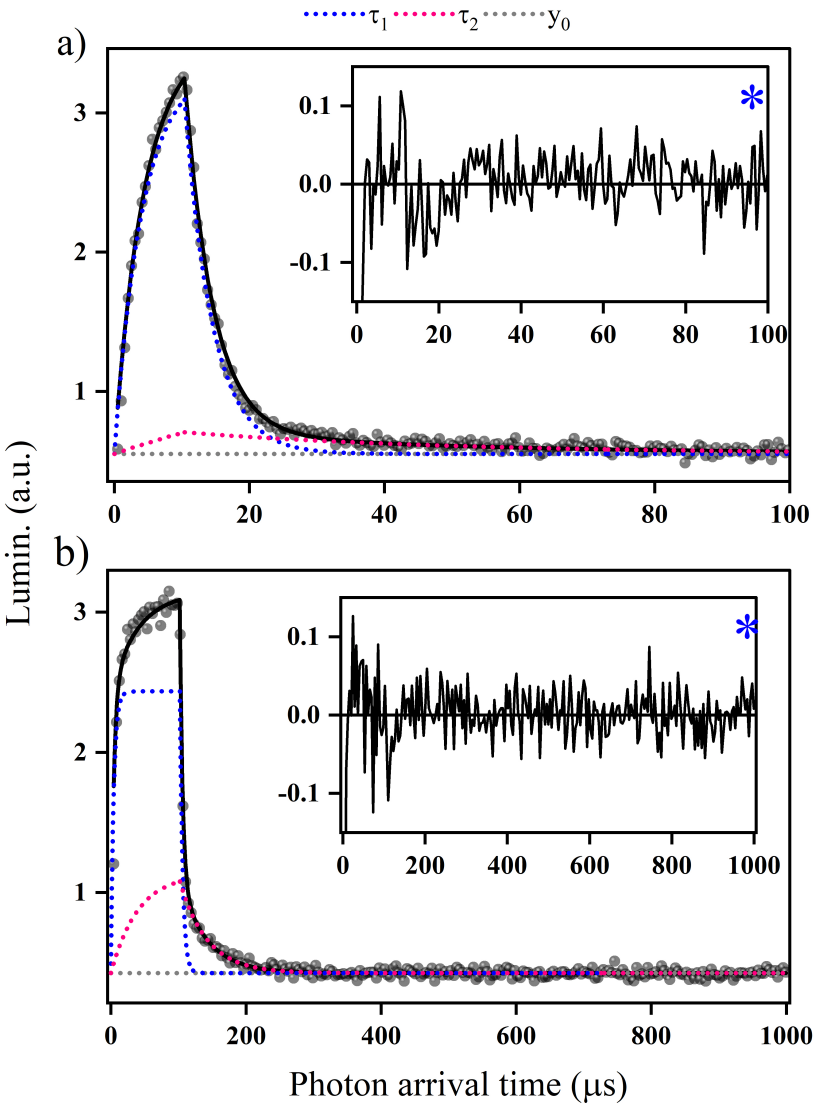

Figure 5: PATDs fitting for the Tb-doped compound using two pulse widths: a) 10 μs and b) 100 μs. A biphasic exponential fitting was carried out with the lifetimes shared among the two pulse period datasets. For details about the insets and representation of the individual components, refer to the caption of Figure 4. Dose used ∼185 mGy.

component is unclear.

The Tb-doped compound exhibited two closely overlapped components with lifetimes of 4.1(1) μs and 40.1(30) μs (Figure 5). Most of the signal, however, is due to a slow component, which appears as a constant component. Its lifetime could not be estimated even using a 1000 μs pulse width (Figure S2). Given that the minor UV emission associated with Tb^{3+} centers is typically associated with lifetimes of the order of 415-970 μs (for Tb molar concentration of 1%) [45, 46], we attribute the lifetime components in

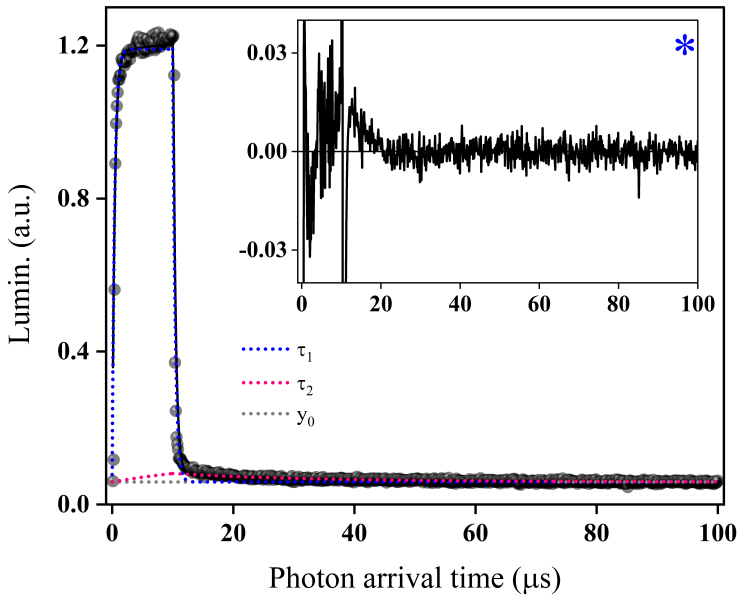

Figure 6: PATD fitting for the Ce-doped compound when a 10 μs pulse width was used. For details about the insets and representation of the individual components, refer to the caption of Figure 4. Dose used ∼185 mGy.

the Tb-doped compound to unidentified luminescence centers. Tb^{3+} emissions in the blue and green regions (main emission at 545 nm) of typical Tb^{3+} centers are not considered here, since the detection window used in the measurements is restricted to the UV.

Ce-doped compound exhibited two components, with estimated lifetimes of $\tau_1 = 0.41(1)$ and $\tau_2 = 23(7)$ μs (Figure 6), with the faster component contributing to 63.4% of the OSL signal. Typical lifetimes associated with 5d → 4f transitions of Ce^{3+} are in the tens of nanosecond timescale, as reported for different compounds [47, 48]. Considering that the lifetime of the Ce^{3+} emission cannot be determined with the present equipment, the observed main lifetime is likely associated with the LED rise and fall times. Minor components with lifetimes ranging from 98 μs and 2.2 ms could also be observed (Figure S2). These secondary components including the 23 μs lifetime component may be associated with shallow trapping centers, as suggested by the phosphorescence measurements. Nevertheless, the dominance of the Ce^{3+} emission (faster component) is clearly demonstrated as seen in Figure 6. Although the fast component lifetime could not be accurately estimated, this compound can be further investigated in view of 2D OSL dosimetry applications, since these require fast luminescent centers as Ce^{3+} emission. Currently there is no commercial available OSL system for 2D dosimetry and recent attempts us-

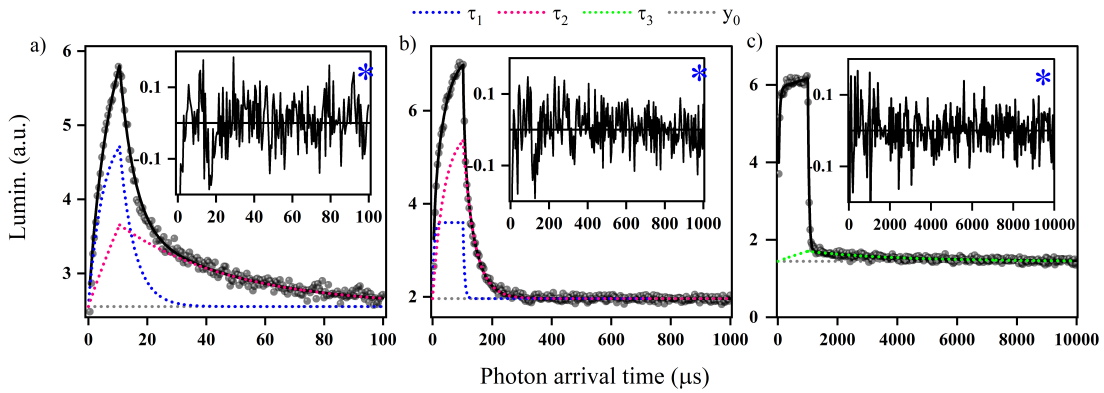

Figure 7: PATDs fitting for the Ag-doped compound using three pulse widths: a) 10 μs; b) 100 μs and c) 1000 μs. A biphasic exponential fitting was carried out with the lifetimes shared among 100 μs and 1000 μs pulse period datasets. For the 10000 μs pulse period, a fitting was carried out individually and only the slower component is discriminated in the graph. For details about the insets and representation of the individual components, refer to the caption of Figure 4. Dose used ~185 mGy.

ing MgB_4O_7-based films have shown some limitations, i.e., significant fading and OSL sensitivity changes [49].

The PATDs for the Ag-doped compound (Figure 7) revealed components with lifetimes $\tau_1 = 5.0(2)$ μs and $\tau_2 = 38.9(9)$ μs, but these contributed only 6.5% (τ_1) and 14.7% (τ_2) to the overall signal (based on the 1000 μs pulse period, Figure 7b), respectively. Most of the OSL is associated with a long luminescence lifetime component (78.8%) which appears as a constant in the PATDs. A component with a lifetime of $\tau_3 = 2.9(5)$ ms was also observed (Figure 7c). This slow component as well as the dominant constant component are probably associated with shallow trapping centers introduced by Ag- doping. The TL curves (emission starting at 60 °C) of Ag-doped CBO reported in a previous work support this interpretation [37].

The ~39 μs component in Ag-doped compound is likely due to the presence of Ag^+ luminescent ions. Ag^+ luminescent centers in Ag-doped SrB_4O_7 crystals, which are responsible for a 290 nm emission, were found to be associated with an 11 μs lifetime [42]. Furthermore, Ag^+ ions in Ag-doped alkali halides were shown to be responsible for an emission with lifetime in the microsecond range, with a 34 μs lifetime at room temperature [50,51]. In Ag-doped aluminophosphate glasses, Ag^+ ions were also shown to be associated with decay components within the same timescale (1.3 and 11.7 μs lifetimes) [52]. The minor component with $\tau_1 = 5.0$ μs reported in the present work could not be

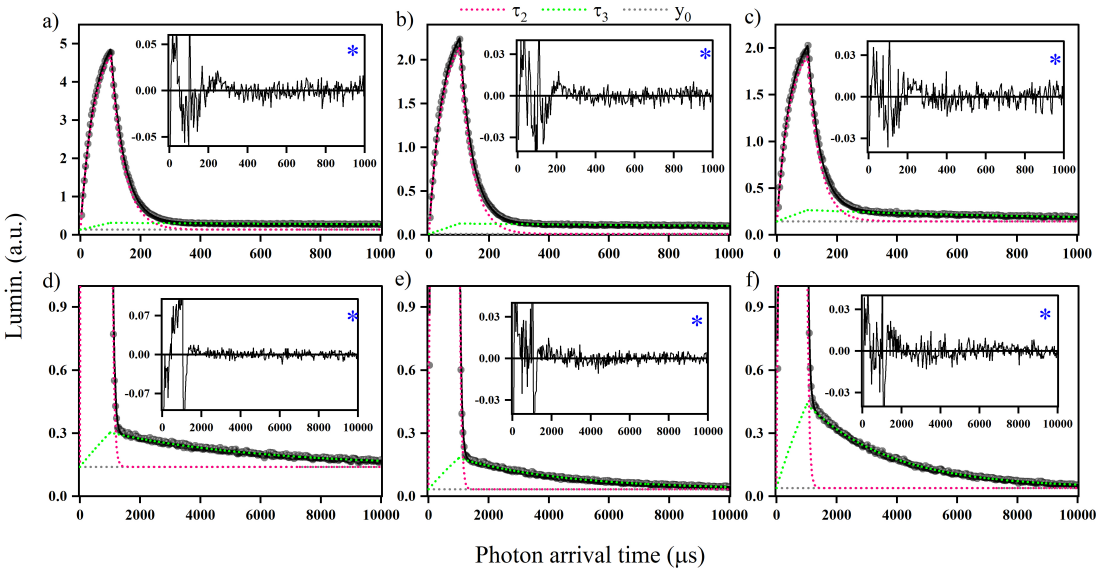

Figure 8: PATDs fitting of the Gd-Ag-codoped compounds using two pulse widths (100 μs and 1000 μs). a) and d) Gd-Ag(1); b) and e) Gd-Ag(2); c) and f) Gd-Ag(3). For a better estimation of the lifetimes, a biphasic exponential fitting was carried out individually for each PATD. For details about the insets and representation of the individual components, refer to the caption of Figure 4. For the 10000 μs pulse period, the y-axis was scaled up for better discrimination of the slower individual components.

identified.

Luminescence lifetimes of codoped compounds

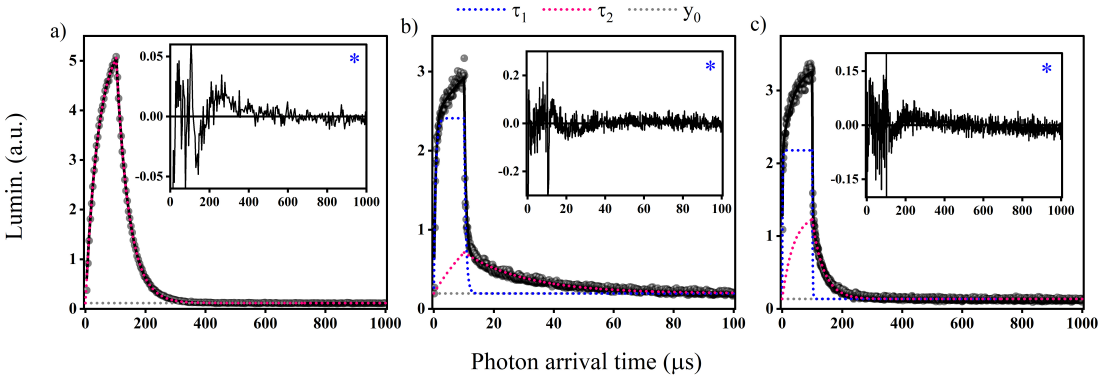

Figure 9: PATDs fitting of two different samples: a) Tb-Ag-codoped compound using a 100 μs pulse width; b) and c) Ce-Ag-codoped compound using two different pulse widths (10 μs and 100 μs). The fitting for the Ce-doped compound was performed individually for each timescale. For details about the insets and representation of the individual components, refer to the caption of Figure 4.

The Gd-Ag-codoped compounds exhibited two main lifetime components, with τ_2 varying between 41.0(3) µs and 44.6(2) µs and τ_3 varying between 2.79(4) ms and 5.1(2) ms, depending on the relative Gd/Ag dopant concentration (Gd/Ag ratio increases from left to right, Figure 8). τ_2 values are similar to that of Ag-doped compound (39 µs), attributed to Ag^+ ions. Although τ_3 of the Gd-Ag(3)-codoped compound (2.8 ms) is similar to the 2.3 ms component of the Gd-doped compound, τ_3 of Gd-Ag(1)-codoped compound was considerably higher (5.1 ms, with substantial constant luminescence). This seems to be related to additional slower components as Ag amount increases, which can be caused by an introduction of shallow trapping centers. Energy transfer between the Gd and Ag ions is excluded, because τ_3 decreases with the increase in the Gd/Ag concentration, when the opposite would be expected [43]. A faster component (τ_1 ~1.8 - 6.1 µs lifetimes) was also observed, but its contribution to the PATDs compared to τ_2 was negligible (Figure S3).

A test was carried out to evaluate the reproducibility of the measured PATDs using different aliquots of the Gd-Ag(3)-codoped compound. The results from the three different aliquots did not present significant changes in the luminescence lifetimes or in their relative contributions to the PATDs. Excluding the constant component, the relative contribution

Table 2: OSL emissions and the estimated lifetimes for each combination of dopants. Unless specified by the footnotes, each lifetime was estimated considering a biphasic exponential fitting and based on different pulse widths: τ_1 (10 µs), τ_2 (100 µs) and τ_3 (1000 µs). The relative contributions (R_i) to the PATDs were calculated by using the estimated lifetimes and the pre-exponential factors (S_i) for a specific pulse width (for italic and bold R_i, the pulse widths used were 10 and 100 µs, respectively. For the others, a 1000 µs pulse width was used). R_{y_0} corresponds to the relative contribution from the constant component (y_0). For the Gd-Ag- and Tb-Ag-codoped compounds, the minor contribution from the fast components (see Supplementary Materials) was not taken into account.

Dopants	OSL emissions (nm)	Lifetimes (µ*s*)						
		τ_1	R_1	τ_2	R_2	$\tau_3(x10^3)$	R_3	R_{y_0}
Gd	310	4.3(2)[a]	6.7%	2263(20)[b]	66.9%	–	–	26.4%
Tb	–	4.1(1)[c]	**28.8%**	40.1(30)[c]	**10.2%**	–	–	**61.1%**
Ce	–	<0.41(1)	*63.4%*	23.5(69)	*3.5%*	2.2(2)[d]	–	*33.1%*
Ag	295	5.0(2)[c]	**6.5%**	38.9(9)[c]	**14.7%**	2.9(5)	–	**78.8%**
Gd-Ag(1)	311, 325	1.8(1)	–	44.6(2)	65.9%	5.1(2)	12.1%	22.0%
Gd-Ag(2)	311, 330	4(1)	–	42.5(2)	67.7%	3.6(2)	20.4%	11.9%
Gd-Ag(3)	311, 340	6.1(8)	–	41.0(3)	48.5%	2.79(4)	39.4%	12.1%
Tb-Ag	332	4.0(7)	–	42.8(2)[a]	83.7%	30(9)	16.3%	–
Ce-Ag	–	<0.59(1)	**60.8%**	38.2(5)	**35.1%**	1.27(8)	–	**4.1%**

[a] Lifetime estimation using a single component;
[b] Lifetime estimation using a 1000 µs pulse width;
[c] Lifetime estimation using a global fitting among two datasets (10 and 100 µs pulse widths);
[d] Lifetime estimation of the slower component in a three-component exponential fitting.

to the PATDs for the fast and slow components were 56.1, 56.3, 57.4% and 43.9, 43.7, 42.6%, respectively (see Figure S4).

For the Tb-Ag-doped compound, the PATDs showed a well defined component with a 42.8(7) μs lifetime (Figure 9a), similar to the component in the Ag-doped and Gd-Ag-codoped compounds. This result supports the association of the ∼43 μs component with the Ag^+ emission. Secondary components were also observed, but these components played a minor role compared to the 43 μs component (Figure S5).

The Ce-Ag-codoped compound exhibited two main components, one with $\tau_1 =$ 0.59(1) μs and another one with $\tau_2 = 38.2(5)$ μs (Figures 9b and 9c). By similarities with the singly doped compounds, the faster component τ_1 is probably due to Ce^{3+} emission, whereas τ_2 with the Ag^+ emission. As discussed for the Ce-doped sample, however, the estimated value of τ_1 is likely associated with the LED rise and fall times. A component with a $\tau_3 = 1.27(8)$ ms lifetime was also observed, but that was negligible compared to the other two (see Figure S5).

Table 2 summarizes all the OSL emission band peaks as well as the estimated lifetimes along with their relative contribution (main components) to the PATDs for the compounds investigated. The table also shows the relative contribution of the constant components, which are probably associated with slower components.

Wavelength discrimination of the decay components for the Gd-Ag-codoped compound

The previous results suggest that, in CBO, the Gd^{3+} emission (311 nm) is associated with a lifetime of ∼2.8 ms, whereas the Ag^+ emission (∼330 nm) is associated with a lifetime of ∼43 μs. In order to confirm these identifications, PATDs for the Gd-Ag(3)-codoped compound were obtained using interference optical filters that transmit or block the Gd^{3+} emission at 311 nm (IF313 or IF330, respectively). The broad emission band centered at ∼330 nm, associated with Ag^+ centers, should be detected with both filters. The Gd-Ag(3) compound was selected among the other Gd-Ag-codoped compounds since it showed to have less influence of additional slower components (lifetime closer to that of Gd-doped compound - 2.3 ms).

As expected, using the IF330 filter (which blocks the Gd^{3+} emission) the component with a millisecond lifetime is completely eliminated from the PATD (Figure 10)

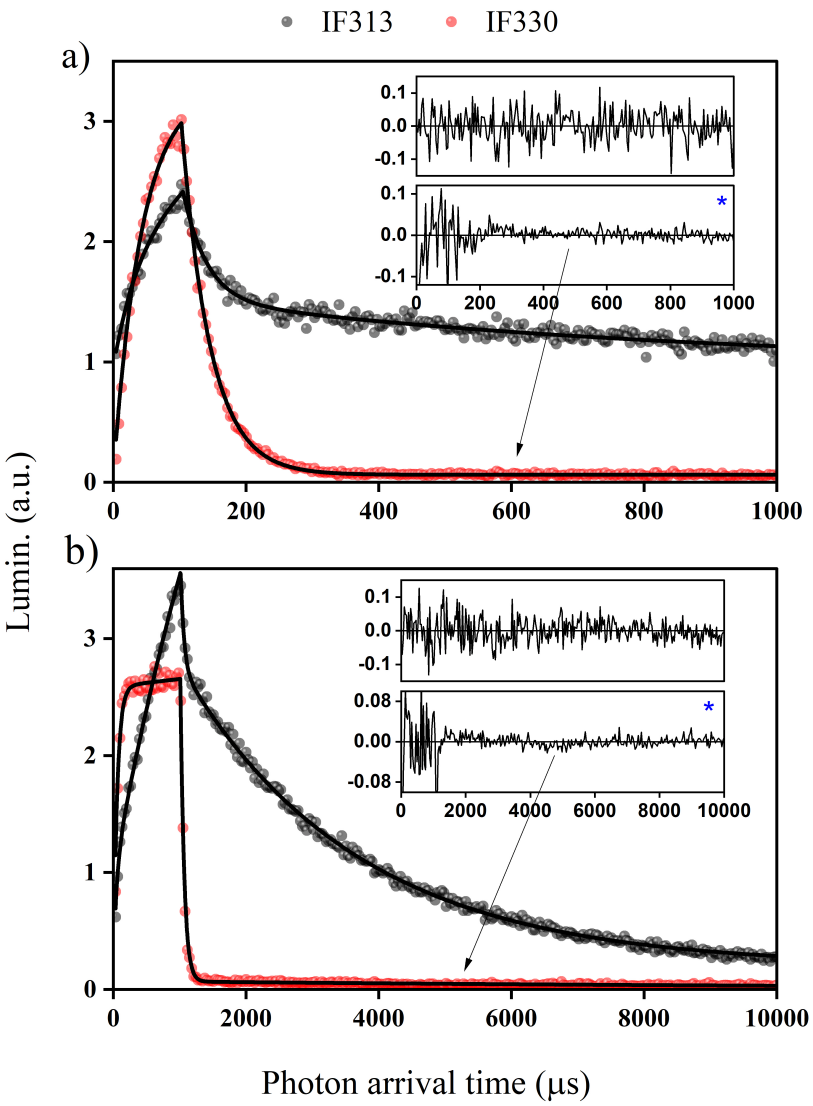

Figure 10: PATDs for the Gd-Ag(3)-codoped compound collected with the narrow-band filters (IF313 and IF330) with two different pulse widths: a) 100 μs and b) 1000 μs. The insets correspond to the fitting residuals of the PATDs obtained with the different filters.

and only a 43.1(4) μs lifetime component is observed. Conversely, using the IF313 filter (which transmits the Gd^{3+} emission and blocks part of the Ag^{+} emission) the main PATD main component presented a lifetime of 2.651(28) ms. Therefore, these results confirm the original identifications.

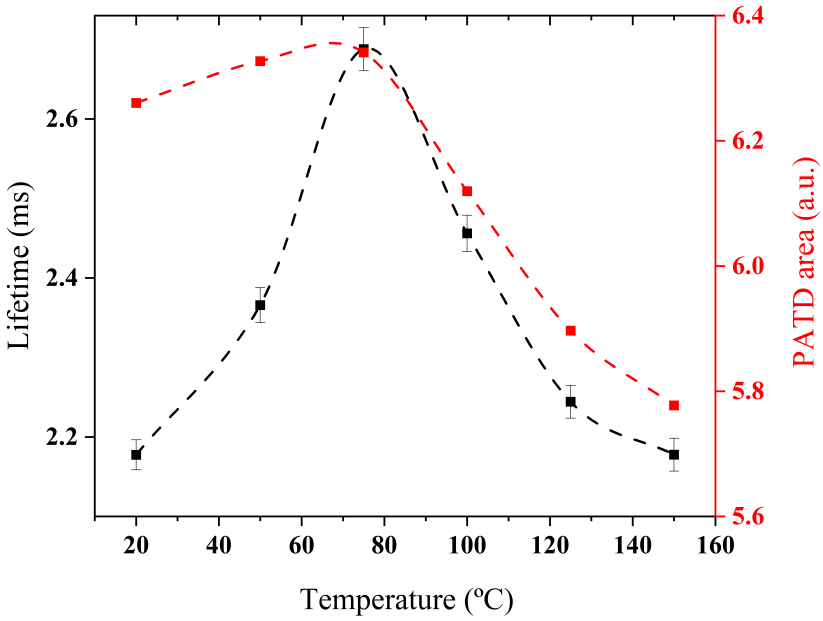

Figure 11: Lifetimes and PATDs as a function of temperature for the Gd-doped compound. The lifetimes were obtained using a single-component exponential fitting for each temperature and the error bars represent their uncertainties. The PATDs are expressed as the integral under the fitted curves. The data was recorded using a 10000 µs pulse period (pulse width: 1000 µs). To export the data, a 32.768 µs bin width was used.

Luminescence lifetimes as a function of temperature

The luminescence thermal quenching of the compounds was investigated for Gd- and Tb-doped, as well as for Gd-Ag- and Tb-Ag-codoped compounds considering both lifetimes and integrals under the PATDs. For the Ce-doped compounds, these measurements were not performed since the main component lifetime could not be estimated at room temperature.

For the Gd-doped compound, the 2.3 ms component corresponds to $^6P_J \rightarrow {}^8S_{7/2}$ forbidden transitions of Gd^{3+} and, therefore, thermal quenching is expected to be negligible (weak coupling between ground and excited states). Indeed, the experimental lifetimes at room temperature and 150 °C were the same, but an anomalous increase was observed at intermediate temperatures (Figure 11). This effect is probably caused by the influence of shallow trapping centers, as observed with an Al_2O_3:C samples [3]. The overall luminescence (PATD area) decreased less than 10 % over the same temperature range. For the Tb-doped compound, thermal quenching of the main decay component was analyzed as well. Although the origin of this component could not be elucidated, the results exhibited

a strong thermal quenching over the temperature range analyzed (Figure S6).

Thermal quenching for the luminescence of Ag-codoped compounds was also investigated. That was performed focusing on the common ∼43 µs lifetime component of Gd-Ag- and Tb-Ag-codoped compounds. All samples presented similar behavior with significant thermal quenching in the temperature range analyzed (Figure 12). That suggests that the common luminescent center characterized by a 43 µs lifetime is strongly affected by the lattice. The different combinations of dopants do not seem to have a significant influence on the thermal quenching of the common luminescence, which followed the equation for the Mott-Seitz model with similar fitting parameters. In addition, Figure S7 shows the thermal quenching considering the overall luminescence, which showed to be in a good agreement with the temperature dependence of the lifetimes for the Ag-codoped compounds. Ag^+ emission is known to have strong thermal quenching up to room temperature [42, 50]. Even though the temperature range used in the present study is higher compared to that of the reported works, the significant thermal quenching of Ag^+ emission is supported.

Conclusions

The results support the association of the 311 nm emission characteristic of Gd^{3+} centers and the ∼2.3 ms luminescence lifetime in the Gd-doped compounds. The negligible thermal quenching confirms the weak coupling between ground and excited states. The narrow emission and long luminescence lifetimes make Gd-doped compounds of interest for dosimetry applications, because the Gd^{3+} emission can be easily isolated either using optical filters or time-resolved measurements (e.g. POSL).

Ce-doping successfully introduced a fast component with lifetime faster than the LED rise and fall times (< 500 ns), but the simultaneous introduction of shallow trapping centers and a resultant strong phosphorescence did not allow for the OSL emission spectra to be collected. Nevertheless the OSL lifetime is consistent with Ce^{3+} emission. Materials with fast luminescence lifetimes such as Ce-doped CBO can be useful in laser-scanning imaging for 2D OSL dosimetry. Nevertheless, one must investigate a new synthesis method or introduce a codopant that could lead to a more stable trapping center while minimizing the role of shallow trapping centers.

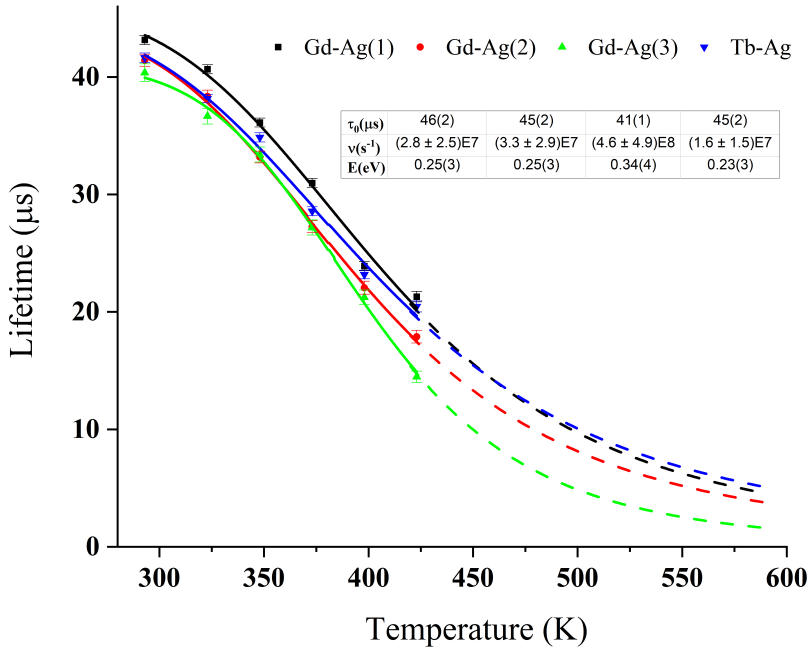

Figure 12: Dependence of lifetimes on temperature for Gd-Ag- and Tb-Ag-codoped compounds in a single graph. The lifetimes correspond to that one of the dominant component of a biphasic exponential fitting. The error bars are the uncertainties related to the estimated lifetimes. The solid lines represent the fitted curves according to the equation $\tau = \tau_0/(1 + \tau_0 \nu \exp(-E/kT))$, where ν and E represent the frequency factor and activation energy, respectively. The dashed lines are the extrapolation for higher temperatures. The parameters in the table from left to right correspond to the legends in the same order. All data were recorded using a 400 μs pulse period (pulse width: 100 μs). To export the data, a 4.096 μs bin width was used.

For the Ag-doped compounds, a broad emission centered at 295 nm in singly-doped and at ~330 nm in co-doped compounds, associated with a lifetime in the 39-45 μs range, was observed, which is probably associated with Ag^+ ions. The variations in the band emissions may be related to the influence of the host or other defects introduced by co-doping on the Ag^+ emission. The thermal quenching of the 43 μs lifetime component in the Ag-codoped compounds supports this interpretation, showing a strong influence of the lattice in the luminescent emission. The lifetime of the Ag-doped samples is intermediate between that of Ce- and Gd-doped samples, being of potential interest for both laser-scanning imaging and applications using POSL. In addition, Ag^+ seems to compete with other recombination centers (e.g. Gd^{3+} or Ce^{3+}). Therefore, Ag-codoping seems to improve the luminescence in CBO by providing an additional recombination route.

Although the exact lifetime estimations can be influenced by factors such as the relative intensity of the emission bands and the presence of shallow trapping centers, the

results demonstrate the value of TTTR-POSL measurements combined with a systematic study of doped and co-doped compounds, which gives insights about the recombination mechanisms in OSL materials. The information on CBO presented here should be useful for future developments of this material.

Acknowledgements

This research was partially funded by Brazilian agencies Fundação de Amparo à Pesquisa do Estado de São Paulo (FAPESP CEPID-NEUROMAT 13/07699-0), Coordenação de Aperfeiçoamento de Pessoal de Nível Superior (CAPES, Finance Code 001) and Conselho Nacional de Desenvolvimento Científico e Tecnológico (CNPq Grant 304107/2019-0). We are grateful to Eldereis de Paula for the technical support regarding the irradiation of samples. The Risø TL/OSL-DA-20 reader (DTU Nutech) was acquired with partial support from the Swiss National Science Foundation (REquip project 206021_177028).

References

[1] G. Blasse and B. C. Grabmaier, *Luminescent Materials*. Springer-Verlag, 1994.

[2] H. Qin, D. Wu, J. Sathian, X. Xie, M. Ryan, and F. Xie, "Tuning the upconversion photoluminescence lifetimes of $NaYF_4$:Yb^{3+}, Er^{3+} through lanthanide Gd^{3+} doping," *Scientific Reports*, vol. 8, no. 12683, 2018.

[3] M. S. Akselrod, N. Agersnap Larsen, V. Whitley, and S. W. S. McKeever, "Thermal quenching of F-center luminescence in Al_2O_3:C," *Journal of Applied Physics*, vol. 84, no. 6, pp. 3364–3373, 1998.

[4] R. J. Clark, I. K. Bailiff, and M. J. Tooley, "A preliminary study of time-resolved luminescence in some feldspars," *Radiation Measurements*, vol. 27, no. 2, pp. 211–220, 1997.

[5] M. L. Chithambo and R. B. Galloway, "On the slow component of luminescence stimulated from quartz by pulsed blue light-emitting diodes," *Nuclear Instruments*

and Methods in Physics Research Section B: Beam Interactions with Materials and Atoms, vol. 183, no. 3, pp. 358–368, 2001.

[6] E. G. Yukihara and S. W. S. McKeever, *Optically stimulated luminescence: fundamentals and applications*. Wiley, 2011.

[7] M. L. Chithambo, *An Introduction to Time-Resolved Optically Stimulated Luminescence*. Morgan and Claypool Publishers, 2018.

[8] I. K. Bailiff, "Characteristics of time-resolved luminescence in quartz," *Radiation Measurements*, vol. 32, no. 5, pp. 401–405, 2000.

[9] M. L. Chithambo, "The analysis of time-resolved optically stimulated luminescence: I. Theoretical considerations," *Journal of Physics D: Applied Physics*, vol. 40, pp. 1874–1879, mar 2007.

[10] M. L. Chithambo, "The analysis of time-resolved optically stimulated luminescence: II. Computer simulations and experimental results," *Journal of Physics D: Applied Physics*, vol. 40, pp. 1880–1889, mar 2007.

[11] M. Wahl, "Time-correlated single photon counting," technical note, PicoQuant, 2014.

[12] M. Wahl and S. Orthaus-Mueller, "Time Tagged Time-Resolved Fluorescence Data Collection in Life Sciences," technical note, PicoQuant, 2014.

[13] W. Becker, *Advanced Time-Correlated Single Photon Counting Techniques*. Springer, 2005.

[14] M. L. Chithambo, C. Ankjærgaard, and V. Pagonis, "Time-resolved luminescence from quartz: An overview of contemporary developments and applications," *Physica B: Condensed Matter*, vol. 481, pp. 8–18, 2016.

[15] T. Lapp, M. Jain, C. Ankjærgaard, and L. Pirtzel, "Development of pulsed stimulation and photon timer attachments to the Risø TL/OSL reader," *Radiation Measurements*, vol. 44, no. 5, pp. 571–575, 2009.

[16] J. S. Nyemann, P. Balling, and E. G. Yukihara, "Recombination lifetimes of LiF:Mg,Cu,P for pulsed optically stimulated luminescence," *Journal of Luminescence*, vol. 234, no. 117924, 2021.

[17] L. Bøtter-Jensen, S. W. S. McKeever, and A. G. Wintle, *Optically Stimulated Luminescence Dosimetry*. Elsevier, 2003.

[18] M. L. Chithambo, A. N. Nyirenda, A. A. Finch, and N. S. Rawat, "Time-resolved optically stimulated luminescence and spectral emission features of α-Al_2O_3:C," *Physica B: Condensed Matter*, vol. 473, pp. 62–71, 2015.

[19] W. M. Yen, S. Shionoya, and H. Yamamoto, *Phosphor Handbook*. CRC Press, 2007.

[20] L. D. Carlos, R. A. S. Ferreira, V. de Zea Bermudez, B. Julián-López, and P. Escribano, "Progress on lanthanide-based organicinorganic hybrid phosphors," *Chemical Society Reviews*, vol. 40, pp. 536–549, 2011.

[21] S. SeethaLekshmi, A. Ramya, M. Reddy, and S. Varughese, "Lanthanide complex-derived white-light emitting solids: A survey on design strategies," *Journal of Photochemistry and Photobiology C: Photochemistry Reviews*, vol. 33, pp. 109–131, 2017.

[22] K. Kuriki, Y. Koike, and Y. Okamoto, "Plastic optical fiber lasers and amplifiers containing lanthanide complexes," *Chemical Reviews*, vol. 102, no. 6, pp. 2347–2356, 2002.

[23] S. K. Gupta, J. P. Zuniga, M. Abdou, M. P. Thomas, M. De Alwis Goonatilleke, B. S. Guiton, and Y. Mao, "Lanthanide-doped lanthanum hafnate nanoparticles as multicolor phosphors for warm white lighting and scintillators," *Chemical Engineering Journal*, vol. 379, no. 122314, 2020.

[24] E. Yukihara, E. Milliken, L. Oliveira, V. Orante-Barrón, L. Jacobsohn, and M. Blair, "Systematic development of new thermoluminescence and optically stimulated luminescence materials," *Journal of Luminescence*, vol. 133, pp. 203–210, 2013.

[25] L. Oliveira, E. Yukihara, and O. Baffa, "Lanthanide-doped MgO: A case study on how to design new phosphors for dosimetry with tailored luminescent properties," *Journal of Luminescence*, vol. 209, pp. 21–30, 2019.

[26] L. Yuan, Y. Jin, Y. Su, H. Wu, Y. Hu, and S. Yang, "Optically stimulated luminescence phosphors: Principles, applications, and prospects," *Laser & Photonics Reviews*, vol. 14, no. 2000123, 2020.

[27] V. Altunal, V. Guckan, A. Ozdemir, A. Ekicibil, F. Karadag, I. Yegingil, Y. Zydhachevskyy, and Z. Yegingil, "A systematic study on luminescence characterization of lanthanide-doped BeO ceramic dosimeters," *Journal of Alloys and Compounds*, vol. 876, no. 160105, 2021.

[28] P. Dorenbos and A. J. J. Bos, "Lanthanide level location and related thermoluminescence phenomena," *Radiation Measurements*, vol. 43, no. 2, pp. 139–145, 2008.

[29] M. W. Swinney, J. W. McClory, J. C. Petrosky, S. Yang, A. T. Brant, V. T. Adamiv, Y. V. Burak, P. A. Dowben, and L. E. Halliburton, "Identification of electron and hole traps in lithium tetraborate ($Li_2B_4O_7$) crystals: Oxygen vacancies and lithium vacancies," *Journal of Applied Physics*, vol. 107, no. 113715, 2010.

[30] E. Pekpak, A. Yilmaz, and G. Ozbayoglu, "An overview on preparation and TL characterization of lithium borates for dosimetric use," *The Open Mineral Processing Journal*, vol. 3, pp. 14–24, 2010.

[31] O. Annalakshmi, M. Jose, U. Madhusoodanan, J. Sridevi, B. Venkatraman, G. Amarendra, and A. Mandal, "Thermoluminescence mechanism in rare-earth-doped magnesium tetra borate phosphors," *Radiation Effects and Defects in Solids*, vol. 169, no. 7, pp. 636–645, 2014.

[32] S. Watanabe, E. F. Chinaglia, M. L. F. Nascimento, and M. Matsuoka, "Thermoluminescence Mechanism In $Li_2B_4O_7$:Cu," *Radiation Protection Dosimetry*, vol. 65, no. 1-4, pp. 79–82, 1996.

[33] A. V. Porotnikov, I. . Ogorodnikov, S. V. Kudyakov, A. V. Kruzhalov, and S. L. Votyakov, "EPR of hole centers in nonlinear $LiBO_3$ crystals," *Physics of the Solid State*, vol. 39, no. 8, pp. 1224–1227, 1997.

[34] I. Ogorodnikov, L. I. Isaenko, A. Kruzhalov, and A. Porotnikov, "Thermally stimulated luminescence and lattice defects in crystals of alkali metal borate LiB_3O_5 (LBO)," *Radiation Measurements*, vol. 33, no. 5, pp. 577–581, 2001.

[35] L. C. Oliveira and O. Baffa, "Optically and thermally stimulated luminescence of CaB_6O_{10}:Ce,LiCl: Basic properties," *Journal of Luminescence*, vol. 188, pp. 180–187, 2017.

[36] R. D. Shannon, "Revised effective ionic radii and systematic studies of interatomic distances in halides and chalcogenides," *Acta Crystallographica Section A*, vol. 32, pp. 751–767, Sep 1976.

[37] L. V. França and O. Baffa, "Boosted UV emission on the optically and thermally stimulated luminescence of CaB_6O_{10}:Gd,Ag phosphors excited by X-rays," *Applied Materials Today*, vol. 21, no. 100829, 2020.

[38] M. Eichelbaum and K. Rademann, "Plasmonic enhancement or energy transfer? On the luminescence of gold-, silver-, and lanthanide-doped silicate glasses and its potential for light-emitting devices," *Advanced Functional Materials*, vol. 19, no. 13, pp. 2045–2052, 2009.

[39] J. A. Jimenez, "Enhanced UV emission of Gd^{3+} in glass by Ag^{+} co-doping," *Materials Letters*, vol. 159, pp. 193–196, 2015.

[40] BIPM, IEC, IFCC, ILAC, ISO, IUPAC, IUPAP, and OIML, "JCGM 100:2008 - Evaluation of measurement data - Guide to the expression of uncertainty in measurement," 2008.

[41] W. T. Carnall, P. R. Fields, and K. Rajnak, "Electronic Energy Levels of the Trivalent Lanthanide Aquo Ions. II. Gd^{3+}," *The Journal of Chemical Physics*, vol. 49, no. 10, pp. 4443–4446, 1968.

[42] A. Meijerink, M. M. E. van Heek, and G. Blasse, "Luminescence of Ag^{+} in crystalline and glassy SrB_4O_7," *Journal of Physics and Chemistry of Solids*, vol. 54, no. 8, pp. 901–906, 1993.

[43] R. Reisfeld, E. Greenberg, R. Velapoldi, and B. Barnett, "Luminescence quantum efficiency of Gd and Tb in borate glasses and the mechanism of energy transfer between them," *The Journal of Chemical Physics*, vol. 56, no. 4, pp. 1698–1705, 1972.

[44] A. Kumar, D. K. Rai, and S. B. Rai, "The effect of modifiers on the fluorescence and life-time of Gd^{3+} ions doped in borate glasses," *Spectrochimica Acta Part A: Molecular and Biomolecular Spectroscopy*, vol. 57, no. 13, pp. 2587–2591, 2001.

[45] B. Zhang, S. Ying, L. Han, J. Zhang, and B. Chen, "Color-tunable phosphor of $Sr_3YNa(PO_4)_3F:Tb^{3+}$ via interionic cross-relaxation energy transfer," *RSC Advances*, vol. 8, pp. 25378–25386, 2018.

[46] J. F. M. dos Santos, I. A. A. Terra, N. G. C. Astrath, F. B. Guimarães, M. L. Baesso, L. A. O. Nunes, and T. Catunda, "Mechanisms of optical losses in the $^5D_4$ and $^5D_3$ levels in Tb^{3+} doped low silica calcium aluminosilicate glasses," *Journal of Applied Physics*, vol. 117, no. 053102, 2015.

[47] V. Bachmann, C. Ronda, and A. Meijerink, "Temperature quenching of yellow Ce^{3+} luminescence in YAG:Ce," *The Journal of Chemical Physics*, vol. 21, pp. 2077–2084, 2009.

[48] S. K. Sharma, Y.-C. Lin, I. Carrasco, T. Tingberg, M. Bettinelli, and M. Karlsson, "Weak thermal quenching of the luminescence in the $Ca_3Sc_2Si_3O_{12}:Ce^{3+}$ garnet phosphor," *Journal of Materials Chemistry C*, vol. 6, pp. 8923–8933, 2018.

[49] N. Shrestha, D. Vandenbroucke, P. Leblans, and E. Yukihara, "Feasibility studies on the use of MgB_4O_7:Ce,Li-based films in 2D optically stimulated luminescence dosimetry," *Physics Open*, vol. 5, p. 100037, 2020.

[50] C. Pedrini, "Spectroscopic investigation of isolated silver ions in lithium chloride single crystal," *Journal of Physics and Chemistry of Solids*, vol. 41, no. 6, pp. 653–657, 1980.

[51] C. Pedrini, H. Chermette, and F. Gaume-Mahn, "Luminescence properties and electronic structure of Cu^+ and Ag^+ impurity centers occupying ideal lattice sites in alkali halides," *Journal of Luminescence*, vol. 24-25, pp. 213–216, 1981.

[52] J. A. Jimenez, S. Lysenko, G. Zhang, and H. Liu, "Optical properties of silver-doped aluminophosphate glasses," *Journal of Materials Science*, vol. 42, pp. 1856–1863, 2007.

Supplementary Materials

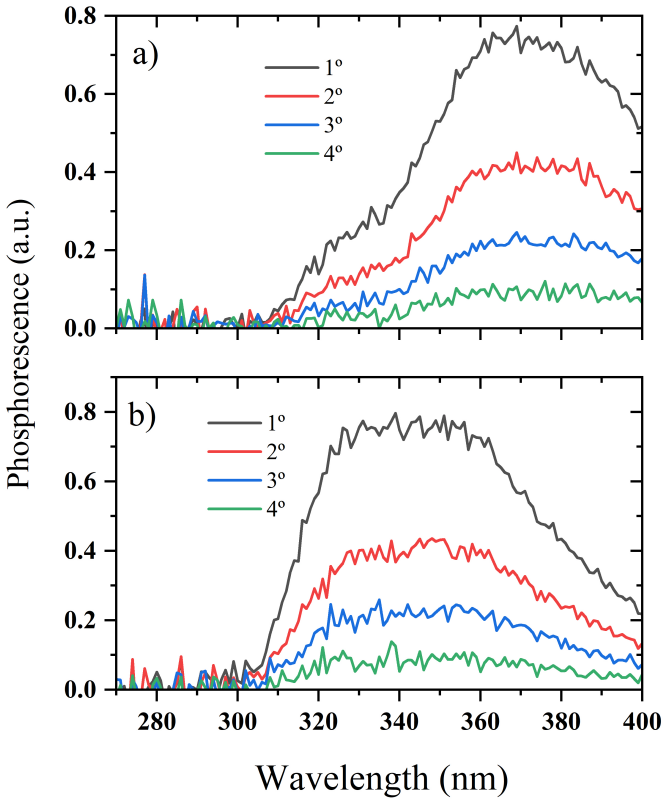

Figure S1: Phosphorescence of the Ce-doped compounds. a) Ce-doped and b) Ce-Ag-codoped compounds. The phosphorescence of these samples were detected using the same system and conditions described for the OSL emission spectra acquisitions, with the excitation slits closed instead (after X-rays irradiation). Several spectra were collected in a row and were subtracted by the last acquisition. The graph legends indicate the order of the spectra acquisition. Dose used: ~500 Gy.

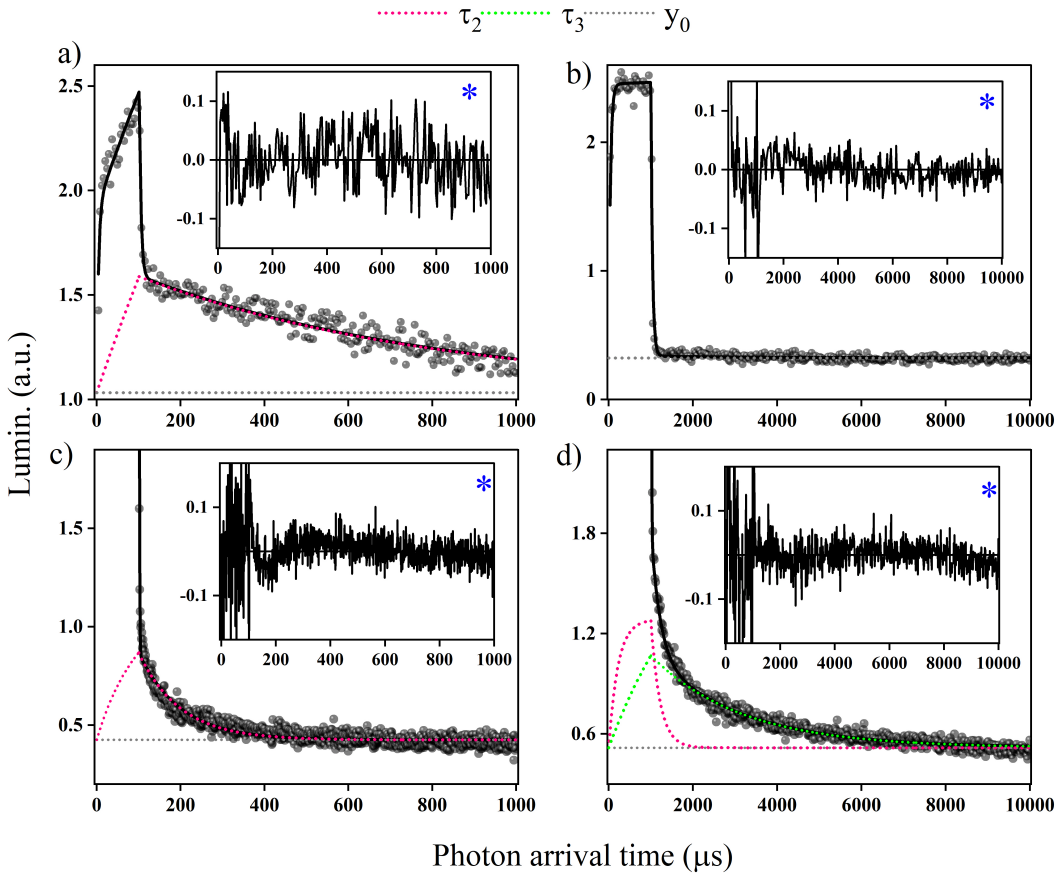

Figure S2: PATDs fitting for the single-doped compounds with other pulse widths. a) Gd; b) Tb; c) and d) Ce. The faster components are not discriminated here since they are reported in the main text. For some PATDs, the y-axis was scaled up for better discrimination of the slower individual components. The insets show the residuals from the exponential fitting and the blue star indicates that the y-axis was adjusted for better visualization of the overall residuals.

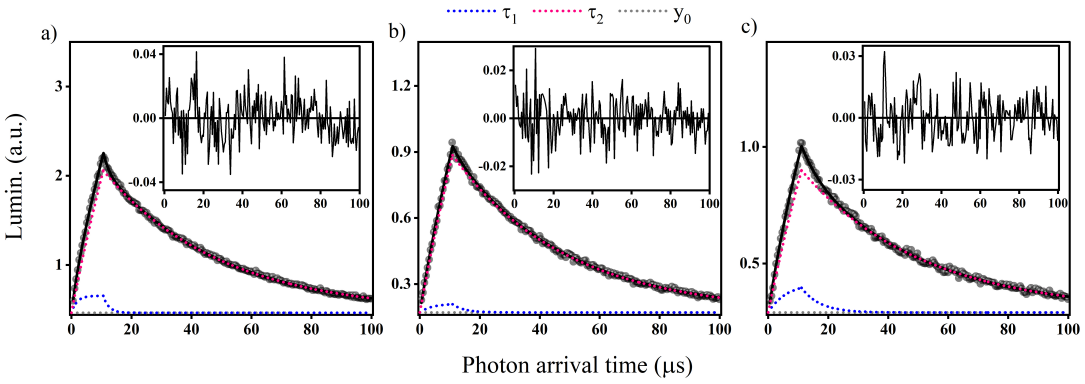

Figure S3: PATDs fitting of the Gd-Ag-codoped compounds with a 100 μs pulse interval. a) Gd-Ag(1); b) Gd-Ag(2) and c) Gd-Ag(3). The second component is the same dominant component as seen with a 100 μs pulse width (main text). For the insets, refer to the caption of Figure S2.

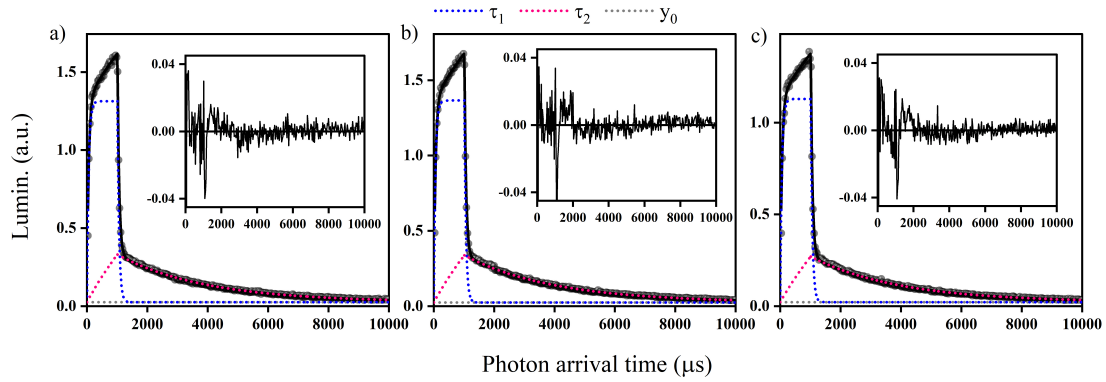

Figure S4: PATDs fitting for three different aliquots of Gd-Ag(3) when a 1000 μs pulse width was used. For the insets, refer to the caption of Figure S2.

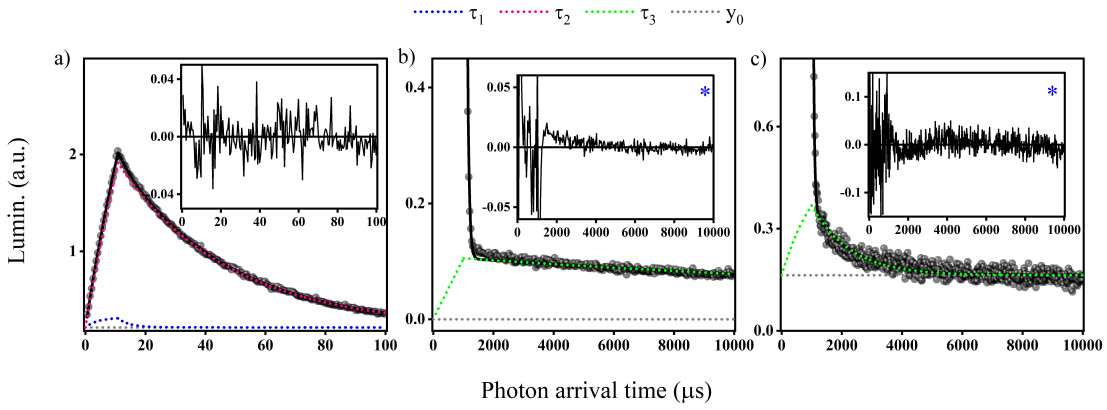

Figure S5: PATDs fitting of the Tb-Ag- and Ce-Ag-codoped compounds with other pulse widths: a) 10 μs and b) 1000 μs pulse widths for the Tb-Ag-codoped compound and c) 1000 μs for the Ce-Ag-codoped compound. The faster components for b) and c) are not discriminated here since they are reported in the main text. For the 1000 μs pulse widths, the y-axis was scaled up for better visualization of the slower individual components. For the insets, refer to the caption of Figure S2.

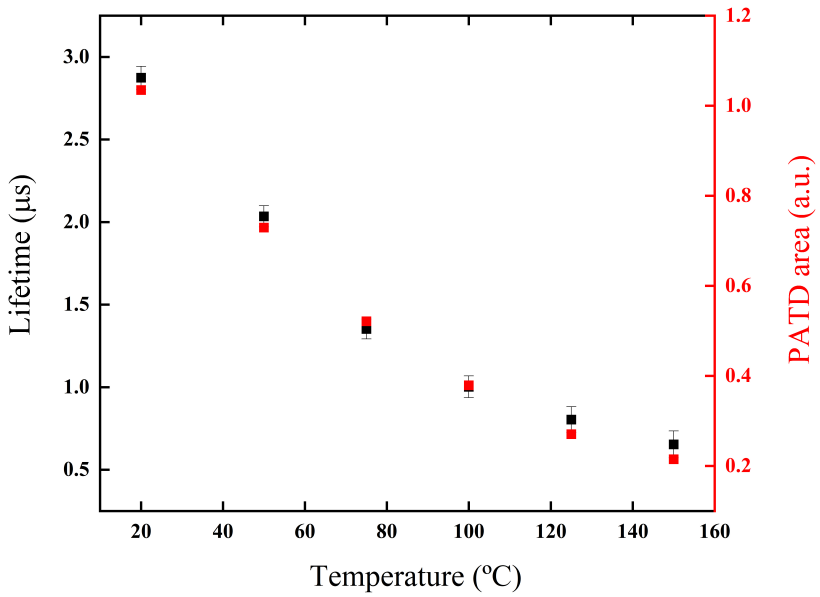

Figure S6: Lifetimes and PATDs as a function of temperature for the Tb-doped compound. Only the main component of a biphasic exponential fitting was considered. The PATDs are expressed as the integral under the curves of the main components only. The error bars are the uncertainties related to the estimated lifetimes. It is worth mentioning that the mismatch between the lifetime estimation at room temperature and the value already presented (refer to the Table 2 in the main text) is due to the different approaches used for the estimations. The data was recorded using a 50 μs pulse period (pulse width: 10 μs). To export the data, a 0.512 μs bin width was used. Dose used ~ 7.4 Gy.

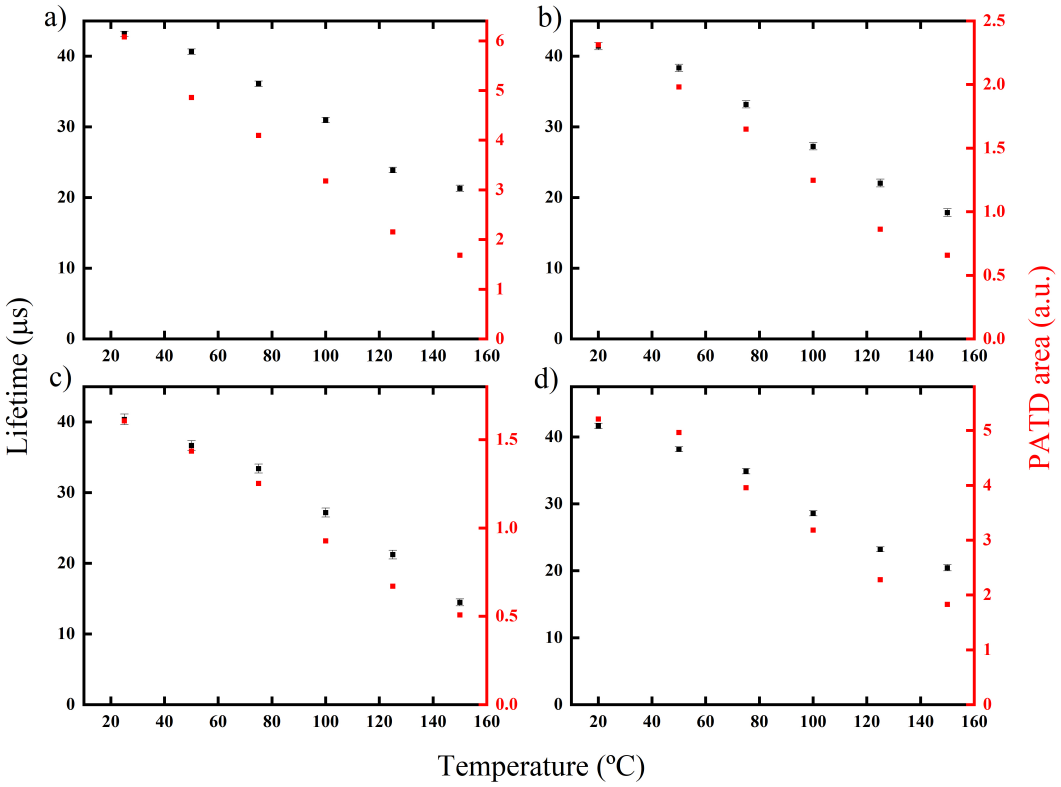

Figure S7: Comparison of lifetimes and PATDs as a function of temperature for Gd-Ag- and Tb-Ag-codoped compounds at different graphs. a) Gd-Ag(1); b) Gd-Ag(2); c) Gd-Ag(3) and d) Tb-Ag. The lifetimes correspond to the dominant component of a biphasic exponential fitting. The PATDs are expressed as the integral under the curves of the dominant components only. The error bars are the uncertainties related to the estimated lifetimes. All data were recorded using a 400 µs pulse period (pulse width: 100 µs). To export the data, a 4.096 µs bin width was used.

V. General Conclusions

The effectiveness of using lanthanide and silver doping in the CaB_6O_{10} host for its use as an OSL phosphor was demonstrated. The ability of activating the phosphor using different dopants, i.e., Ce^{3+}, Ag^{+} or Gd^{3+} allows for the luminescence lifetime tuning in a wide time-range: from nanoseconds to milliseconds. This addresses both 2D laser scanning dosimetry, as well as pulsed OSL dosimetry requirements using the same basic compound. It is recommended that new investigations using the Ag-doped CBO be carried out to verify the feasibility of a mid-range lifetime OSL phosphor (40 μs) in 2D laser scanning dosimetry applications.

Furthermore, the phosphors exhibited high-sensitivity, even comparable to the commercial OSL detectors based on Al_2O_3:C (using U340 Hoya filters) and wide linear dose-range with no signs of saturation. It is noteworthy that, the basic chemical precursors, e.g. acid boric and calcium carbonate, used for producing the CBO phosphors provides a low-cost procedure, combined with a relatively simple synthesis method. It was also demonstrated that the synthesis method is reliable, as suggested by the reproducibility tests.

In addition, the isotopically boron enriched phosphors demonstrated their feasibility after neutron irradiations. However, it is recommmended to evaluate how neutron-sensitive are the new OSL phosphors compared with TLD-600 and MgB_4O_7:Ce,Li phosphors.

One should keep in mind that the fading after irradiation of both Gd,Ag- and Tb,Ag- codoped compounds, i.e., ∼30% after 24 h following stability must be considered for practical applications. To address that, new synthesis routes, i.e., change of thermal treatment profiles, should be explored.

At last, the energy-response dependence of the new OSL phosphors should be taken into account for personal and medical dosimetry applications.